UNIVERSITY OF
BIRMINGHAM

CHARACTERISATION OF 2D AND 3D ORAL KERATINOCYTE CULTURES

by

Erum Khan

A thesis submitted to
The University of Birmingham
for the degree of
DOCTOR OF PHILOSOPHY

School of Dentistry
The University of Birmingham
January 2012

Abstract

Oral keratinocyte behaviour were analysed in two and three dimensional cultures of an immortalised human H400 cell line and primary rat keratinocytes (PRKs) using a novel method of quantitative microscopy, RT-PCR data and immunohistochemistry profiles. Monolayer cultures were established in high and low calcium media at different cell densities and analysed prior to generating 3D organotypic cultures (OCs) on de-epidermalised dermis (DED), polyethylene terephthalate porous membrane (PET) and collagen gels for up to 14 days. H400 and PRKs proliferation in monolayer cultures was greater in low calcium medium compared with high calcium medium. Gene expression analysis indicated that adhesion and structural molecules including E-cadherin, plakophilin, desmocollin-3, desmogleins-3 and cytokeratins-1, -5, -6, -10, -13 were up-regulated by days 6 and 8 compared with day 4 in high calcium medium. Immunohistochemical profiles and gene expression data of OCs on DED recapitulated those of normal oral epithelium. The final thickness of OCs as well as the degree of maturation/stratification was significantly greater on DED compared with other scaffolds used. Quantitative microscopy approaches enabled unbiased architectural characterisation of OCs and the ability to relate stratified organotypic epithelial structures to the normal oral mucosa. H400 and PRK OCs on DED at the air liquid interface demonstrated similar characteristics in terms of gene expression and protein distribution to the normal tissue architecture.

THIS THESIS IS DEDICATED TO MY DEAR PARENTS

GULNAZ AND AHMED ALI KHAN

Acknowledgements

I would like to thank Professor Gabriel Landini, Dr Richard Shelton, Dr Paul Cooper and Dr John Hamburger for their support, guidance and patience throughout my PhD. I am really honoured to have them as my supervisors. Many thanks to all my post graduate desk-fellows, past and present particularly Jennifer, Lisa, Zoe, Eisha, Jonathan, Owen, Joceline and James who remained kind, helpful and cooperative during my PhD. I am highly thankful to Michael for making the effort to proof read my thesis.

I would like to extend my appreciation to the other members of the academic staff at the School of Dentistry including Gay Smith, Michelle Holder, Dr. Kevin Carter, Sue Fisher and especially Sue Finney for her assistance in histological techniques at the laboratory. Thanks also go to the porters at the building of Birmingham Dental Hospital.

I would like to thank my parents especially my mom for her emotional support which gave me great comfort and made it possible for me to do my degree. Many thanks go to Idrees for his patience, guidance and endless support. In addition, I am highly grateful to my lovely sister Almas, brothers Farhan and Noman for their support, affection and constant belief in me.

I would also like to acknowledge the Liaquat University of Medical and Health Sciences for financial support and the University of Birmingham for providing an opportunity to pursue my PhD.

Table of Contents

List of Figures

Unless stated otherwise all figure images represent my own work

List of Tables

Abbreviations

ALI	Air liquid interface
BM	Basement membrane
bp	Base pair
Ca^{2+}	Calcium ion
$CaCl_2$	Calcium chloride
CGC	Collagen-glycosaminoglycan-chitosan
cDNA	Complementary de-oxyribonucleic acid
2D	Two dimensional
3D	Three dimensional
CK	Cytokeratin
DAB	3, 3-diaminobenzidine reagent
DED	De-epidermalised dermis
df	Degrees of freedom
DMSO	Dimethyl sulphoxide
ECM	Extracellular matrix
EDTA	Ethylenediaminetetraacetic acid
EGF	Epidermal growth factor
FCS	Foetal calf serum
GSH	Glutathione-SH
GAGs	Glycosaminoglycans
GAPDH	Glyceraldehyde-3-phosphate dehydrogenase
HC	High calcium
HEPES	4-(2-hydroxyethyl) piperazine-1-ethanesulfonic acid
H&E	Haematoxylin and eosin
HTA	Human tissue authority
IHC	Immunohistochemistry
IMS 99	Industrial methylated spirit 99 %
IL	Interleukin
IgG	Immunoglobin G
LC	Low calcium
K	Keratin
KGF	Keratinocyte growth factor
$MnCl_2$	Manganese chloride
mA	Milliampere
mRNA	Messenger ribonucleic aid
MCGs	Membrane-coated granules
MTT	[3-(4, 5-Dimethyl thiazole-2-yl)-2, 5-diphenyl tetrazolium bromide]
NADPH	Nicotinamide adenine dinucleotide phosphate

NADH	Nicotinamide adenine dinucleotide
PDGF	Platelet derived factor
PAS	Periodic acid-Schiff reaction
PBS	Phosphate buffered saline
PET	Polyethylene terephthalate
PKC	Protein kinase C
PFA	Paraformaldehyde
PRKs	Primary rat keratinocytes
SD	Standard deviation
SIOX	Simple Interactive Object Extraction
Sq-RT-PCR	Semi-quantitative reverse transcriptase-polymerase chain reaction
rcf	Relative centrifugation force
ROI	Region of interest
TAE	Tris-acetate EDTA
Tm	Annealing temperature
TGF-α	Transforming growth factor-α
TGF-β	Transforming growth factor-β
V-cells	Virtual cells
UV	Ultraviolet

CHAPTER 1 INTRODUCTION

1.1 Oral mucosa

The oral mucosa is a mucous membrane lining the oral cavity that interfaces anteriorly with the skin at the lips and posteriorly with the oesophagus. The oral mucosa is involved in several functions in the mouth including protection, sensation, secretion and absorption. It protects deeper tissues and organs including the underlying connective tissue, salivary glands, salivary ducts and muscles from the environment of the oral cavity (Sloan *et al.*, 1991) Structurally, oral mucosa is similar to the skin and the mucous membrane of the oesophagus and cervix (Squier and Brogden, 2011) and shows regional variation in thickness, composition and type of covering epithelium (Presland and Dale, 2000).

1.1.1 Classification of oral mucosa

According to functional demand and tissue features, the oral mucosa has been categorised into three groups, which are the masticatory (~60 % of total surface area), lining (~25 % of total surface area) and specialised mucosa (~15 % of total surface area) (Squier and Kremer, 2001). The masticatory mucosa is lined by keratinised stratified squamous epithelium, tightly attached to the underlying tissue by a collagenous connective tissue. This type of mucosa is found on the hard palate, gingiva and the masticatory surfaces of the dental arches in the edentulous mouth and the lateral borders of the tongue. The epithelium of masticatory mucosa is frequently orthokeratinised but may be parakeratinised (such as gingiva, palate) (Figure 1.1). The masticatory epithelium is inextensible and tolerates significant physical stress due to its underlying convoluted lamina propria (Presland and Dale, 2000). The numerous elongated papillae enable the epithelium to resist shear forces generated during chewing (Nanci, 2007).

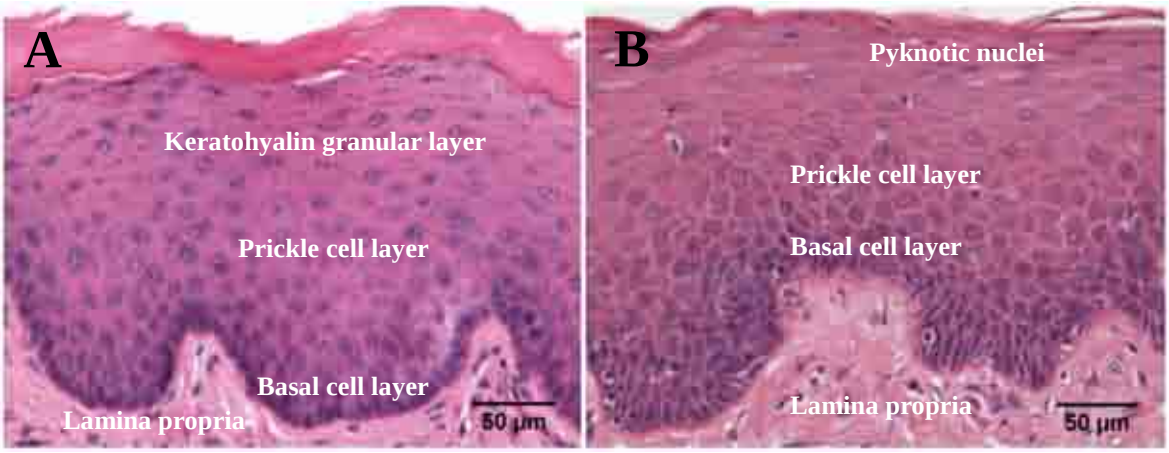

Figure 1.1. Structure of keratinised and parakeratinised oral mucosa. Five micron histological cross section of oral mucosal tissue stained with haematoxylin and eosin (H&E). (**A**) Adult rat tongue, showing keratinised stratified squamous epithelium with a distinct superficial layer of keratin, and (**B**) adult human gingiva, showing parakeratinised stratified squamous epithelium in which the superficial layer of cells retain shrunken (pyknotic) nuclei. The labels show the approximate locations of the different histological features within the tissue.

The connective tissue of the lamina propria contains collagenous fibres that bind the epithelium tightly to the underlying bone-mucoperiosteum or directly to fibrous submucosa. These fibres are thicker and more organised than those present within the lining mucosa (Avery and Daniel, 2005; Nanci, 2007).

The lining mucosa comprises of a non-keratinised stratified squamous epithelium supported by a more elastic and flexible connective tissue compared with the masticatory mucosa. The lining mucosa is a highly vascularised and relatively thin, consequently it appears a brighter red than masticatory mucosa (Nanci, 2007; Young *et al*., 2000). The lining mucosa is present in the cheeks, vestibule, soft palate, floor of the mouth, mucogingival junction and ventral surface of the tongue which require flexibility to accommodate chewing, speech or swallowing of food (Squier and Brogden, 2011). The specialised mucosa covers the dorsum of the body or papillary portion of the tongue and can be present as a mosaic of keratinised and non-keratinised epithelium (Squier and Kremer, 2001). A 'V' shaped groove, the sulcus terminalis, divides the tongue into the anterior two thirds of the body and the posterior third or base (Nanci, 2007).

The anterior portion of the tongue is covered by pointed filiform papillae, which are keratinised extensions of the epithelium and forms a rough, abrasive surface that aid in the disaggregation of food. Fungiform (fungus-like in appearance) papillae are present at the tip of the tongue and are smooth round structures covered with a non-keratinised epithelium and are associated with taste buds. At the posterior limit of the tongue there is a row of circumvallate papillae surrounded by a deep circular groove which contain numerous taste buds. On the outer edges of the tongue there are foliate

papillae which are also embedded with taste buds and provide taste sensation (Squier and Brogden, 2011). The mucosa covering the base of the tongue contains aggregations of lymphoid tissue that are commonly referred to as the lingual tonsils (Nanci, 2007; Kamata, 1992).

1.1.2 Principal patterns of maturation (keratinisation)

The principal patterns of maturation are represented by keratinised and non-keratinised epithelia (Smack *et al.*, 1994). As cells migrate from the basal layer to the outer (cornified) surface of epithelia, they accumulate cytoplasmic protein filaments (cytokeratins) and undergo a program of terminal differentiation which results in the production of the so-called stratum corneum, characteristic of keratinised epithelium (Presland and Jurevic, 2002; Watt and Green, 1982). Differentiating cells enter the prickle cell layer where specific proteins are synthesised and retained, including involucrin and profilaggrin which are precursors for the thickening of the cell envelope (Rice and Green, 1977). The mature (cornified) cells become larger, flattened (hexagonal), filled with keratin and also lack visible nuclei and other organelles (Fukuyama *et al*., 1976; Trott and Banoczy, 1962), they are surrounded by an external lipid matrix which contributes to the epithelial barrier. This pattern of maturation is termed orthokeratinisation (Adams, 1976) and histologically, the squames are stained bright pink with eosin (eosinophilic) (Figure 1.1 A) (Becker *et al*., 2008; Young *et al.*, 2000). In parakeratinised epithelium, shrunken or pyknotic (darkly stained) nuclei are retained in much of the superficial layers (typically in parts of the hard palate and much of the gingiva) (Figure 1.1 B).

In healthy oral epithelium, parakeratinisation is a normal event, whereas in skin this process is sometimes associated with pathological conditions such as psoriasis (Nanci, 2007). The rate of cell proliferation is highest in thin non-keratinised regions such as the floor of the mouth and the underside of the tongue as compared with the thicker keratinised regions including the palate and gingivae (Thomson *et al*., 1999).

The pattern of regional epithelial maturation is also associated with different turnover rates which represent the time taken for a cell to divide and migrate through the entire epithelium (Squier and Kremer, 2001) (Table 1.1). The fastest turnover rate is present on the dorsal surface of the tongue, followed by the buccal mucosa, floor of the mouth, the hard palate, the ventral surface of the tongue (Cutright and Bauer, 1967). Non-keratinised buccal epithelium turns over more rapidly than keratinised gingival epithelium (Chandra *et al*., 2010) and this results in accelerated healing of lesions in this type of epithelium (Squier and Brogden, 2011). Indeed it has been reported that it takes ~1-3 weeks to renew buccal epithelia, compared with 4-10 weeks in the epidermis (Winning and Townsend, 2000). The induction of epithelial proliferation and differentiation is reportedly modulated by four main factors which are i) soluble inducers, ii) cell-cell interactions, iii) cell-matrix interactions and iv) cell polarity and shape (Freshney and Freshney, 2002).

Table 1.1. **Turnover time range (days) in different epithelia.**

Tissue region	Turnover time, days
Dorsal tongue	10
Labial mucosa	14
Buccal mucosa	14
Floor of mouth	20
Hard palate	24
Ventral tongue	25
Gingiva	41
Skin	27

(Chandra *et al*., 2010; Cutright and Bauer, 1967; Squier and Kremer, 2001)

Soluble inducers are biologically active molecules including hormones, vitamins and paracrine factors (molecules secreted from fibroblasts with their receptors preferentially found on epithelial cells). Examples of these paracrine factors include keratinocyte growth factor (KGF), epidermal growth factor (EGF), transforming growth factor-α (TGF-α), transforming growth-β (TGF-β), platelet derived factor (PDGF), interleukin-1 (IL-1) and interleukin-6 (IL-6) (Alberts *et al.*, 2008; Feliciani *et al*., 1996). The rate of cell proliferation is consequently the result of interaction between positive and negative regulators which act through complex control networks. Typically the binding of these factors to cell surface receptors results in the activation of intracellular kinases, phosphatases and transcription factors leading to expression of proteins involved in cell cycle regulation and differentiation (Squier, 1968; Squier and Kremer, 2001).

Reportedly high-density monolayers undergo differentiation faster than low-density cultures (Freshney and Freshney, 2002) and the process of cell migration and differentiation is also modulated by cell-matrix interaction. Indeed keratinocyte proliferation is promoted by interaction with the extracellular matrix (ECM) derived molecules of collagen type-I and -IV and fibronectin, while laminin-1 and laminin-5 inhibit keratinocyte migration (O'Toole *et al.*, 1997). Indeed integrin receptors present at focal adhesion sites mediate cell-matrix and cell-cell interactions and initiate various signalling processes (Hynes, 1992). Notably the α2β1 integrin receptor is present in basal keratinocytes and mediates migration on collagens type I and IV whereas, the α5β1 integrin receptor controls keratinocyte locomotion in response to fibronectin (Kim *et al.*, 1992).

1.2 Structure of oral mucosa

The oral mucosa consists of an epithelium supported by a loose connective tissue, termed the lamina propria. There is a thin junction complex between the epithelium and lamina propria which is referred to as the basement membrane (BM).

1.2.1 Oral epithelium

The oral epithelium undergoes constant renewal and repair to maintain the defence barrier of the oral mucosa and consists of several cell layers (Smith and Everett, 1962). The stratified and squamous epithelium consists of several cell layers including the stratum basale, stratum spinosum, stratum granulosum and if the epithelium is keratinised the superficial layer is termed the stratum corneum (Figure 1.1 A, Figure 1.2 A). In non-keratinised epithelium, the cells at the stratum basale differentiate into stratum spinosum and stratum intermedium leading to the superficial layer (Figure 1.2 B). The stratum basale is a single layer of undifferentiated keratinocytes that is anchored to the basal lamina. These basal cells proliferate and asymmetrically divide either to give i) stem cells which maintain the population of dividing cells or ii) transit cells which differentiate and migrate through the layers (basal to superficial) of the oral epithelium. Notably these basal cells adhere to the underlying basal lamina via the α3β1 integrin receptor which has an affinity for laminin-5 (Dogic *et al.,* 1998).

Moreover, hemidesmosomes bind with the α6β4 integrin cell receptor to further anchor basal cells to the basement membrane (Carter *et al.,* 1990). In the stratum spinosum the keratinocytes are relatively large compared with the basal cells (Chandra *et al.,* 2010) and appear irregularly polyhedral in shape with delicate spines protruding from their surfaces and therefore are termed ‘prickle cells’.

(A) **(B)**

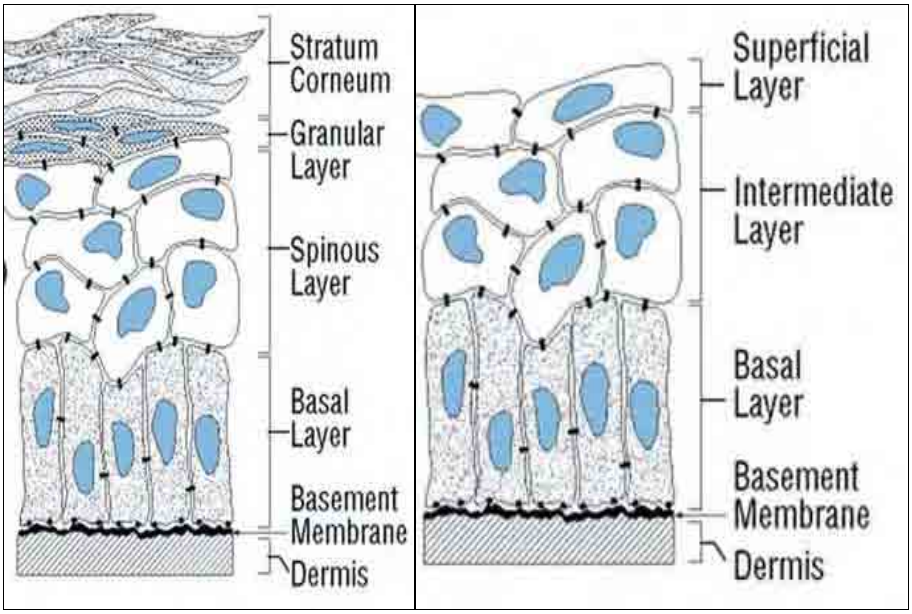

Figure 1.2. **Different stratified layers of squamous epithelium**. Schematic diagram (Presland and Jurevic, 2002) showing the different stratified layers within (A) keratinised and (B) non-keratinised squamous epithelium. In keratinised epithelia, basal (columnar) keratinocytes differentiate into spinous (polygonal), granular (keratohyalin granules present in the cytoplasm of keratinocytes) and corneum (flat keratinocytes without nuclei) cell layers. In non-keratinised epithelia basal keratinocytes (columnar) differentiate into intermediate (polygonal) and superficial (flat nucleated) cells layers.

These cells begin accumulating lipids, keratins and specific proteins including involucrin, profilaggrin and other precursors for the thickening of the cell envelope. The stratum granulosum is characterised by flat cells which include intracellular membrane-coated granules (MCGs) containing lipids. At the boundary between the granular and cornified layers, these MCGs migrate to the superficial aspect of the keratinocytes (Squier and Kremer, 2001). The membrane of the MCG fuses with the plasma membrane of keratinocyte and the lipids are extruded into the extracellular space of the surface layer (Matoltsy, 1976; Elias and Friend, 1975) thereby providing flexibility and a permeability barrier to the stratified squamous epithelium (Squier and Kremer, 2001). The stratum corneum comprises flat and hexagonal cells which contain dense cytokeratin filaments (Steinert *et al*., 1983) which are surrounded by an external lipid matrix (Elias and Friend, 1975; Madison *et al.*, 1987).

In non-keratinising epithelia, there is less accumulation of lipids and cytokeratins compared with keratinising epithelia. In addition the cytokeratin filaments do not accumulate as bundles and the mature cells on the outer surface of non-keratinised epithelia are relatively larger, flat and retain nuclei and other organelles compared with keratinised epithelia. During injury, keratinocytes flatten out towards the wound and the number of gap junctions increases to enable rapid cell-to-cell communication (Nanci, 2007).

1.2.1.1 Cells of the oral epithelium

Keratinocytes are the major cell type present within the epithelia of both the epidermis and oral epithelium. The progenitor cells are situated in the basal layer in thin epithelia (such as the floor of the mouth) and in the lower two or three cell layers in

thicker epithelia (such as the cheek and palate). The progenitor layer(s) comprises two distinct cell populations which include stem cells, a relatively small population which retain the proliferation potential of the tissue (Watt, 1998) and a large population of dividing cells which undergo cellular differentiation before desquamation at the epithelial surface (Squier and Kremer, 2001). In addition to keratinocytes, there are other minor cell populations present within the basal and prickle cell layers of the oral epithelium. Indeed, the presence of Langerhan's cells, lymphocytes, Merkel cells and leukocytes have all been reported (Nanci, 2007).

1.2.1.2 Cytokeratins/keratins

Keratins are members of the 10 nm intermediate filament multigene family (Hansson *et al.,* 2001). The family is comprised of twenty keratins and is divided into two major types based on their molecular weight ranging from 40-68 kDa and their isoelectric point (pH) ranging from 5.2-7.8 (Moll *et al.,* 1982). Each keratin exists in several pH variants of different isoforms of both type I and type II keratins (Smack *et al.,* 1994).

Type I keratins include the K9-K20 members, which have molecular weights ranging from 40-64 kDa and have acidic pH whereas, type II keratins (K1-K8) have molecular weights ranging from 52-68 kDa and exhibit a neutral or basic pH (Su *et al.,* 1994). Keratin filaments extend from the nucleus to the plasma membrane providing a cytoskeleton within the keratinocyte. Keratins interact with desmosomes and hemidesmosomes which enable cell-to-cell adhesion (Magin *et al.,* 2007) and basal cell interaction with basement membrane and connective tissue, respectively. Keratins are expressed in a tissue-specific manner in different combinations of pairs that determine

epithelial cell development and stages of differentiation (Table 1.3) (Smith and Everett, 1962; Clausen *et al.*, 1986). Alteration in the expression of keratins appears to be of biological and pathological significance, for example in oral squamous cell carcinoma the expression of K4/K13 is commonly dys-regulated (Sakamoto *et al*., 2011).

1.2.1.2.1 Basal cell layer keratin expression

K5/K14 are usually expressed initially in basal cells of stratified squamous epithelium (Blumenberg and Tomic-Canic, 1997). K5/K14 are therefore regarded as specific markers for basal cells of stratified squamous epithelia however their expression can be additionally detected in the suprabasal compartment (Blumenberg and Tomic-Canic, 1997). K19 can also be detected in the basal cell layer of different oral epithelial subtypes (Sawaf *et al*., 1990) (Table 1.3). Notably, hereditary epidermal disorders can result from mutations in keratin genes indeed epidermolysis bullosa simplex, which results in skin blisters, is caused by genetic mutations in the K5/K14 genes (Coulombe *et al.*, 2009).

Table 1.2. **Distribution of classes and specific pairing of type I (neutral-basic) and type II (acidic) keratins in oral and other epithelial tissues** (Hansson *et al*., 2001).

Type II Size (kDa)	**Type I** Size (kDa)	**Distribution in epithelium**	**Distribution in oral epithelium**
K1 (68)	K10(56.5)	Suprabasal, keratinising stratified	Suprabasal cells of buccal epithelium, basal cells of gingiva and dorsal tongue
K2e/K2p(66)	K11(56)	Suprabasal, keratinising stratified	
K3(64)	K12(55)	Suprabasal, keratinising	Suprabasal cells of gingiva and sulcular epithelium
K4(59)	K13(51)	Suprabasal, non-keratinising stratified	Suprabasal cells of buccal, lingual epithelium, attached gingiva and hard palate
K5(58)	K14(50)	Basal cells, keratinising	Basal cells of buccal epithelium, gingiva, suprabasal cells of gingiva, tongue
	K15(50)	Basal cells, keratinising and non-keratinising	
	K17(46)	Basal cells, keratinising and non-keratinising	
K6(56)	K16(48)	Suprabasal, high cell turnover stratified	Suprabasal cell layer of gingiva, tongue and buccal mucosa
K7(54)	K19(40)	Simple (gastrointestinal) epithelia	Basal and suprabasal cells of buccal epithelium, basal cells of gingiva, tongue
K8(52)	K18(45)	Simple (secretary) epithelia	
K9(64)		Suprabasal, palmoplantar	
	K20(46)	Simple (urothelium) epithelia	

1.2.1.2.2 Keratin expression during epithelial differentiation

Keratins K1/K10 have been described as early markers of the epithelial differentiation process (Stark *et al.*, 1999) as they are predominantly expressed in the basal and suprabasal layers of keratinised and non-keratinising stratified squamous epithelium (Bloor *et al.*, 2001; Bloor *et al.*, 2000). The K4/K13 molecules are expressed primarily in suprabasal cells of non-keratinising stratified squamous epithelium such as buccal, lingual and oesophageal epithelia (Pang *et al.*, 1993). However, subsequent work has also demonstrated their expression in the suprabasal cell layers of the foetal epidermis, the attached gingiva and the hard palate (Morgan and Su, 1994). The K4/K13 keratins are also expressed in tissue culture by primary keratinocytes cultured at the air-liquid interface (ALI) (Bloor *et al.*, 1998).

Keratin K3 has also been detected in the suprabasal layer of gingiva and sulcular epithelium (Juhl *et al.*, 1989) while K6/K16 and K17 are expressed during wound healing in suprabasal cells of the epidermis (Freedberg *et al.*, 2001; Blumenberg and Tomic-Canic, 1997). Notably K6/K16 are expressed in suprabasal cells of the gingiva and tongue and are also detected in the non-keratinising buccal mucosa as well as in the cornea (Su *et al.*, 1994). K19 is also expressed in the suprabasal cell layer of buccal epithelium and is considered a marker of differentiation (Morgan and Su, 1994).

1.2.1.3 Specialised cell junctions in the epithelium

Desmosomes and hemidesmosomes (Figure 1.3 A) are located at the cell membrane and maintain cohesion between cells and regulate epithelial permeability (Squier and Brogden, 2011; Mackenzie and Binnie, 1983a). These structures enable

cell-cell binding in addition to facilitating the keratinocytes interaction with the basal lamina. Intracellularly these junctions also connect the keratin cytoskeleton to the cell surface (Presland and Jurevic, 2002).

Specifically, desmosomes are structures providing tight adhesion between adjacent cells (Figure 1.3 A) and consist of two principal groups of desmosomal cadherin molecules, namely members of the desmoglein-3 and desmocollin families (Garrod and Chidgey, 2008). Desmosomal cadherin proteins are attached to cytoplasmic keratin filaments via the desmosomal plaque (Kowalczyk *et al*., 1999; Kowalczyk *et al*., 1994) which includes proteins such as plakoglobin, desmoplakins, plakophilins, envoplakin and periplakin (Matoltsy, 1975) (Figure (1.3 B). Desmosomal cadherins mediate cell adhesion by calcium-dependent interaction between their extracellular protein components.

In addition to desmosomes, E-cadherin and P-cadherin (termed classical cadherins) membrane proteins establish cell-to-cell adherens junctions between epithelial cells enabling their attachment via the cytoplasmic actin proteins (Green and Jones, 1996). Adherens junctions are characterised by the adhesive function of E-cadherin which depends upon its association with cytoplasmic proteins, termed catenins (α-, β-, and γ-catenins) that link the cytoplasmic terminal tail of E-cadherin to the actin cytoskeleton (Lewis *et al*., 1994). Adherens junctions are intercellular junctions and crucial for epithelial adhesion (Niessen, 2007).

Hemidesmosomes enable the anchoring of the intermediate filament cytoskeleton to the basement membrane (Garrod, 1993). In palatal epithelium, the hemidesmosomes enable the epithelium to withstand high mechanical loads of up to 700 Newtons (Bale and White, 1982). Laminin-receptors on the cell surface provide

bridge-like structures which ensure the stability of connection and communication between the basal lamina and the epithelial cells. Non-integrin glycoproteins present on the cells, bind with collagen and other ECM components in the epithelium (Stevens and Lowe, 2005).

Figure 1.3. **Structure of desmosome and hemidesmosome**. Schematic diagrams showing (A) desmosome and hemidesmosome structures. Desmosomes bind adjacent keratinocytes and hemidesmosomes anchor the intermediate filament cytoskeleton of the keratinocytes to the basement membrane adapted (Presland and Jurevic, 2002), and (B) desmosomal tight junctions, enabling keratin cytoskeleton connection to the cell surface and keratinocytes binding with one another via desmosomal cadherins (plakoglobin, desmoplakin and plakophilin) (Jamora and Fuchs, 2002).

(A)

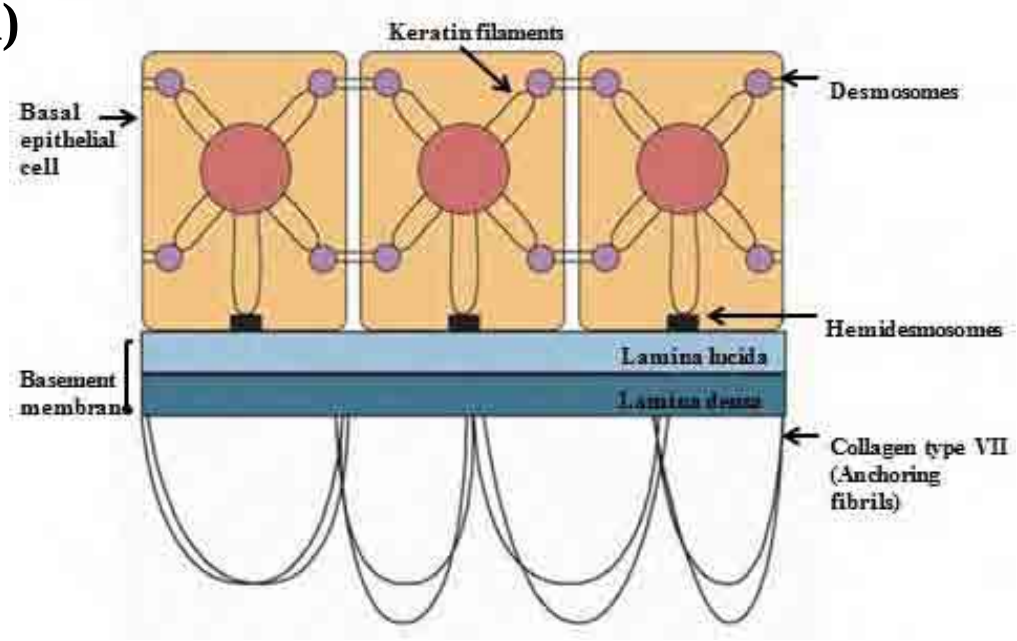
Keratin filaments
Desmosomes
Basal epithelial cell
Hemidesmosomes
Lamina lucida
Basement membrane
Lamina densa
Collagen type VII (Anchoring fibrils)

(B)

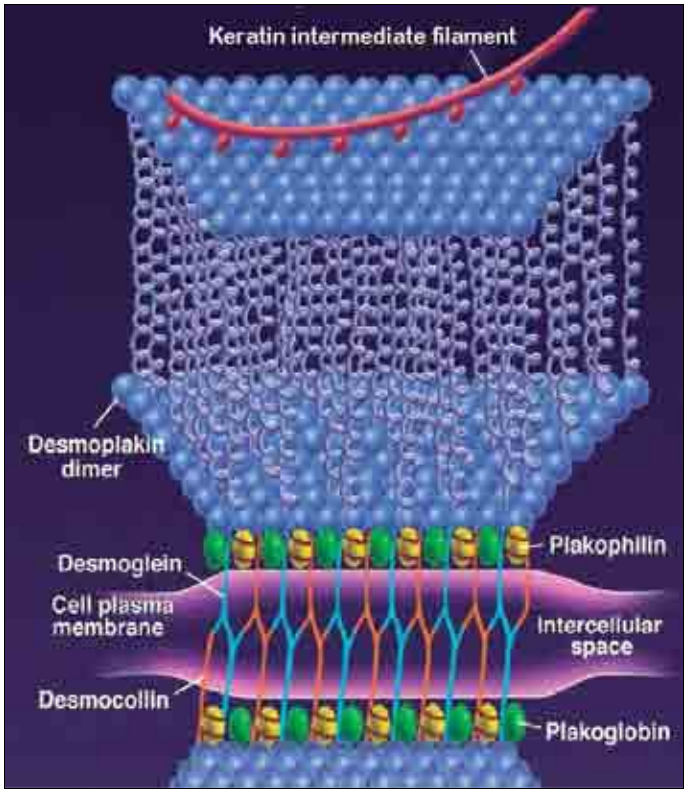
Keratin intermediate filament
Desmoplakin dimer
Plakophilin
Desmoglein
Cell plasma membrane
Intercellular space
Desmocollin
Plakoglobin

1.2.2 Basement membrane

The junction of the oral epithelium and lamina propria is an undulating interface termed the basement membrane (BM) where papillae of connective tissue interdigitate with epithelial ridges. The BM cushions and supports the epithelium and acts as a filtration barrier for both the epithelium and connective tissue (Nanci, 2007). The BM is also present around muscles, nerves, capillaries and fat cells depicted in Figure 1.4 (Leeson *et al*., 1985). The architectural appearance and composition of the BM varies from site to site and depends upon the masticatory loads placed on it. For instance, the BM of palatal mucosa that bears a high mechanical stress during mastication is thicker with more prominent rete ridges as compared with those of buccal mucosa (Bale and White, 1982). In histological sections stained with haematoxylin and eosin (H&E) the BM is not visible as it has no affinity with this stain. The BM is however detectable as a pink/purple band using the periodic acid-Schiff reaction (PAS) (Nanci, 2007) due to this stains affinity for the complex carbohydrates of proteoglycans found in the reticulin fibres of the BM (Figure 1.4 A) (Young *et al.,* 2000). BMs can also be identified in histological tissue sections (although not particularly distinctively) with silver (black) staining techniques as shown in Figure 1.4 B (Leeson *et al.*, 1985).

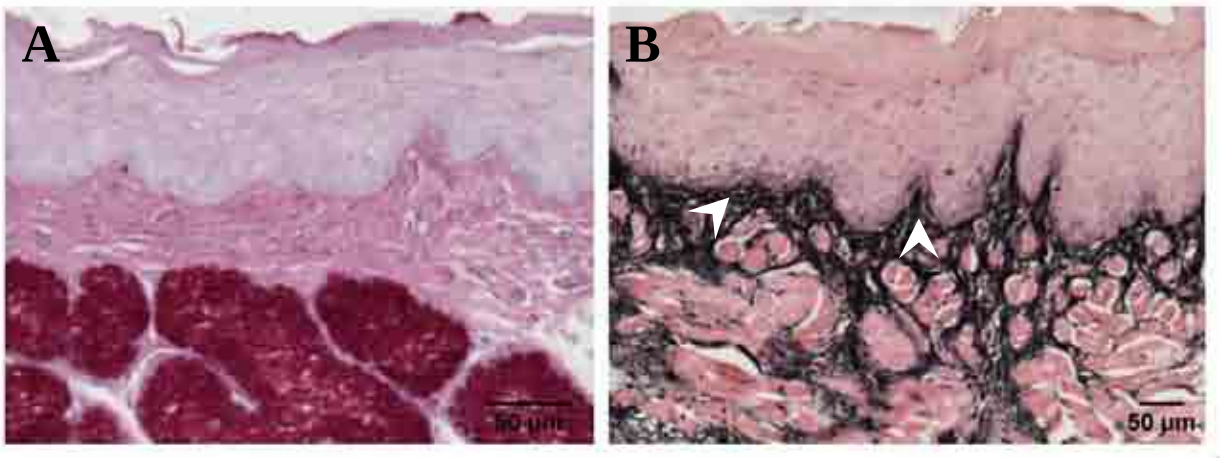

Figure 1.4 **Periodic acid Schiff and methamine silver staining of rat tongue**. Five micron histological cross sections of adult rat tongue stained with (A) Periodic acid Schiff (PAS) showing the presence of collagen fibres within the basement membrane (pink), striated muscle of tongue (dark pink), salivary gland (magenta) due to an affinity of PAS for proteoglycans, glycogen and glycoprotein (complex carbohydrates), respectively. (B) methamine silver staining showing a fused network of reticulin fibres of collagen type I and III in the lamina propria (dark black areas shown by white arrow heads), though collagen IV in the basement membrane is not marked distinctly.

Transmission electron microscopy has also demonstrated that the BM is composed of three layers or laminae, including the lamina lucida, lamina densa and lamina reticularis which comprise fibres and ground substances (Avery and Daniel, 2005). The lamina lucida is located towards the epithelial side of the basal lamina and is an electron-lucent band of 10-60 nm width comprising laminin, integrin and entacin proteins as well the dystroglycan glycoprotein. Laminin-5 (previously known as kalinin, epiligrin, and nicelin) is an important adhesive component which anchors the filaments of the lamina lucida and is secreted by keratinocytes (Marinkovich *et al*., 1993; Verrando *et al*., 1993). The lamina densa is a 20-300 nm thick electron-dense band which is located between the lamina lucida and the lamina reticularis (Squier and Kremer, 2001). The fibroreticular lamina (or lamina reticularis) is produced by the cells of the connective tissues and is comparatively more fibrous than the lamina lucida (Avery and Daniel, 2005). The lamina reticularis is attached to the basal lamina by anchoring fibrils of type VII collagen and micro-fibrils (fibronectin, laminin) of ECM (Stevens and Lowe, 2005).

Studies have demonstrated that the protein content of the BM plays a key role in regulating clot formation, inflammation, re-epithelialisation, angiogenesis and wound contraction (O'Toole *et al*., 1997). Inherited defects of β4 integrin and collagen type XVII result in a separation of the epithelium-lamina propria interface at the lamina lucida level. This decreases hemidesmosome attachments and is manifested as the mucosal blisters seen in pemphigoid (McGrath *et al.*, 1995).

Within the BM, several collagen fibre types are embedded in a ground substance composed of glycosaminoglycans (GAGs) and serum derived proteins which are highly hydrated (Nanci, 2007; Young *et al*., 2000). Collagens represent a large

family of fibrillar glycoproteins and each collagen fibre is composed of many macrofibrils, each consisting of microfibrils which in turn comprise a number of molecules of tropocollagen (Young *et al.*, 2000). Tropocollagen consists of three polypeptide chains entwined into a triple helix structure (Pauling and Corey, 1951; Becker *et al*., 2008). Collagen type IV and VIII are found within the BM with collagen IV being exclusive and particularly abundant in the BM of the oral mucosa (Becker *et al*., 1986). Immunohistochemical analysis indicates collagen type IV appears as a continuous band in BMs and around blood vessels, salivary glands and nerve fascia (Figure 1.5). Laminin, which has a similar immunohistochemical distribution as type IV collagen (Becker *et al.*, 1986), is a glycoprotein and principal constituent of the anchoring filaments formed by the association of three gene products for the α, β, and γ chains (Burgeson *et al*., 1994). Laminin connects the BM with hemidesmosomes of the basal lamina (O'Toole *et al*., 1997) and its major function is to enable cell adhesion by interacting with integrins (Dogic *et al*., 1998). Laminin also regulates cell behaviour by mediating cell signals between the ECM and the cell interior via transmembrane receptors (Aumailley and Krieg, 1996). Indeed together with collagen type IV, laminin has been demonstrated to be an important regulator of oral epithelial cell differentiation in gingival tissue cultures (Tomakidi *et al.*, 1998). Fibronectin is a glycoprotein and also an essential component of the BM, distributed throughout the lamina propria and sub-mucosa in a reticular pattern (Salonen *et al*., 1984). The fibroreticular lamina anchors the BM to the adjacent ECM by extension of lamina densa into fibroreticular lamina where it interacts with collagen type III. Collagen type VII anchoring fibrils and hemidesmosomes connect the BM with the underlying ECM (Avery and Daniel, 2005; Young *et al*., 2000).

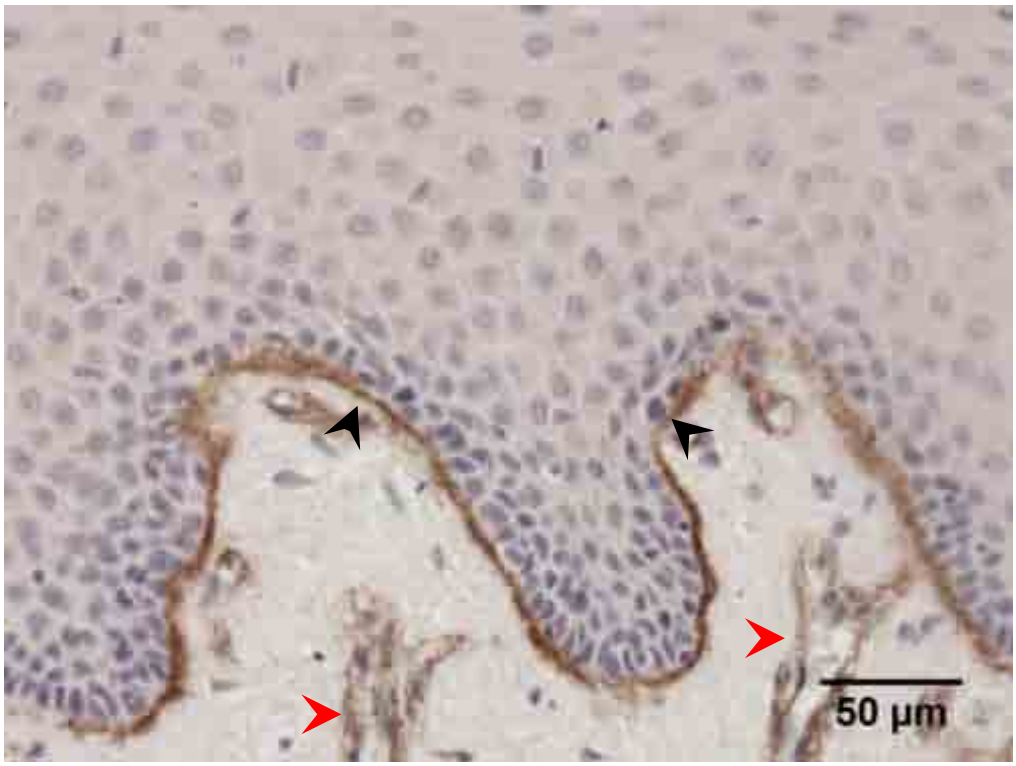

Figure 1.5. **Collagen type IV staining of adult human gingiva**. Five micron histological cross section of adult human gingiva stained with anti-collagen type IV antibodies. Collagen type IV is detected in the basement membrane which is highlighted as a fine continuous band (black arrow head) located between the epithelium and lamina propria. Collagen type IV staining is also detected around blood vessels (red arrow heads).

1.2.3 Lamina propria

The lamina propria is a loose connective tissue present beneath the epithelium (Figure 1.1). It contains capillaries and a network of collagen type I fibres while deeper layers contain collagen type III, elastic fibres, such as elastin, and glycoproteins (Sear *et al.*, 1980). The vascular component of the lamina propria contains extensive capillary loops in the papillae between the epithelial ridges (Leeson *et al.*, 1985). Lymphatic vessels, nerve endings and the ducts of salivary glands are also found within the lamina propria (Avery and Daniel, 2005).

1.2.3.1 Cells of the lamina propria

Fibroblasts are the major mesenchymal cell type within the lamina propria and are responsible for synthesising ground substance and collagen fibres (Sloan *et al*., 1991). Light microscopy analysis reveals fibroblasts as fusiform (cigar-shaped) or stellate (star-shaped) morphologically with long processes that tend to lie parallel to bundles of collagen fibres (Figure 1.6). Fibroblasts contain numerous mitochondria, granular endoplasmic reticulum and a prominent Golgi complex, which indicate the cells collagen associated synthetic activity. Fibroblasts play a key role in regulating tissue integrity (Nanci, 2007) and have a relatively low rate of proliferation in adult oral mucosa except during wound healing when their numbers increase rapidly to enable repopulation of the injury site. Indeed fibroblasts can exert contractile forces and develop cytoplasmic actin filaments to facilitate active wound closure. In certain diseases, such as gingival overgrowth, fibroblasts may be activated and secrete more ground substance than is usual (Squier and Kremer, 2001).

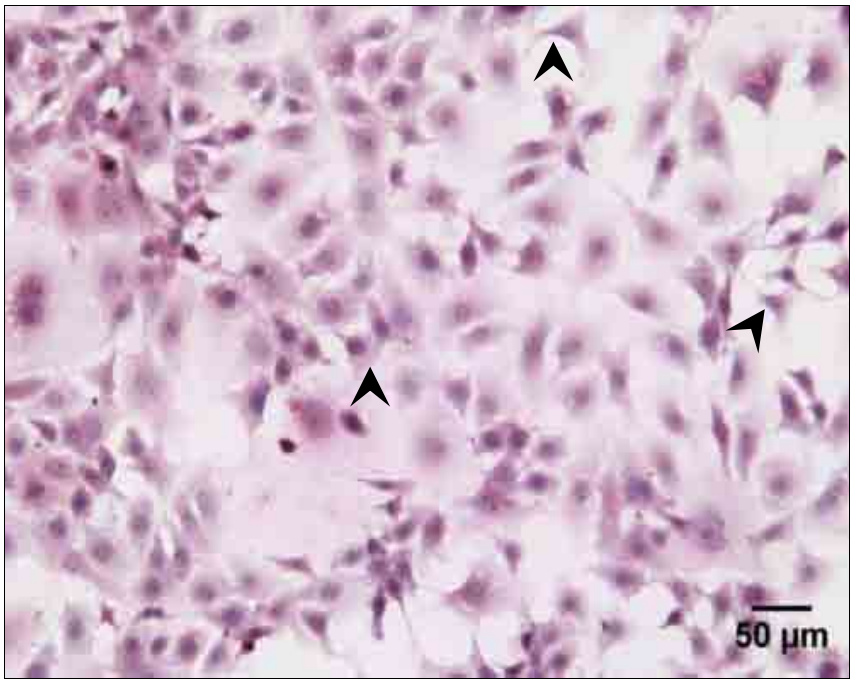

Figure: 1.6. **Typical stellate structure of NIH/3T3fibroblasts**. H&E stained histological image showing typical stellate (black arrow heads) nature of NIH/3T3 fibroblasts cultured as a monolayer.

1.2.3.2 Fibres and ground substance in the lamina propria

Collagen (types I and III) and elastin together with fibronectin are the major fibres in the lamina propria (Pachence, 1996) (Becker *et al*., 2008). Elastin is the principal protein of the elastic fibres of the lamina propria. The other component of the elastic fibre is a glycoprotein with a microfibrillar morphology (Squier and Brogden, 2011). Initially, elastic fibres consist entirely of aggregates of microfibrils, each 10 to 20 nm in diameter. However on maturation elastin is deposited within the microfibril matrix as a granular material until it becomes the predominant component accounting for more than 90 % of the fibres present in most regions of the oral mucosa (Becker *et al.*, 2008; Young *et al*., 2000).

Although the ground substance of the lamina propria appears to be amorphous when visualised by light or electron microscopy, it consists of heterogeneous protein-carbohydrate complexes permeated by tissue fluids (Nanci, 2007). Chemically these complexes can be subdivided into two distinct groups: proteoglycans and glycoproteins (Young *et al*., 2000). The proteoglycans consist of a polypeptide core to which GAGs (consisting of hexose and hexuronic acid residues) are attached. In the oral mucosa the proteoglycans are represented by hyaluronic, heparin sulphate, versican, decorin, biglycan and syndecan (Squier and Brogden, 2011).

1.3 Sub-mucosa

The sub-mucosa is present in different areas of the oral cavity, including the floor of the mouth, the ventral surface of the tongue and the alveolar, buccal and labial mucosa. The underlying sub-mucosa in the cheeks contains adipocytes and minor mixed salivary glands, interspersed with connective tissue fibres that bind the mucous

membrane to the underlying musculature (Sloan *et al.,* 1991). The underlying sub-mucosa of the floor of the mouth, as well as the sublingual mucous glands, contains adipose tissue and the connective tissue papillae (Avery and Daniel, 2005; Mefi *et al.*, 2000). In the lateral anterior regions of the hard palate, the sub-mucosa contains adipose tissue, while in the midline of the hard palate, no sub-mucosa is present. The lateral regions of the palatine mucosa contain both adipose and glandular sub-mucosa that extends posteriorly into the soft palate. In the ventral surface of the tongue the sub-mucosa is not clearly distinguishable as it merges with the connective tissue that lies between the muscle bundles of the tongue (Avery and Daniel, 2005).

1.4 Tissue engineering (TE)

TE is an interdisciplinary field which applies the principles of engineering and life sciences to develop biological substitutes to maintain or restore tissue functions (Sipe, 2002; Baum and Mooney, 2000; Alexander *et al*., 1995; Skalak and Fox, 1988). TE of oral mucosa has the potential to contribute to treatment and rehabilitation for a range of oral diseases including congenital defects, acquired disease (such as cancer, periodontal disease and trauma) (Hildebrand *et al*., 2002; Zdrahala and Zdrahala, 1999). Currently tissue engineered autograft (tissue sourced from the same organism) and allograft (tissue extracted and cultured from a different organism of the same species) approaches are being developed (Lee, 2000). TE approaches can include two types of tissue construct generation utilising *in vitro* and *in vivo* approaches. *In vitro* tissue engineering includes the isolation and expansion of tissue specific cells with seeding onto scaffolds used to generate engineered tissue/organs (Lanza *et al*., 2007; Moharamzadeh *et al.,* 2007; Kaigler and Mooney, 2001; Baum and Mooney, 2000; Lee, 2000). This approach has been used to attempt to reconstruct several different tissues *in vitro* including skin dermis, cartilage and bone reconstruction (Chan and Leong, 2008; Feinberg *et al.,* 2005; Ma and Elisseeff, 2005). Notably *in vitro* labelling of cultured and subsequently grafted gingival keratinocytes showed that the transplanted keratinocytes integrated into the newly formed mucosal epithelium (Lauer and Schimming, 2001). Oral mucosa engineering is a relatively new field and there are relatively few studies reported in the literature regarding the *in vitro* reconstruction of full thickness oral mucosa equivalents composed of both an epithelium and a lamina propria. Indeed the *in vivo* performance of engineered oral mucosa has not yet been satisfactorily tested and therefore significant work is still required before this field is able to benefit patients.

In vivo TE envisions a process of mediating the healing and regeneration of living tissue by promoting the growth and differentiation of cells within the patient at the site of injury potentially via the use of a biodegradable scaffold (Lanza *et al*., 2007). Ideally such scaffolds should be biocompatable and contain a system of interconnecting channels formed by a physical-chemical or mechanical means enabling cell communication and nutrient diffusion.

1.4.1 Scope of tissue engineering

Previously, TE research has been undertaken for a range of tissues and organs including skin, blood vessels, bone, cartilage, muscle and heart (Langer and Vacanti, 1993). Major challenges still however remain to be overcome with regards to their successful application and these include: risk of infection, time scale to produce engineered tissue and regulatory issues (Sipe, 2002). In addition, engineering of structural and fully functional tissues and organs remains challenging (Cancedda and De Luca, 1993). Indeed while Kaigler (Kaigler and Mooney, 2001) reported engineered skin that did not contain hair or glandular structures and that its architecture only moderately resembled that of the normal dermis, (Navsaria *et al*., 2004) reconstructed head and neck full-thickness skin for burn injuries which successfully incorporated hair follicle structures.

TE approaches have been applied to generate human oral mucosal equivalents not only for treatment and closure of surgical wounds but also for facilitating studies on the biology and pathology of oral mucosa (Kinikoglu *et al*., 2009). Studies have been performed using tissue engineered oral mucosal equivalents for intra-and extra-oral treatment which have provided favourable histological and clinical outcomes (Lauer and Schimming, 2001). Indeed the ideal engineered oral mucosa should resemble the normal oral mucosa and should be composed of an outer layer of stratified squamous epithelium and an underlying layer of

dense connective tissue. Current limitations with regards to the generation of epithelial sheets for grafting on superficial oral mucosal defects include their fragility and relatively low engraftment rates (Cooper *et al*., 1993; Clugston *et al*., 1991).

Cooper *et al* (1993) reported that the presence of a dermis assisted in epithelial graft adherence, epithelial maturation and minimised wound contraction, while encouraging the formation of a basement membrane. In skin tissue engineering, the gold standard has been the use of a split-thickness graft containing all of the epidermis and a proportion of the underlying dermis (MacNeil, 2008). However, for the mucosal grafts, limitation of donor tissue size, which is generally of a much smaller area compared with skin, is a problem (Ueda *et al*., 1991). Treatment of oral defects with skin grafts has been attempted, however due to physiological differences between skin and mucosa, such as hair growth and pattern of keratinisation, limit application of this approach (Izumi *et al*., 2003).

1.4.2 Applications of engineered oral mucosa

Applications for tissue engineered oral mucosa include their use clinically and for *in vitro* test/models system and several of these are described below (Lee, 2000).

1.4.2.1 Clinical applications

The most successful application of tissue engineering to date is the development of skin equivalents. Indeed skin tissue is needed for adjunctive aesthetic treatment of burns, invasive cancers, gunshot injury, major abrasions and knife lacerations (Baum and Mooney, 2000). Engineered skin products, with both dermal and epidermal components, using a combination of cells and various polymer carriers were the first tissue engineered products reported for clinical use (Kaigler and Mooney, 2001). Indeed application of tissue engineered skin was demonstrated to promote further tissue regeneration and remodelling by stimulating

local secretion of growth factors and cytokines which contributed to the tissue repair (Lee, 2000).

Currently, a range of commercially available skin substitutes are available for clinical applications (Otto *et al*., 1995). For instance, Dermagraft is initially used for burn wound coverage and subsequently replaced with autologous skin grafts (Purdue, 1997). While, split skin grafts have been used to cover extensive oral mucosal defects, hyperkeratosis and growth of hair were the major disadvantages observed (Sauerbier *et al*., 2006). Unlike engineered skin, tissue engineered human oral mucosa has not yet been commercialised for clinical applications. Within dental surgery the engineering of oral mucosa and gingiva is important in the treatment of gingival recession, periodontal implant reconstruction and maxillofacial reconstructive surgery (Igarashi *et al*., 2003; Schmelzeisen *et al*., 2002; Kaigler and Mooney, 2001). Indeed TE oral mucosa has been used to cover defects in various surgical procedures like vestibuloplasty, freeing of the tongue and prelamination of the radial flap (Sauerbier *et al*., 2006).

1.4.2.2 *In vitro* test system model application

In vitro applications of three-dimensional oral mucosa models include analyses of biocompatibility, biological responses, disease models and wound healing (Enoch *et al*., 2008). Specifically TE oral mucosa has been used to evaluate the biological effects of biomaterials, responses to infectious or toxic agents and molecular/cellular changes under pathological conditions (Le, 2000). The air-liquid interface (ALI) culture method (Klausner *et al.*, 2007) is routinely used as this approach enables improved structural and functional tissue recapitulation compared with relatively simple monolayer culture (Rosdy and Clauss, 1990).

1.5 Role of scaffolds

A scaffold is defined as an artificial supporting structure used for growing cells into three dimensional tissue structures and ideally should demonstrate porosity and appropriate mechanical stability and integrity. Biodegradability (can be a result of enzyme activity) and is often an important factor of a scaffold as it is preferably resorbed by the surrounding tissues without the need for further surgical intervention (Palsson and Bhatia, 2003). Other properties scaffolds should usually demonstrate include promotion of cell attachment and migration, retention and delivery of biochemical factors and nutrients, and the ability to exert certain mechanical and biological influences which modify cell behaviour (Muschler *et al*., 2004).

The use of different natural and synthetic biodegradable materials as potential scaffolds has been investigated. Thus far promising results have been obtained from the culture of oral mucosal cells on various types of substrate including porcine skin (Xiong *et al*., 2008), human cadaver dermis (Izumi *et al*., 2003; Izumi *et al*., 2000), alginate/fibrin-based materials (Alaminos *et al*., 2007) and collagen-based materials (Luitaud *et al*., 2007).

1.5.1 Collagen scaffolds

Collagen is a naturally occurring protein that constitutes 30 % of all protein in the human body (Lee and Mooney, 2001) and is a major component of ECMs (Alberts *et al*., 2008) of mammalian connective tissues including skin, bones, cartilage, tendons and the vasculature (Orgel *et al*., 2006). Collagen forms triple helical structures of polypeptide chains (Lee *et al*., 2001) packed in microfibrils which can be processed into porous scaffolds in the form of hydrated gels for the encapsulation of cells. Collagen type I, such as rat tail collagen (comprised of triple α-helices), self-assembles under appropriate environmental conditions (Pachence, 1996) to form a fibrillar substrate which is responsible for its mechanical stability.

Collagen hydrogels have been reported to provide a suitable substrates for keratinocytes to form multilayers on and also to prevent epithelial cell invasion and island formation in the sub-epithelial layers (MacCallum and Lillie, 1990). The limitations of collagen gels are their relatively weak mechanical properties (compressive strength) which occur following formation (Roy et al., 2010). While cross-linking collagen with glutaraldehyde can enhance the physical strength of the gels (Lee and Mooney, 2001; Rault et al., 1996) this approach can form toxic and immunogenic components. Notably, scaffolds comprising collagen-chitosan (Ma et al., 2003), collagen-elastin (Hafemann et al., 1999), collagen-glycosaminoglycan (Ojeh et al., 2001) and collagen-glycosaminoglycan-chitosan (CGC) (Black et al., 2005, Vaissiere et al., 2000) were found to be more biologically stable and better suited for tissue engineering of oral epithelium purposes.

1.5.2 PET

PET is a synthetic porous membrane (resin) produced by the combination of ethylene glycol and terephthalic acid monomers. PET is available for laboratory research in the form of cell culture inserts and it has been used previously for the reconstruction of epithelia and tissues *in vitro* (Moharamzadeh *et al*, 2008). In PET culture inserts, cells are nourished from both sides of the surface as a consequence of pores introduced during manufacture. This porosity enables two different chambers to be established in cell cultures above and below the PET membrane (Chambard *et al*., 1983; Guguen-Guillouzo and Guillouzo, 1986; Saunders *et al*., 1993). PET cell culture inserts are also useful for establishing co-cultures, where cells grow in close proximity to another cell population in the same culture environment, but without direct contact between them. These co-cultures are used, for example, to study mesenchymal-epithelial interactions between normal cells as well as in tumour development by enabling

stimulation through paracrine growth factors (Hofland *et al*., 1995; Gache *et al*., 1998). PET cell inserts can also be used to culture cells at the air liquid interface (Ponec *et al*., 1988) to induce keratinocyte stratification *in vitro.*

In addition to porous membranes, PET in the form of nanofibrous scaffolds (Li *et al*, 2002; Yoshimoto *et al*, 2003; Ma *et al*, 2005) has been found to increase cellular attachment, proliferation, and differentiation compared with traditional scaffolds like collagen (Smith *et al, 2008*). Recent studies demonstrated that PET nano-fibres improved fibroblast attachment (Storrie *et al*, 2007) and adsorption of integrin binding protein components of the ECM (fibronectin and laminin) which resulted in increased expression of integrins (Woo *et al*, 2007).

1.5.3 De-epidermalised dermis (DED) as a scaffold

DED can be used as a substrate for keratinocyte growth and is prepared from split thickness skin by the removal of the epidermis and dermal fibroblasts from the dermis (Moharamzadeh *et al.,* 2007). DED has good durability and an ability to retain its structural properties (retain an intact basement membrane after removal of epidermis) (Duncan *et al*., 2005), even following freezing and preservation in glycerol (Krejci *et al.,* 1991; Heck *et al.,* 1985) thereby providing a suitable environment for 3-dimensional cell culture of epithelia. Due to the compatibility of DED with oral mucosa, it has recently been used to engineer human hard palate mucosal epithelium (Cho *et al*., 2000). A recent study on the implantation of oral mucosal substitutes composed of acellular dermis and autologous oral keratinocytes in dogs was however reported as unsuccessful, probably due to insufficient vascularisation after implantation (Ophof *et al*., 2002). There is however one clinical trial of implantation reported which utilised DED tissue engineered oral mucosa which resulted in improved healing (MacNeil *et al.,* 2011).

1.6 Two dimensional (2D) monolayer and three dimensional (3D) organotypic cultures (OCs)

2D monolayer cultures of oral keratinocytes have proved useful in basic biological research. Initially Rheinwald and Green (1975) introduced a method of growing single layer human keratinocytes in *vitro*, using a feeder layer of NIH/3T3 fibroblasts but conventional cell culture techniques in a standard culture medium (Costea *et al*., 2005). The monolayer of fibroblast cells produced a relatively low amount of ECM which facilitated keratinocyte morphogenesis, adhesion and the formation of the complex dermal-epithelial junctions. Subsequently it has been shown that the nature and origin of the underlying fibroblasts influence the phenotype of the overlying epithelium (Locke, 2007; Moharamzadeh, 2007; Lee, 2000).

Organotypic epithelial structures can also be engineered using primary or immortalised keratinocytes (Wan *et al*., 2007; Boelsma *et al*., 1999). OCs of keratinocytes on three dimensional scaffolds at the ALI facilitate the construction of multilayer sheets of epithelium which resemble native epithelium, demonstrating differentiation and BM formation, differential cytokeratin expression and superficial keratinisation (Rosdy and Clauss, 1990). Stratifying squamous epithelia (from skin and mucosa) differ regionally in the suprabasal expression of structural and differentiation markers and in OC systems *in vivo*-like patterns of differentiation can be recapitulated (Igarashi *et al.*, 2003). Several studies have reported successfully generating engineered oral mucosa by culturing oral keratinocytes with or without fibroblasts on collagen (Rouabhia and Deslauriers, 2002; Masuda, 1996), de-epidermalised dermis (DED) (Boelsma *et al.*, 1999) and polyethylene terephthalate (PET) (Moharamzadeh *et al.*, 2008). Different techniques have also been used for OC in the absence of an underlying dermis or connective tissue by using a mitotically inhibited murine 3T3

fibroblasts feeder layer (Rheinwald and Green, 1975). In past research has been performed on effects of high and low calcium in keratinocytes proliferation and differentiation of monolayer cultures. However, H400 and PRKs (tongue source) were never cultured on DED, collagen and PET to generate OCs. Generated organotypic cultures (OCs) have been characterised on the different scaffolds using histological (Costea *et al*., 2005) and immunohistochemical analyses (Zacchi *et al*., 1998) to determine the degree of keratinocyte proliferation and differentiation, in addition transmission electron microscopy (Moharamzadeh *et al*., 2008) has been used to determine ultrastructural features of OCs, including tonofilaments (cytokeratins) and desmosomal junctions. Although detailed microscopic quantitative characterisation in comparison with normal mucosal architecture has not been performed previously.

In the present study a semi-automated quantitative imaging method was applied for architectural characterisation of OCs generated on the three different scaffolds of DED, collagen and PET. This approach enabled determination of the thickness of OCs on a morphological basis. In addition, OCs and normal oral epithelium were compared histologically using immunohistochemical and polymerase chain reaction (PCR) gene expression analyses for structural markers.

Quantitative microscopy approaches enable reproducible and quantitative morphological tissue characterisation and provide significant insights into structure and dynamics at the cell and tissue level (Huang and Murphy, 2004). Quantitative methods based on mathematical morphology (Vila Torres *et al.,* 1994), stereology (Garcia *et al*., 2007; Haug, 1972; Li *et al*., 2009) and image processing principles (Liu *et al.,* 2004) have provided a better understanding of the architectural characteristics of tissue samples compared with subjective visual assessment (Landini and Othman, 2003). Various applications of quantitative microscopy have been used to characterise 2D and 3D morphological

information, including average size, shape, number and the colour intensity of each object in the entire image (Chen and Murphy, 2004; Murphy *et al.*, 2003; Boland and Murphy, 2001). Characterisation of thickness and cell layer analysis in histological sections of a tissue can also be determined using semi-automated quantitative imaging methods. Determination of cell layer level in histological sections of epithelia is based on binary morphological reconstructions which determine the layer level with reference to the outermost or innermost layers of the tissue. Microscopic quantification of architectural organisation can provide a precise description and compartmentalisation of morphological data. Moreover, automated imaging methods also provide an opportunity to analyse large data sets in a short time and at low cost (Landini and Othman, 2002).

1.7 Culture conditions

Various culture media have been used to generate monolayer and OCs. Medium composition plays an important role in optimisation of growth and differentiation of OCs (Costea *et al*., 2005). For OC of keratinocytes, Dulbecco's modified Eagle medium (DMEM) is commonly used but supplemented with several regulators of cell growth and differentiation including epidermal growth factor (EGF), insulin (Neely, 1991), adenine (Cook *et al*, 1995), hydrocortisone (Ponec and Boonstra, 1987), and cholera toxin (Okada *et al*., 1982).

In addition human keratinocytes can be grown in medium containing a reduced concentration of calcium ions (0.1 mM compared with 1.2-1.8 mM in standard medium formulations) (Leigh and Watt, 1995). Notably keratinocytes are prevented from stratifying at low calcium concentrations as desmosomes and intercellular adherens junction do not assemble appropriately. Nonetheless, under these conditions keratinocytes initiate terminal differentiation (Hennings *et al.*, 1980) within the monolayer and on further addition of calcium ions, the differentiating cells migrate to form a suprabasal cell layer (Watt, 1989).

1.8 Cell growth and culture characterisation

Currently there are a variety of analytical approaches available which enable determination of growth kinetics in cell culture systems. The MTT [3-(4, 5-Dimethyl thiazole-2-yl)-2, 5-diphenyl tetrazolium bromide] assay is however one of the most widely used methods and has been used to measure cell proliferation and viability of keratinocytes (Newby *et al*., 2000). This assay is a relatively simple and rapid and can be easily adapted for high-throughput analysis (Mosmann, 1983) and advantages of this approach are its accuracy, reliability and its throughput capacity (Denizot and Lang, 1986). This method has been used to assay cytotoxicity of potential medicinal agents and other toxic materials which may come into contact with the oral mucosa (Klausner *et al*., 2007). The MTT assay was first described by Mosmann (1983) and utilises the activity of a dehydrogenase enzyme active in the mitochondrial respiratory chain to convert a yellow MTT substrate, taken up by living cells, to a purple formazan compound (Molinari *et al*., 2005; Mosmann, 1983). Subsequent spectrophotometric analysis can be used to determine cell numbers and metabolic activity (Klausner *et al*., 2007; Freimoser *et al*., 1999).

1.9 Aims and objectives

The overall aim of this work was to generate and characterise cultures using novel method of quantitative microscopy to enable identification of the most appropriate methods for generating/engineering oral mucosa *in vitro*. This aim was addressed by means of the following objectives:

- Identification of the effects of high and low calcium concentrations on keratinocyte proliferation in monolayer cultures using an immortalised human oral keratinocyte cell line (H400) and primary rat tongue keratinocytes (PRKs).

- Determination of adhesion and structural molecule expression including E-cadherin, plakophilin, desmocollin-3, desmogleins-3 and cytokeratin 1, 4, 5, 6, 10, 13 in low- and high-density H400 monolayer cultures to determine the effect of cell-cell contact using the reverse transcriptase polymerase chain reaction.
- Localisation of structural and differentiation markers including E-cadherin, desmogleins-3, involucrin and cytokeratin 5, 6, 10, 13 in H400 and PRK monolayer cultures to identify structural and maturation proteins of oral epithelium using immunohistochemistry.
- Characterisation of the architectural arrangement of keratinocyte cultures in terms of epithelial thickness and cell layer numbers in 3D H400 and PRK OCs generated on the three different types of scaffold materials including DED, collagen and PET for defined culture periods using image analysis to provide a quantitative comparison with normal oral mucosa.
- Analysis of structural and differentiation markers in 3D OCs epithelium using immunohistochemistry to identify tissue arrangement generated *in vitro*.
- Gene expression analysis of proliferation, structural and differentiation molecule transcripts of 3D OCs using the reverse transcriptase polymerase chain reaction to compare with normal oral epithelium levels.

CHAPTER 2 MATERIALS AND METHODS

2.1 Epithelial tissue isolation

Primary rat keratinocytes (PRKs) were obtained from neonatal albino Wistar rats (1-2 days old) humanely sacrificed by cervical dislocation. Rodent tongues were swabbed with a 5 % solution of iodine (Sigma, UK) in 70 % ethanol to disinfect the tissues and then excised using a disposable scalpel no: 10 (Swann-Morton, UK). Excised samples (1.5x1 cm sections) were stored in 0.25 % trypsin-0.02 % ethylene diamine tetra acetic acid (EDTA) (Invitrogen, UK) overnight at 2 ºC to detach the epithelial layer from the sub-mucosa. PRKs from the dorsal surface of the tongue samples were removed by scraping and vigorous pipetting (Ophof *et al*., 2002) for 5 minutes prior to establishing cultures.

2.2 2D monolayer cell cultures

2.2.1 Primary rat keratinocyte (PRK) culture

PRKs were seeded onto a prepared feeder layer of NIH/3T3 mouse embryonic fibroblast**s** ($8x10^3$ cell/cm^2) (see section **2.2.3**) which had previously been treated with 8 µg/ml mitomycin C (150 µl in 20 ml of solution) (Sigma, UK) to inhibit growth (Rheinwald and Green, 1975; Blacker *et al*., 1987) in 75 cm^2 flasks (Easy flask 75 FILT Nunclon DSI, Denmark) for 2 hours at 37 °C. PRKs with feeder layers (feeder layer enabled keratinocytes to grow in colonies) (Hunt *et al*., 2009; Wan *et al*., 2007) were cultured in 3:1 DMEM high glucose (Biosera, UK): Hams-F12 (Sigma, UK) supplemented with 10 % foetal calf serum (FCS) (Biosera, UK), 10 mM 4-(2-hydroxyethyl) piperazine-1-ethanesulfonic acid (HEPES) buffer (Sigma, UK), 200 mM L-glutamine (Sigma, UK), 0.4 mg/ml hydrocortisone (Sigma, UK), 100U/ml penicillin G, 100 mg/ml streptomycin, 5 mg/ml insulin (Sigma, UK), 10 ng/ml epidermal growth factor (Sigma, UK), 8 ng/ml cholera toxin (Sigma, UK) and 1.25 mg/ml amphotericin B (Sigma, UK).

2.2.2 Immortalised H400 keratinocyte culture

Immortalised H400 keratinocytes, a human oral alveolar cancer cell line was first used by professor Prime *et al* in 1990 at the University of Bristol (Prime *et al*., 1990) were cultured in keratinocyte medium, all sourced as previously described.

2.2.3 Fibroblast culture

The NIH/3T3 a mouse embryonic fibroblast cell line (Todaro and Green, 1963) was used as a feeder layer for PRKs. Cultures were originally maintained in the sources previously described.

All monolayer cell cultures were incubated at 37 ºC in an atmosphere of 5 % CO_2 and 95 % humidity. Medium was changed on day 3 after initial seeding and subsequently changed every 2 days unless otherwise stated (Ophof *et al*., 2002).

2.2.4 Sub-culture of cells

Once cultures had reached 80-90 % confluence in 75 cm^2 cell culture flasks the medium was removed and 4 ml of 0.25 % (w/v) trypsin: 1mM EDTA (Invitrogen, UK) was added to the flask and cultures were incubated at 37 ^oC in 5 % CO_2 for 5-10 minutes to detach the monolayer. Once detached, an equal volume of supplemented DMEM containing 10 % FCS was added to neutralise the trypsin activity. The detached cell suspension was then transferred into a 15 ml universal tube and centrifuged (Eppendorf Centrifuge model 5415D, UK) at 6,000 relative centrifugation force (rcf) for 2 minutes to pellet the cells.

2.3 3D organotypic cultures (OCs)

2.3.1 OCs on de-epidermalised dermis (DED)

Glycerol-preserved skin (Euro Skin Bank, Beverwijk, Netherlands) was washed in distilled water and stored in phosphate buffered saline (PBS) containing 100 U/ml penicillin G, 100 mg/ml streptomycin, at 37 ºC for 10 days. The epidermis was removed by mechanical scraping, using a disposable scalpel no: 10 (Swann-Morton, UK) to produce de-epidermalised dermis (DED) which was further dissected into 2 cm^2 square sections (Wan *et al.*, 2007). In this study, to minimise variation between DED squares, the required samples were sectioned from a single DED sheet. A stainless steel ring of 1 cm^2 internal area with one end bevelled (Duncan *et al*., 2005) was placed on the reticular side of the DED (Livesey *et al*., 1995). This surface of the DED comprised dense irregular connective tissue and vessel channels which were suitable for fibroblast infiltration. 1 ml of a 3T3 fibroblast cell suspension ($5x10^5$ cells/ml, passage 6) was seeded inside the ring and cultured for 24 hours. The ring was removed at this stage and replaced back on the papillary surface. Following this, H400 or PRKs ($1x10^6$ cells/ml) were seeded on the papillary surface (directly over the basal lamina which supports keratinocyte proliferation and migration) (Pins *et al*., 2000) within the ring and grown submerged in standard keratinocyte culture medium for 7 days (Boelsma *et al*., 1999). Keratinocytes on the papillary surface were raised to the air liquid interface (ALI) by lifting the DED on stainless steel meshes and cultured for 3, 5, 7, 10 and 14 days (Figure 2.1 A).

2.3.2 OCs on collagen hydrogels

Collagen hydrogels were synthesised by mixing 6 ml of 4 mg/ml sterile rat collagen type 1 (Invitrogen, UK) in a buffer solution of 0.5 ml of 1N NaOH, 1 ml of PBS and 0.5 ml of

distilled water. This mixture was poured into 24-well plates and incubated at 37 ºC until a firm gel was formed (~2h). Hydrogels were rinsed with standard keratinocyte culture medium prior to cell seeding. PRKs and H400 cells ($1x10^6$ cells/ml seeded) were cultured separately on the collagen hydrogels immersed in medium for 7 days. Cultures were raised to the ALI for up to a further 14 days of culture (Figure 2.1 B) (Costea *et al*., 2003; Igarashi *et al*., 2003).

2.3.3 OCs on polyethylene terephthalate (PET)

PRKs and H400 keratinocytes ($1x10^6$ cells/ml) were cultured on 24-well cell culture inserts, containing polyethylene terephthalate (PET) membranes (Greiner Bio-One, UK) of 0.4 μm pore size while 3T3 fibroblasts were seeded beneath the inserts for 7 days in standard keratinocyte culture medium. Media was subsequently removed from the surface of the insert (while media remained in the well) to enable exposure of the monolayer of cells to the ALI for 14 days (Figure 2.1 C).

All OCs were cultured overall for a maximum of up to 14 days at 37 ºC in an atmosphere of 5 % CO_2 and 95 % relative humidity as initially cells were immersed in culture medium for 7 days on a scaffold which was then raised to the ALI for up to a further 14 days. Medium was changed every 2-3 days. All OC samples were processed for histological evaluation (see section **2.6.4**); immunohistochemical analysis (see section **2.6.4**, **2.6.5**) and RT-PCR analyses (see section **2.10**).

Figure 2.1. **Generation of OCs of H400 and PRKs at air liquid interface for 14 days.** Photographs demonstrating the different approaches used for generation of OCs of H400 and PRKs at ALI for 14 days. **(A)** 2 cm^2 piece of DED was seeded with keratinocytes inside a stainless steel ring and submerged in keratinocyte culture medium for 7 days. Subsequently, keratinocytes on DED were raised to the ALI on stainless steel grids. **(B)** Keratinocytes cultured on collagen for 7 days raised to the ALI using stainless steel grids and **(C)** keratinocytes seeded on PET for 7 days were raised to the ALI by removing media from the surface of the insert.

(A)

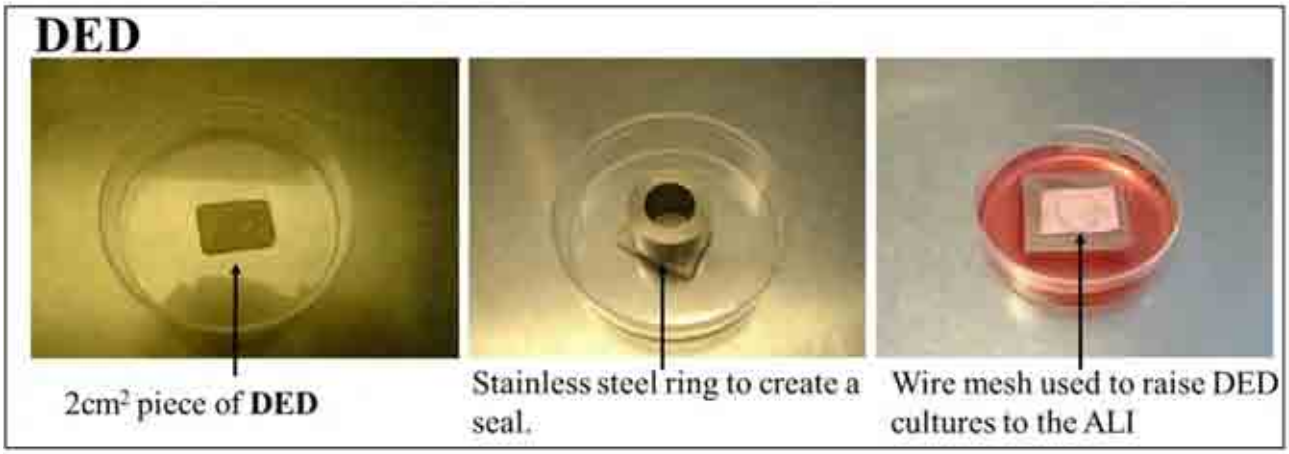
DED
2cm² piece of DED
Stainless steel ring to create a seal.
Wire mesh used to raise DED cultures to the ALI

(B)

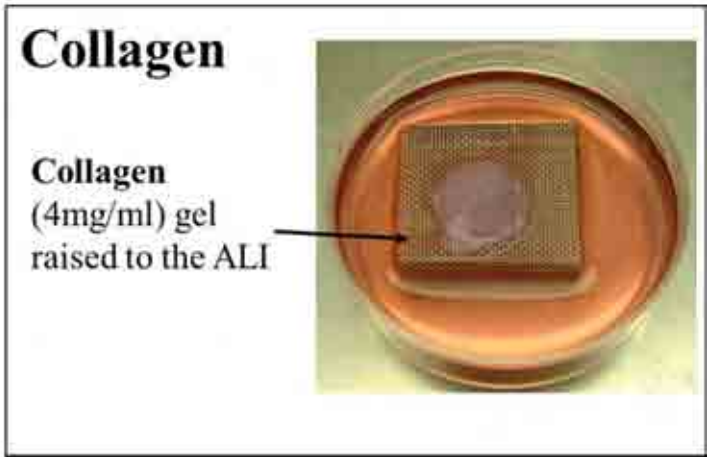
Collagen
Collagen (4mg/ml) gel raised to the ALI

(C)

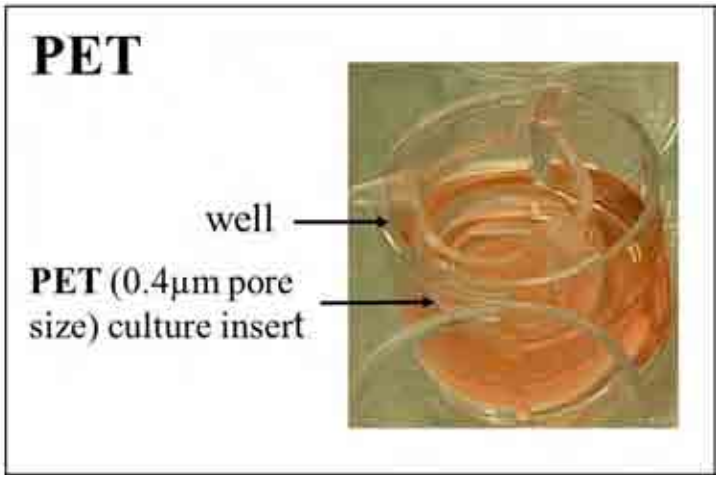
PET
well
PET (0.4µm pore size) culture insert

2.4 Assessment of H400 monolayer cell culture proliferation in high and low calcium containing media

To compare the effects of high and low calcium on PRK and H400 growth, cells were cultured as previously described in high glucose media (DMEM high glucose without calcium chloride) (Biosera, UK) supplemented with either 0.1 mM or 1.8 mM calcium chloride ($CaCl_2$ Sigma, UK).

2.4.1 MTT [3-(4, 5-dimethylthiazol-2-yl)-2, 5-diphenyltetrazolium bromide] assay for cell viability

A stock solution of sterile-filtered 5 mg/ml MTT (Sigma, UK) in DMEM (Biosera, UK) was prepared and stored at 4 °C in darkness to avoid degradation. Cells were initially seeded in 24-well plates at $1x\ 10^3$ in 24-well plates each and cultured for 1, 3, 6, 8, 10 and 12 days in high and low calcium media with four replicates of each condition. Media was removed from wells and cells were washed with PBS prior to addition of 300 µl per well of MTT reagent and incubated for 4 hours at 37 ºC. Subsequently 300 µl lysis buffer solution (0.1 N hydrochloric acid in isopropanol) (Sigma, UK) was added into each well and pipetted carefully to ensure that formazan crystals attached to the surface of the well plate were completely dissolved. The absorbance of the solution in each well was then determined using a multiwell plate reader (ELx 800 Universal Microplate reader, Bio-Tek Instruments, Cole-Parmer, UK) using a wavelength of 570 nm and within 1 hour of completing the assay.

2.4.2 Semi-automated cell counting

Determination of cell numbers and culture area covered using an automated approach utilising light microscopy was investigated. H400 keratinocytes ($0.5x10^3$) were cultured in high and low calcium media on glass coverslips (22 x 22 mm) (Deck gläser, Germany) within

35 mm petri dishes (Sigma, UK) for 4, 6 and 8 days. Monolayer cell cultures were stained with haematoxylin only (H-only) to identify cell nuclei (see section **2.6.4**). Fifteen images of H400 monolayer cell cultures in high and low calcium media at 4, 6 and 8 days each were captured using a digital camera (QImaging Micropublisher 3.3, Canada) attached to an Olympus BX50 microscope (Olympus Optical Co. Ltd, Tokyo, Japan) using a 10x objective (generating images with a field width of 1406.5 μm). The area covered by the cultures was calculated as a percentage of total field area for all culture images using the image intensity at a fixed threshold range (0-225) which was determined experimentally by trial and error using ImageJ (Rasband, 2011). To determine the area of cell coverage in μm^2, the percentage of coverage area was multiplied by the total area of the image (at 10X the captured field of view was 1406.5 x 1054.9 μm) and divided by 100 to obtain values in μm^2. The average area of cells was evaluated by dividing cell coverage area of the image in square micrometres by the total number of cells present in the image.

The total number of cells in the image was estimated by two different methods: i) a manual count and ii) an automated (machine) approach using ImageJ software. Manual counting was performed by selecting the cells' nuclei in H-only images using the ImageJ Point tool. Automated cell counting was achieved using the ImageJ command for identifying regional maxima (or minima if the image greyscale was inverted). Maxima are regions of pixels that are surrounded by strictly lower greyscale values. This procedure can be applied within a "noise" tolerance value to avoid over detection of maxima that are close to the value of the surrounding lower grey values. To determine which operation was closer to the manual cell count, the numbers of cells counted manually were compared with data obtained by the automated cell counting using the maxima approach depending on different noise tolerance values (ranging from 2 to 100 in greyscale units). The maxima approach with noise tolerance

22 showed the best power correlation with manual counts (R^2=0.9636) depicted in Figure 2.2 and therefore this method was used to estimate total number of cells cultured in high and low calcium media.

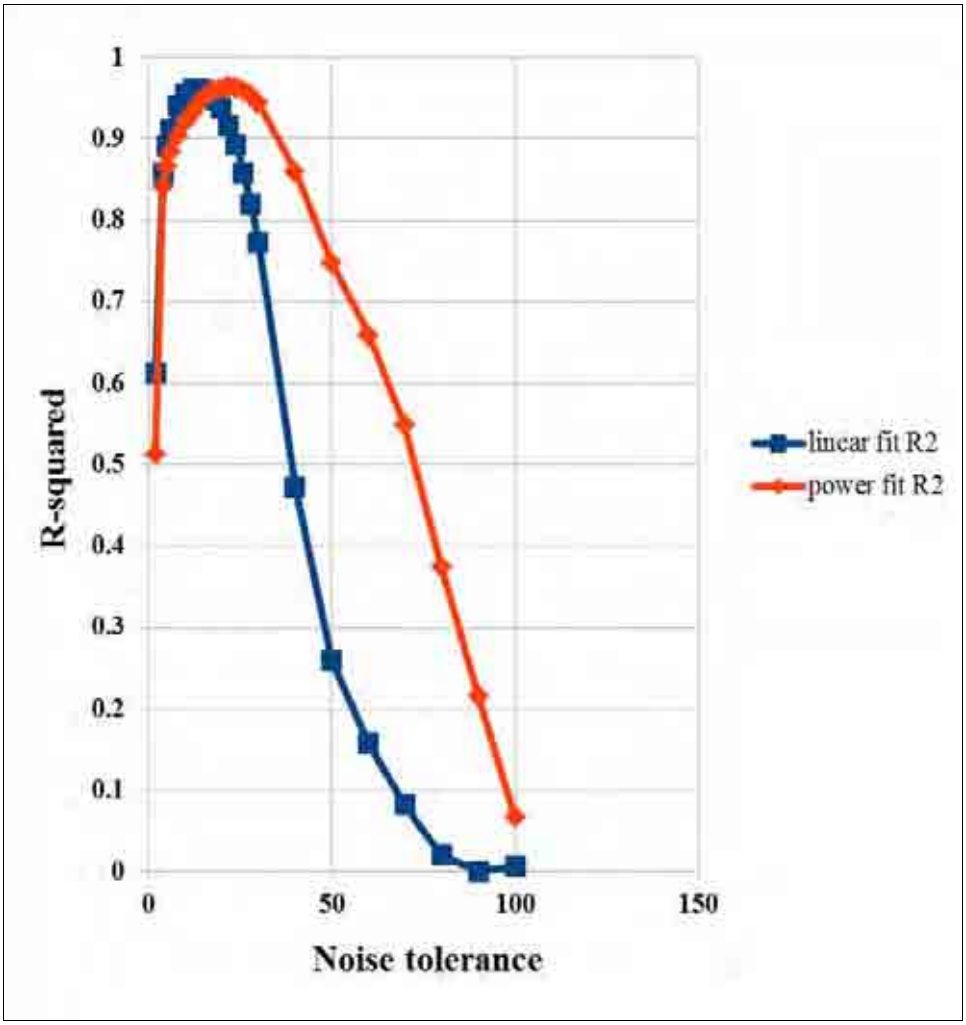

Figure 2.2. **Correlation between manual and machine estimates of cell counting**. Graph demonstrating the relationship between the correlation (R-squared) of the regression (linear in blue, power in red) between manual counting and machine estimates of cell numbers at various noise tolerance settings of the local maxima procedure used to detect the cells. The maxima approach with noise tolerance 22 had the highest power regression (R^2=0.9636).

2.5 Statistical analysis of monolayer cell cultures

Cell numbers within H400 monolayer cultures grown for 4, 6 and 8 days in high and low calcium media were analysed using the univariate general linear model analysis and a Tukey post-hoc test (SPSS V17) (SPSS Inc, USA).

2.6 Histological techniques

2.6.1 Extraction of normal rat oral epithelium

Normal tongue tissue (approximately 1.5x1 cm) from a 6 week old albino Wistar rat was dissected using a disposable surgical scalpel blade no: 10 (Swann-Morton, UK). Dissected specimens were washed in PBS for 2 minutes and fixed in 10 % neutral buffered formalin (Surgipath Europe Ltd, UK) at room temperature for 24 hours.

2.6.2 Fixation of H400 and PRK monolayer cell cultures, OCs and tissue samples

Paraffin sections of adult human gingiva (periodontal surgery waste tissue, School of Dentistry Tissue Bank, UK) and rat tongue tissue were used as positive controls for staining. Human gingiva, rat tongue tissues, H400 and PRK OCs samples were washed in PBS and fixed in 10 % neutral buffered formalin (Surgipath Europe Limited, UK) at room temperature for 24 hours. The tissue samples were trimmed and transferred into labelled cassettes and stored in 70 % industrial methylated spirit IMS 99 (Genta Medicals, UK) until routine tissue processing was performed automatically using a Shandon Citadel 1000 Tissue Processor (ThermoFisher Scientific, UK).

Monolayer cell cultures of NIH/3T3 fibroblasts, H400 and PRKs cultured on glass coverslips (22x22 mm) (Deck gläser, Germany) were fixed in dry acetone for 15 minutes (at room temperature) and air dried for 10 minutes.

2.6.3 Paraffin wax embedding of tissue sections

A thermal and cryo-console (Sakura Tissue–Tek TEC IV Embedding Console System 4714, Netherlands) were used to embed processed wax-impregnated tissue samples and OCs at 60-75 °C. Embedding of tissue in wax was followed by cooling the cassettes immediately over the cryo-console at -5 °C. A rotatory microtome (Leica RM 2035, Leica instruments GmbH, Germany) was used to cut 4-5 µm sections from paraffin embedded tissue blocks using stainless steel disposable microtome blades (S35 or R35) (Feather microtome blades, Japan).

2.6.4 Cell and tissue staining

H400 and PRKs (in high and low calcium media) cultured on glass coverslips for 3, 5 and 7 days were stained manually with haematoxylin only (H-only). NIH/3T3 mouse embryonic fibroblasts cultured on glass coverslips were stained manually with haematoxylin and eosin (H&E). Each glass coverslip was mounted using xylene based mounting media XAM (Merck Ltd, UK). Cells were treated with Gill's III haematoxylin solution (Surgipath Europe Ltd, UK), for 2 minutes and 20 seconds and rinsed in water for 5 minutes. Cells were subsequently treated with 0.3 % acetic acid (Merck Ltd, UK) and 0.3 % hydrochloric acid (Merck Ltd., Genta Medical) for 30 seconds in each solution followed by rinsing in water for 5 minutes. Following Scott's tap water (Surgipath Europe Ltd, UK) substitute treatment for 2 minutes, cells were rinsed with water for 5 minutes and stained with eosin solution (Surgipath Europe Ltd, UK) [(0.5 % alcoholic eosin diluted 1:1 with 100 % industrial methylated spirit 99 (IMS) (Genta Medicals, UK)] for 1 minute. Cells were rinsed in water for 5 minutes and then treated with 100 % industrial methylated spirit 99 (IMS) (Genta Medicals, UK) followed by xylene (Genta Medical, UK) for 2 minutes in each.

Paraffin embedded tissues samples of human gingiva, rat tongue and H400 and PRK OCs were stained with H&E using an automated staining machine (Thermo Shandon Linistain GLX Random Access Stainer, UK) and the reagents as mentioned above.

2.6.5 H400 and PRK monolayer cell culture and paraffin embedded tissue sample immunostaining

Monolayers of H400 and PRKs cultured on glass coverslips and paraffin embedded tissue sections of human gingiva, rat tongue and 14 day OCs of H400 and PRKs were used for IHC analysis. Five µm paraffin sections of tissue samples were mounted on Menzel-Glaser Suprafrost Plus glass slides (Thermo Fisher, UK), deparaffinised in two changes of xylene for 3 minutes each and rehydrated in graded ethanol (100 %, 95 % and 70 % for 2 minutes each). Tissue sections were pre-digested with trypsin or pre-heated in 0.01M citrate buffer pH 6.0 (2 minutes) at 97 ºC in a commercial microwave oven (Sharp Easy Chef II, 850W; maximum setting) for 50 minutes (5x10 minutes periods) to unmask antigenic sites. Slides were then placed in a plastic horizontal slide carrier in a plastic beaker, with a loose fitting lid, containing anti-bumping granules and sufficient citrate buffer (1.1L for 50 minutes) to keep the sections constantly submerged during the entire boiling period.

Tissue sections were blocked for endogenous peroxidase using 3 % H_2O_2 in PBS for 10 minutes to reduce background staining followed by blocking of non-specific sites of the tissue samples using goat serum. After incubation with the primary antibodies (see Table 2.1) the sections were stained with the avidin-biotin-peroxidase complex system (Str AviGen Biogenex, USA). Bound peroxidase was visualised using 3, 3-diaminobenzidine reagent (DAB) (Sigma, UK) and tissue sections were counterstained with Mayer's haematoxylin.

Table 2.1. Details of primary antibodies used in immunohistochemical analysis.

Primary antibody	Reactive species	Isotype	Clone	Concentration used	Antigen retrieval method
Anti-cadherin (mouse monoclonal)	human,	IgG1	HECAD-1	1:200	Microwave incubation
Anti-cadherin (rabbit monoclonal)	Human, rat , mouse	IgG	[EP913(2)Y]	1:200	Microwave incubation
Anti-desmoglein (mouse monoclonal)	human, rat	IgG1	3G133	1:400	Trypsin
Anti-involucrin (mouse monoclonal)	human	IgG1	SY5	1:800	Trypsin
Anti-cytokeratin 1 (rabbit polyclonal)	human, rat, mouse	IgG	ab93652	1:200	Trypsin
Anti-cytokeratin 10 (mouse monoclonal)	human, rat, dog	IgG1	DE-K10	1:200	Trypsin
Anti-cytokeratin 13 (mouse monoclonal)	human, mouse, rat	IgG	AE8	1:200	Trypsin
Anti-cytokeratin 5, 6 (mouse monoclonal)	human, mouse, rabbit	IgG1	D5/16B4	1:400	Trypsin
Anti-Ki67 (rabbit polyclonal)	human, mouse, rat	IgG	ab66155	1:1000	Microwave incubation
Anti-collagen IV (mouse monoclonal)	human	IgG1	CIV22	1:50	Microwave incubation
Anti-laminin-5 (mouse monoclonal)	human	IgG1	P3H9-2	1:200	Trypsin
Pan-cytokeratin (mouse monoclonal)	human, rat	IgG1	MNF116	1:200	Trypsin
Mouse IgG1 (mouse monoclonal)	no reaction with any antigen	IgG1	NCM1	1:200	Trypsin

Supplier of primary antibodies was Abcam Cambridge, UK except anti-cytokeratin-5, -6, collagen IV and pan-cytokeratin which were from DAKO, UK.

All antibodies and reagent dilutions were optimised on positive control samples and washes were performed in 0.01 M PBS (pH 7.6). Immunohistochemical analysis for each protein was performed with positive and negative controls to ensure comparability.

2.7 Microscopy

2.7.1 Light microscopy

A total of 90 images (15 images each for H400 monolayer cell cultures in high and low calcium media at 4, 6 and 8 days of culture) were analysed (see section **2.4.2**). A selection of 8 images per group of OCs on DED, collagen, PET and tissue samples of human gingiva and rat tongue stained with H&E were captured using the same microscopy set-up but with a 40x objective which provided a field width of 353.7 µm.

All images were corrected for uneven background illumination and saved in TIFF format. Before correcting the background illumination, the camera white balance function was applied to the illuminated bright field (without a specimen) to compensate for light temperature colour. With the specimen on the microsope stage, the camera brightness control was manually adjusted to guarantee that the pixel distribution in the dark and bright extremes of the histogram was not saturated. Each pixel represented a separate shade of grayscale and the value ranged from dark (0) to light (255) for a full 8 bit scale (2^8=256).

To correct for uneven background illumination, a darkfield image (with the light source blocked) was captured to compensate for the so-called "hot pixels" that output non-zero signal values when there is no incident light on the camera sensor. Following this, a brightfield image was captured by opening the light path and removing the specimen from the microscope. The correction operation on subsequent (specimen) images was performed by calculating the transmittance through the sample. Transmittance is the ratio of light

transmitted through the sample (specimen image) and the light illuminating the sample (brightfield image) and values vary from 0.0 (no light is transmitted) to 1.0 (all light that illuminates the specimen passes through it). This value is subsequently rescaled to span the whole greyscale space of the image storing format (i.e. multiplied by 255 below):

Corrected_image = [(specimen - darkfield) / (background - darkfield)] x 255. At the same time, the offset of the hot pixels is removed by subtraction of the darkfield image from the specimen and background images.

The epithelial compartment of the various organotypic cultures in the H&E stained sections was segmented using a semi-automated method of object extraction called "Simple Interactive Object Extraction" SIOX, (see section **2.8.1**) (Friedland, 2007) which runs under Fiji (http://fiji.sc/). Fiji is software which combines the open source image processing application ImageJ together with a selection of pre-installed plug-ins (Schmid *et al*., 2010). The SIOX method is based on the optical density of the image (in this case histological staining) which is used here to help separating the epithelium from the remainder of the scaffold, followed by histogram thresholding to produce a binary image.

2.7.2 Scanning electron microscopy (SEM)

SEM was used to visualise the features of scaffolds used for cell culture. Samples were fixed in 10 % paraformaldehyde (PFA) overnight, rinsed in PBS for at least 20 minutes and dehydrated through graded solutions of ethanol (Sigma, UK) in distilled water (20 %, 30 %, 40 %, 50 %, 60 %, 70 %, 90 %, 95 %, 100 % for at least 10 minutes each). Samples were then critically point dried from CO_2 in a Bio-Rad E3000 (Polaron, UK) chamber. All dried samples were mounted on 25 mm aluminium stubs (Agar Scientific, UK) using silver in isobutyl methyl ketone (Agar Scientific, UK) and sputter coated with gold (Denton Vacuum

Desk II, USA) for 90 seconds with 30 mA current. Samples were examined using a JEOL JSM-840 SEM (SEMTech Solutions, USA) at an accelerating voltage of 25 kV.

2.8 Image analysis of 3D OCs

2.8.1 Object extraction using the SIOX algorithm

The SIOX procedure (Friedland, 2007) extracts (segments) objects from a colour image based on the concept that foreground objects are comparatively different from the background. In the algorithm, 'foreground' is a set of spatially connected pixels that are of interest to the user while the rest of the image is considered to be 'background'. The user manually selects regions which are known or typical back- and foreground and the algorithm then finds the extent of the two classes of region. These selections can be specified with the mouse to refine the final region of interest (ROI). The robustness of the segmentation relies on the identification of the two classes of regions. The specified ROIs are mapped into a confidence matrix termed 'trimap' to classify the rest of the regions which have not been included in the selections. The 'confidence matrix' is a matrix of the same dimensions as the image specified by the user. Each element of the matrix contains a point number in the interval of 0-1. A value of 0 means known background, a value of 1 represents known foreground whilst 0.5 express unclassified elements. The algorithm generates colour signatures for foreground and background and classifies all image pixels as either foreground or background in the confidence matrix which results in a new output matrix. The algorithm filters out noise using different operations such as erosion, dilation and blurring on the matrix and closes holes up to a specific size, if required. Finally the regions with high values in the confidence matrix are extracted to create a binary image.

2.8.2 Analysis of epithelial thickness in 3D OCs

The thickness of the epithelium in the OC was measured from the binary images (Figure 2.3 A) segmented using SIOX as described above followed by a macro procedure running under ImageJ which measured (using Pythagoras theorem) all possible distances between all points in the bottom (basal) boundary B of the binary image of the epithelium (i.e. the basal boundary) to all points on the surface boundary S.

For an arbitrary point (PB) in B, the thickness of the tissue relative to P_B is given by the shortest distance $D_{min}(P_B,S)$ (that is the minimun distance from P_B to any other point in S). This is repeated for all points in B, therefore the sample's minimum thickness is calculated as the minimum value of the set of 'minimum distances' from B to S. Likewise, the maximum tissue thickness from B to S, is given by the maximum value of the set of 'minimum distances' in D. This approach allows for two maximum thickness values, one measured from B to S and the other from S to B. This is because the set of minimum distances is not symmetrical; the shortest distance from a specific point in S to any point in B does not necessarily coincide with the distance from that point in B to any point in S, unless the set of points define the minimum tissue thickness. In Figure 2.3 B the set of shortest distances from the bottom to the surface is shown as orange lines, while in Figure 2.3 C is shown the set of shortest distances from the surface to the bottom. The longest and shortest lines in these sets are shown in black and highlighted with black (maximum thickness) and red arrows (minimum thickness). Note that the maximum thickness measured from one and the other surface does not necessarily match.

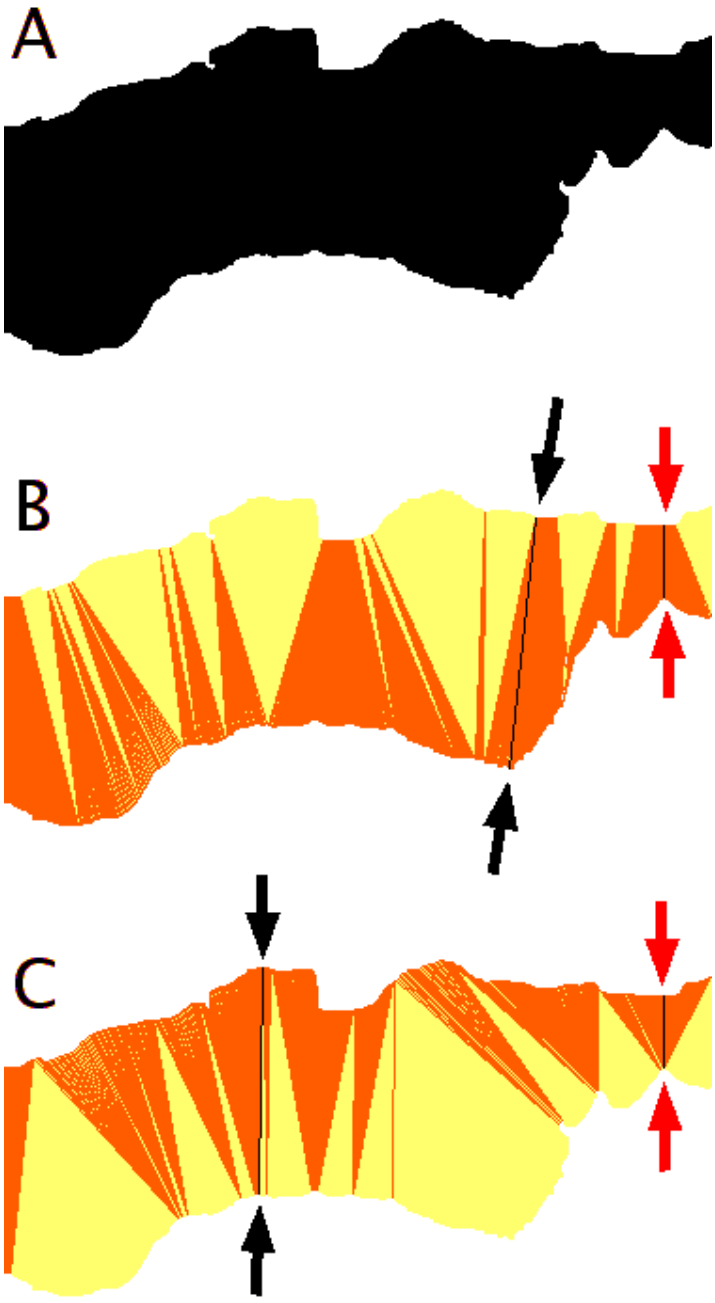

Figure 2.3. **Diagrammatic representation of the steps used to measure the thickness of 14 day OCs. (A)** Binary image of OC, the orange lines represent **(B)** the set of shortest distances from the bottom of the image to the surface and **(C)** the set of shortest distances from the surface to the bottom of the image. The maximum distance in these sets are shown with black arrows and the shortest distances in red arrows.

2.8.3 Analysis of layers in 3D OCs

A total of 128 images were captured at 40x magnification (field width 353.7 µm) and were used for subsequent analysis. Images (8 per group) comprised OCs of H400 or PRK cells grown on DED (for 3, 5, 7, 10 and 14 days), collagen (14 days) and PET (14 days). In addition, rat dorsal tongue mucosa and human gingiva samples were also processed for comparative purposes.

2D or virtual cells (V-cells) are theoretical cells, constructed based on the intensity of the haematoxylin stain of the cell nucleus to generate "seeds" that are subsequently used for partitioning the epithelial profile into non-overlapping discrete areas. This approach has been used before in the analysis the architectural features of normal as well as pathological epithelia for example those of carcinomas (Landini and Othman, 2003), pseudotumours (Abu-Eid and Landini, 2006) and cysts (Landini, 2006).

H&E stained images (Figure 2.4 A) were processed using a colour deconvolution algorithm (Ruifrok and Johnston, 2001) which separated the colour image into (H)-only and eosin-only (E)-only components. The H-only image (Figure 2.4 B) contained mostly nuclear staining and was used to produce the nuclear seeds by means of smoothing (to eliminate non-nuclear features) followed by a morphological reconstruction of the nuclear regions. A process called morphological domes (Landini and Othman, 2003) extracted the darkest regions of pixels corresponding with the nuclei (seeds). The epithelium of OCs was compartmentalised using the SIOX procedure (Figure 2.4 C) and the seeds of watershed segmentation (Vincent, 1993) were used to partition the epithelial compartment into the V-cells (Figure 2.4 D). Once the V-cells were segmented, the layer analysis could be automated using a procedure based on a sequence of binary reconstructions of the V-cells (Figure 2.4 E) which has been described elsewhere (Abu-Eid and Landini, 2006; Landini and Othman, 2004;

Landini and Othman, 2003). In this procedure, the first layer of cells (the basal cell layer) was the set of cells in the epithelial compartment that were adjacent to the empty space below (which was occupied by the lamina propria). The second layer comprised those cells adjacent to the first layer, and so on, until all cells in the image were labelled (Figure 2.4 F). This type of analysis assumes that the section of the epithelium is imaged completely in its full thickness with the free surface orientated towards the upper image border. A summarising flow diagram of the sequence of computerised processing of H&E image for architectural characterisation of OCs is shown in Figure 2.5.

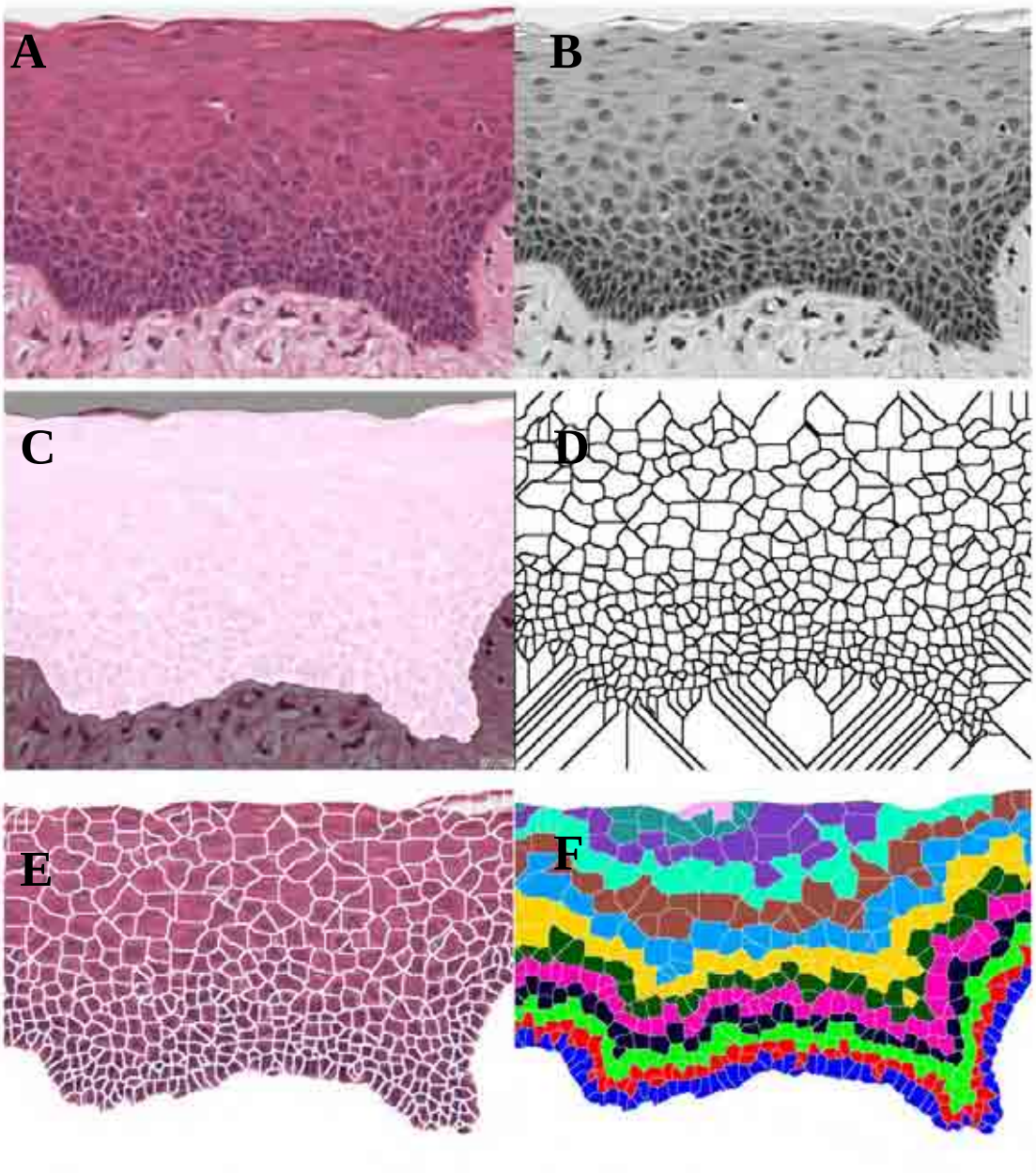

Figure 2.4. **Process sequence of binary reconstructions of V-cells**. Images showing steps in the process sequence of binary reconstructions of V-cells from **(A)** the original image, **(B)** the haematoxylin-only image, **(C)** the epithelial compartment as obtained using the SIOX procedure, **(D)** the watershed partitioning and **(E)** the corresponding results logically combined with the original image. The thickness of the boundaries between the V-cells has been exaggerated for display purposes. In **(F)** are shown the different layers labelled in colours starting from the basal layer (in blue).

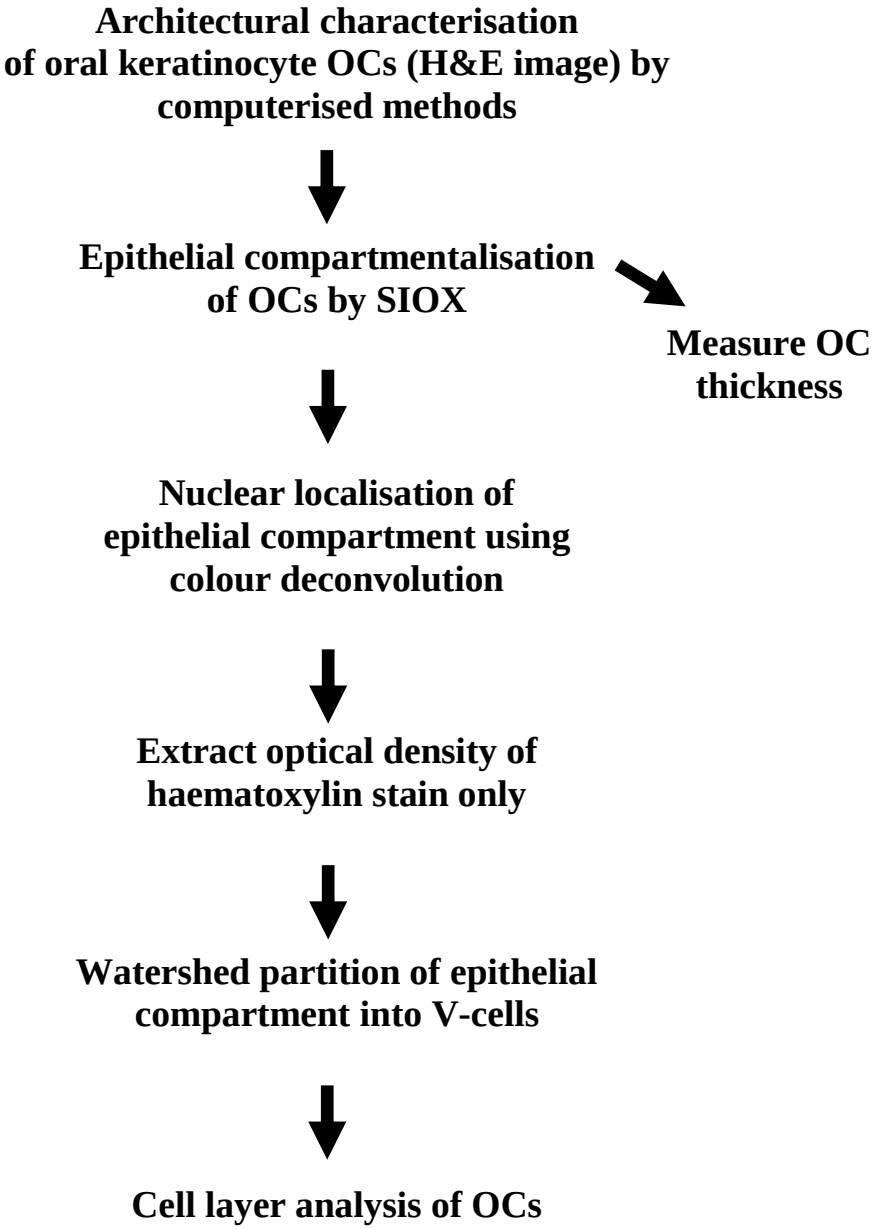

Figure 2.5. Flow diagram providing the sequence for the computerised analysis of H&E images to architecturally characterise OCs.

2.9 Statistical analysis of 3D OC parameters

Statistical significance ($p<0.0001$) of OC thickness differences between the test groups was determined with confidence interval of 95 % using the multivariate general linear model (SPSS V17) (SPSS Inc, USA).

Organising the data by culture days, a multivariate general linear model analysis of the number of layers and number of V-cells per field was performed using the scaffold material (DED, collagen or PET) and the cell type (H400 or PRK) splitting the data output according to the culture times. In the histological sections produced, it was possible to estimate the departure from an absolute transverse section plane perpendicular to the surface of the sample. Given that the PET thickness was constant, three linear measurements of the sectioned PET were performed on each section and a relative correction factor was derived from the ratio of the thinnest PET section and the average of the three measurements per section. This factor corrected the epithelial thickness of all the PET samples data. Unfortunately this kind of correction could not be performed in the other preparations due to the lack of internal reference.

2.10 Ribonucleic acid (RNA) extraction

RNA was extracted from H400 and PRK 2D monolayer cell cultures, 3D OCs on DED, collagen and PET and control human and rat tissue using the Total RNA Isolation System (SV Total RNA Isolation System Promega Corporation, UK) according to the manufacturer's instructions. From cultures, the medium was removed from 25 cm^2 flasks and cells (monolayers) were lysed *in situ* using 175 µl RNA lysis buffer (Promega, UK). Following this 350 µl RNA dilution buffer (Promega, UK) was added in the lysate. For 3D OCs and tissue, samples were homogenised (Ultra-Turrax, Fisher, UK) in 450 µl in RNA

lysis buffer (Promega, UK) and mixed with 900 µl in RNA dilution buffer (Promega, UK). The tubes containing lysates were heated to 70 ºC for 3 minutes followed by cooling at 2-8 ºC and the suspension was centrifuged (Eppendorf Centrifuge, UK) at 10,000 rcf for 10 minutes to pellet debris and tissue remnants. The purified lysate was removed from the pellet debris and samples were transferred onto the spin basket membrane assembly. To enable the binding of RNA to the spin basket membrane, 200 µl 95 % ethanol was mixed in the suspension and centrifuged at 10,000 rcf for 3 minutes. The effluent remaining after centrifugation was discarded and 600 µl RNA wash solution was added to the spin basket membrane. This combination was centrifuged for 1 minute and the final effluent was discarded. To remove contaminating DNA, a fresh DNase incubation mixture of 40 µl yellow buffer solution, 5 µl (0.09 M) manganese chloride and 5 µl DNase I enzyme was prepared. The resultant 50 µl solution was added to the RNA bound to the spin basket membrane and incubated at room temperature for 15 minutes to digest any remaining DNA. To halt the DNase reaction 200 µl DNase stop solution was added to the mixture and centrifuged at 6,000 rcf for 1 minute. DNA-free RNA was eluted in a final volume of 30 µl sterile water (Milward *et al*., 2007).

2.10.1 Complementary de-oxyribonucleic acid (cDNA) synthesis

Following RNA quantification (see section **2.10.4**) cDNA was synthesised by reverse transcribing the isolated RNA, with the reverse transcriptase as a catalyst, and using the Omniscript reverse transcriptase kit (Qiagen, UK). Conditions used were as recommended by the manufacturer. Each reverse transcription reaction was seeded with 1-2 µg of total RNA, combined with 2 µl 10 µM oligo (dT) primer (Ambion, UK) in 0.2 ml PCR tubes (Appleton Woods, UK) to give a final concentration of 1 µM before adjusting the reaction volume to 12 µl by the addition of RNase-free water (Qiagen, UK). The samples were incubated at 80 °C in a UBD1 heat block (Grant Instruments, UK) for 10 minutes and quenched on ice for a further

5 minutes to denature and remove any secondary structure of the RNA which may inhibit the reverse transcription process. Following incubation, 2.0 µl 10xRT Buffer, 2.0 µl 5 mM dNTP mix, 1 µl 10 U/µl RNase inhibitor [diluted to a final concentration of 10 U/µl in 1xRT buffer (Promega, UK)] and 1 µl Omniscript reverse transcriptase were added and mixed in each reverse transcription reaction. To synthesise cDNA the final 20 µl volume reaction mix was incubated for 60 minutes at 37 ºC in a UBD1 heat block (Great Instruments, UK) followed by cooling on ice for 5 minutes. Finally, this reaction mix was incubated for 5 minutes at 93 ºC to inactivate the reverse transcriptase enzyme and rapidly quenched on ice for 5 minutes to minimise cDNA secondary structure formation.

2.10.2 Purification of cDNA

To purify samples of cDNA a micron YM-30 centrifugal filter (Millipore, UK) was used. This purification removes contaminants such as excessive salts, primers, dNTPs, enzymes and remnants of the reverse transcription reaction from the cDNA molecules which may inhibit the subsequent PCR amplification. cDNA was washed twice with 500 µl RNase free water in a Micro tube with centrifugation at 10,000 rcf for 7 minutes to purify and concentrated the cDNA. To collect the cDNA in fresh collecting tubes, the centrifugal filter was inverted into fresh tubes and centrifuged at 1,000 rcf for 3 minutes.

2.10.3 Quantification of nucleic acids

Spectrophotometric analysis was used to determine the concentration of extracted RNA and cDNA in the solution. Once RNA and cDNA were extracted and purified their concentrations were determined using the Biophotometer (Eppendorf, UK) with absorbance values at 260 nm (A_{260}) and 280 nm (A_{280}). 2 µl of stock solution were diluted with 68 µl RNase free water in a Uvette (cuvette) (Eppendorf, UK) and analysed at an absorbance of 260

nm to determine the concentrations of the total RNA and cDNA. Sample concentration (mg/ml) was derived by taking an average value from three dilution factor standards. An absorbance of 1 unit at 260 nm represents approximately 40 µg RNA per ml (A_{260} =1=40 µg/ml) and 50 µg single standard DNA per ml (A_{280} =1=50 µg/ml). The ratio between the A_{260} and A_{280} reading provided an estimate of sample purity with a ratio between 1.8 to 2.1 signifying high purity of the isolated RNA. RNA integrity was also confirmed by visual inspection of samples electrophoresed on 1 % non-denaturing agarose gels stained with SYBR Gold (1:100 in 1x TAE) (Molecular Probes, UK) (see section **2.10.6**).

2.10.4 Semi-quantitative reverse transcriptase-polymerase chain reaction (Sq-RT-PCR)

Sq-RT-PCR assays were performed using the Red Taq PCR system (Sigma, UK). For gene expression analyses, 12.5 µl Red Taq ready reaction mix, 10.5 µl dH_20, 1 µl 25 µM forward and reverse primer (Tables 2a, 2b). Amplification for all the reactions was achieved at 40 cycles except for glyceraldehyde-3-phosphate dehydrogenase (GAPDH) (28 cycles), using a Thermal Cycler (Master Gradient, Eppendorf). The initial denaturation step lasted for 5 minutes at 94 ºC, followed by an amplification cycle consisting of 94 ºC for 20 seconds, 65 ºC for 20 seconds and 72 ºC for 20 seconds ending with a 10 minutes extension at 72 ºC. Following the designated number of cycles, 6 µl of the reaction was removed and the product was visualised on a 1.5 % agarose gel (see section **2.10.6**).

2.10.5 Agarose gel electrophoresis

Agarose powder (molecular grade, Helen Biosciences, UK) was added to 1xTris Acetate EDTA (TAE) (Bioline, UK) buffer at pH 8.3 at a concentration of 1 % (w/v). The mixture (in a conical flask) was heated in microwave oven (Samsung TDS, M1714, Korea) on maximum power (850 W) for 4-5 minutes until the agarose was completely dissolved. The

mixture was cooled to 50-60 ºC under tap water, with constant agitation to prevent uneven solidification of the gel. To enable visualisation of the products under ultraviolet illumination, 0.5 µg/ml ethidium bromide (Sigma, UK) or SYBR Gold (1:100 in 1x TAE) was added to the cooled gel mixture which was then poured into an appropriate sized gel tray (after sealing its border with autoclave tape) and combs were placed in position to form sample loading wells. After solidification at room temperature the gel was transferred into an electrophoresis tank and submerged in 1x TAE running buffer. Samples along with DNA marker (Hyperladder IV, Bioline, UK) were loaded into the wells and electrophoresis was performed at 50-100 V until the Bromophenol blue dye (Sigma, UK) had migrated approximately half to three quarters of the length of the gel.

2.10.6 Image analysis of RT-PCR gels

Following electrophoresis, the sq-RT-PCR gel was subsequently transferred onto the G: Box Chemi HR16 (Syngene, Cambridge, UK) where gels were scanned and images captured before analysis using Gene Tools software (Syngene Cambridge, UK). A rectangular area of equal size was outlined around the PCR product for each sample which enabled the volume density of the amplified products to be obtained. Prior to comparison of relative expression levels between samples, volume density values for each sample were normalised to their respective amplified GAPDH house-keeping gene volume density, which were used as controls. Normalisation was achieved by dividing the obtained sample volume density for each assay by the respective GAPDH volume density values. Normalised expression levels for each sample were then expressed as either a percentage or as relative expression levels of the highest normalised volume density obtained. Each gene analysis was performed in duplicate.

Table 2.2 a. Details of human primer sequences and semi-quantitative RT-PCR conditions.

Gene / Gene symbol	Primer sequence	Product (bp)	T_m °C	GenBank accession number
Glyceraldehyde 3-phosphate dehydrogenase / GAPDH	F-CTAGACGGCAGGTCAGGTCC R-CACCCATGGCAAATTCCATG	597	60°C	NM_0020463
E-Cadherin /HECAD	F-CAAGTGCCTGCTTTTGATGAR R-GCTTGAACTGCCGAAAAATC	339	60°C	NM_004360
Desmoglein-3 / DSG3	F-CACCCTTTTGCCCATAGAAA R-AAGATGGGCATTGAAAGC	391	60°C	NM_001944
Plakophilin 1 / PLP	F-CCCTTCCCCTTAGCACTACC R-TAGTGTGAGGCCAATGTG	345	60°C	NM_001005337
Peripherin / PRPH	F-ACATCGAGATCGCCACCTAC R-ATGCAGACGGAGACGAGACA	336	60°C	NM_006262
Involucrin / IVL	F-GAACAGCAGGAAAAGCACCT R-TAGCGGACCCGAAATAAGTG	332	60°C	NM_005547XM_001130659
Cytokeratin -1 / CK1	F-TGGCAAGACCGAGGTCGATT R-TGTGGGTGGTGGTCACTGCT	392	60°C	NM_0061521.2
Cytokeratin-5 / CK5	F-CCAAGCCAATTGCAGAACCA R-AAATTTGGGATTGGGGTGGG	198	60°C	NM_000424.2
Cytokeratin-6 / CK6	F-GTCCTCAGGCCCCTCTCTGG R-CCCCTGGCAATTTTCTGCAA	317	60°C	NM_005554
Cytokeratin-10 / CK10	F-CCGTGGGCGAGTCTTCATCT R- AGACTTTGTTTTCCATGCATCT	208	60°C	NM_000421.2
Cytokeratin-13 / CK13	F-TCTAATGCCTCTGGTCGCCG R-AGGGCCCACCATCAGGAGAG	197	60°C	X52426.1
Ki67	F-GCCCGGGGACGTAGCCTGTA R-ACCGTCGACCCCGCTCCTTT	385	60°C	NM_002417.3

Table 2.2 b. Details of rat primer sequences and semi-quantitative RT-PCR conditions.

Gene / Gene symbol	Primer sequence	Product (bp)	T_m °C	GenBank accession number
Glyceraldehyde 3-phosphate dehydrogenase / GAPDH	F- CGATCCCGCTAACATCAAAT R-GGATGCAGGGATGATGTTCT	391	60°C	NM_017008
E-Cadherin /HECAD	F- TTCTCCGCGCTCCTGCTCCT R- TTGTCAGCTCCTGGGCCGGT	587	60°C	AB017696
Desmoglein-3	F - ATCCGTGAGGAGTCAACCTG R -CCCGTAGCTCCTCCTAGCTT	371	60°C	XM_001054333
Involucrin / IVL	F - AAGTCCCCAGAGCCAGAACT R - TGTGAGTCATCCAGCTCCTG	308	60°C	NM_022195
Cytokeratin -1 / CK1	F - CCCACCACACCATTAGCTCT R - GCGCTCCGTAAAAGACACTC	369	60°C	NM_001008802
Cytokeratin-5 / CK5	F- AGTGTGCCAACCTCCAGAAT R - AGCCATAGCCAATGTTGCTT	318	60°C	NM_183333
Cytokeratin-6 / CK6	F- GGTGGCTCCCGTGCAGTGTG R- AGGTCAGGCCTCCTGGTGAGC	439	60°C	XR_008355.1
Cytokeratin-10 / CK10	F - TCACCACAGAAATCGACAGC R - GGGTTATTTGCAGGTTTCCA	360	60°C	NM_001008804
Cytokeratin-13 / CK13	F - CCACGAAGAGGAGATGAAGG R - TCCGTCTCTGCCAAGGTACT	333	60°C	NM_001004021
Ki67	F - TGTCACCTGAGCCAGTGAAG R - TGGGGAATCTCAGTCTGTCC	355	53°C	XM_225460.5

T_m=Annealing temperature (°C); bp=base pairs; (F) =Forward primer; (R) = Reverse primer. All DNA primers were manufactured by Invitrogen.

CHAPTER 3 RESULTS

(MONOLAYER CELL CULTURES)

This chapter reports on characterisation of H400 and PRK monolayer cultures in high and low calcium to determine the effects of calcium on cell proliferation using MTT assay and semi-automated image analysis (see section 2.41, 2.42). Moreover, degree of differentiation of keratinocytes at different culture periods and in high and low calcium media was also investigated in this chapter. Semi-quantitative RT-PCR data (see section 2.10.4) and IHC profile (see section 2.6.5) enabled to evaluate the gene expressions and markers of oral keratinocytes proliferation and differentiation.

3.1 Characterisation of monolayer cell cultures

H&E stained NIH/3T3 fibroblasts (Figure 3.1 A), H-only stained H400 (Figure 3.1 B) and PRK (Figure 3.1 C) cultures enabled characterisation of different stages of cell growth using light microscopy. NIH/3T3 fibroblasts appeared stellate, with multiple nucleoli whereas H400 keratinocytes and PRKs exhibited a more polygonal morphology. H-only histological images were used for automated cell counting (see section 3.3) of monolayer cell cultures in high and low calcium media over a range of culture periods.

3.2 Analysis of keratinocyte growth in high and low calcium media

Figure 3.2A shows that using the MTT assay the number of H400 cultured in low calcium medium was statistically higher than those cultured in high calcium medium for 6, 8, 10 and 12 days of culture as determined using the T-test statistical analysis. Similarly, PRK cell numbers were significantly higher in low calcium medium compared with high calcium medium at 4, 6, 8, 10 and 12 days of culture (Figure 3.2 B) using the T-test statistical analysis.

3.3 Semi-automated cell counting in high and low calcium media

The percentage of area coverage of H400 in high calcium at day 4 was 25 % which was increased to 79 % at day 6 and slightly reduced down to 75 % at day 8. The coverage area of H400 in low calcium was increased constantly as 37 %, 93 % and 99 % at day 4, 6 and 8 respectively (Figure 3.5). Data in Figure 3.6 shows the average area of a single H400 keratinocyte computed from the total coverage area divided by the number of counted cells in high calcium medium at day 4 was 1138 μm^2 which slightly reduced (not significantly) to 1087 μm^2 and 902 μm^2 at day 6 and day 8 of culture, respectively. In the low calcium medium, the single cell area was 1235 μm^2 which increased to 1411 μm^2 at day 6 and then reduced down to 1090 μm^2 at day 8 of cultures. The average cell area (H400) in low calcium was significantly different ($P<0.0001$) at 4, 6 and 8 days of cultures.

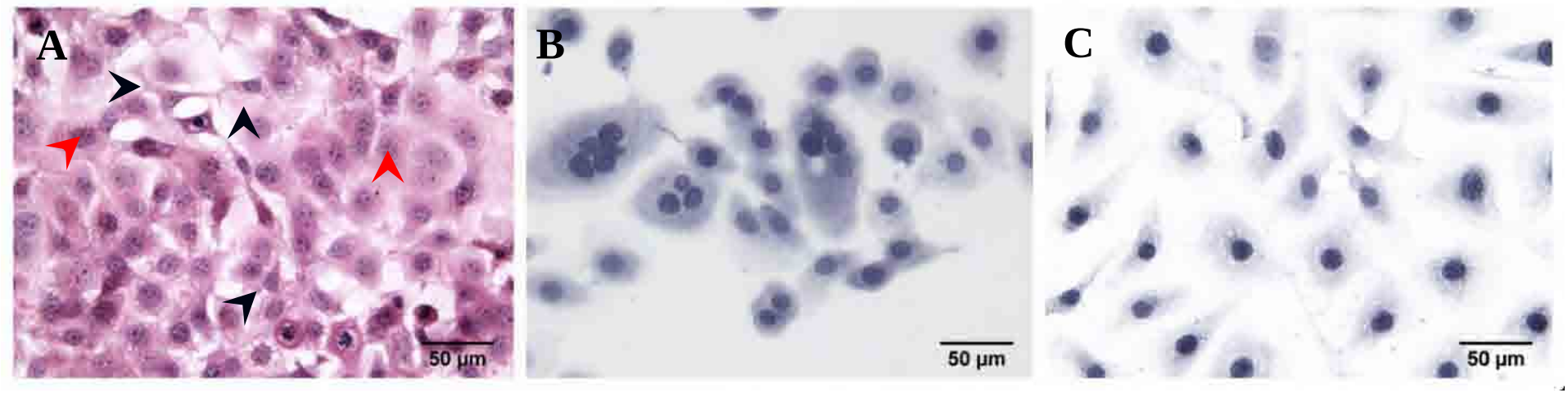

Figure 3.1. **Light photomicrographs of H400, PRK & NIH/3T3 monolayer cell cultures**. Monolayer cell cultures (A) stellate (black arrow heads) NIH/3T3 fibroblasts with multiple nucleoli (red arrow heads) (H&E stained) and (B) rounded H400 (H-only staining) and (C) PRKs (rounded) (H-only staining).

(A)

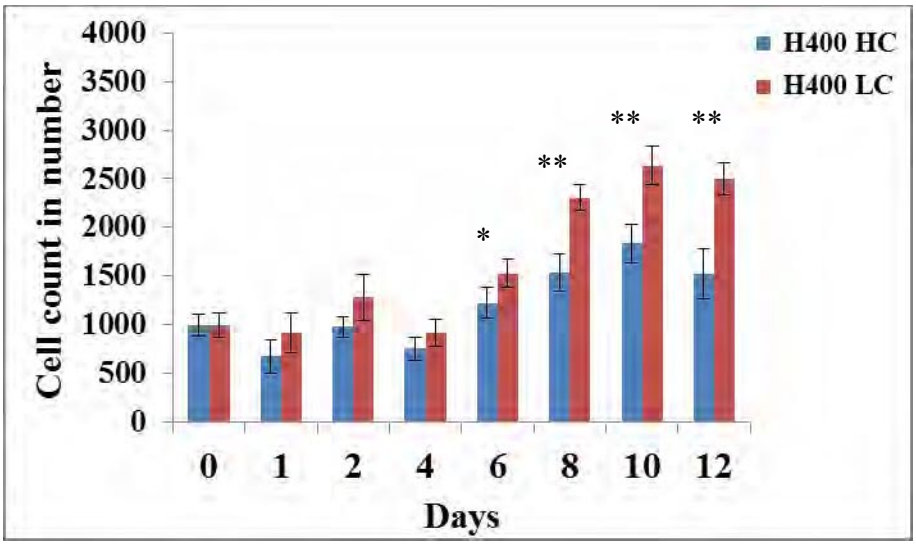

(B)

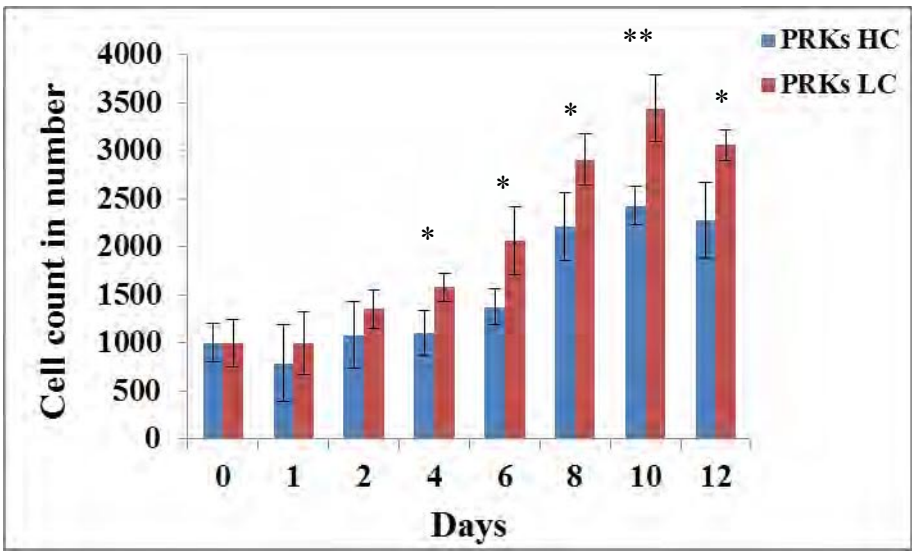

Figure 3.2. **H400 and PRKs count in low and high calcium medium using the MTT assay**. Graphs showing the number of (A) H400 produced in low calcium (LC) medium were significantly higher compared with high calcium (HC) medium. Similarly (B) PRKs cell count in low calcium medium was significantly increased than those cultured in high calcium after all different culture periods (except day 0 when cells were seeded at the same density) as determined using the MTT assay with a T-test (n = 3= replicates). Error bars represent one standard deviation from the mean **P<0.01, *P<0.05).

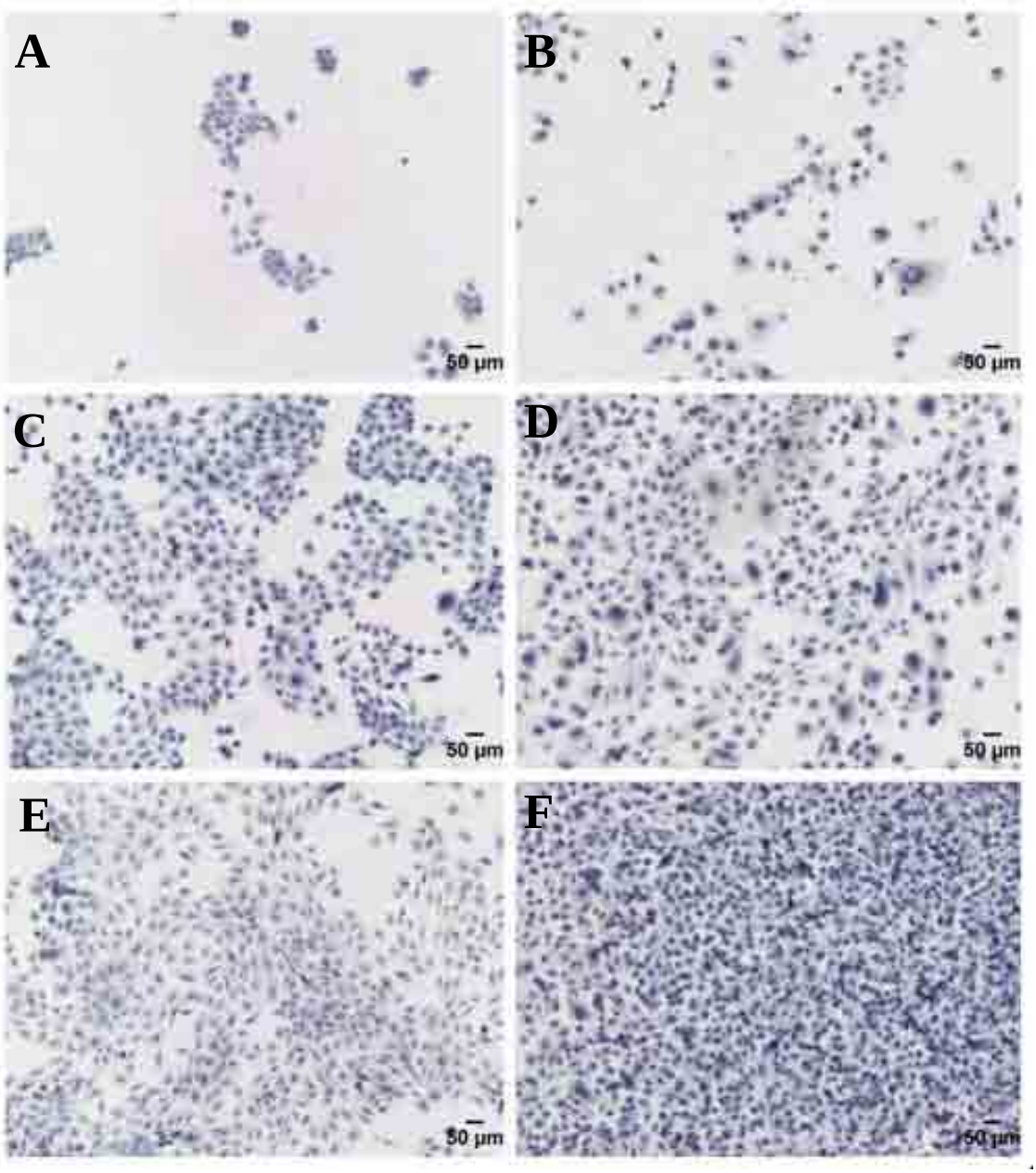

Figure 3.3. **Degree of colonisation of H400 in high and low calcium media**. Light microscopy images of H-only stained cultures of H400 cultured in high (left) and low (right) calcium media. The degree of colonisation of keratinocytes at day 4, 6 and 8 in high calcium media (A, C, E) was comparatively lower than observed in low calcium media (B, D, F) at each time point.

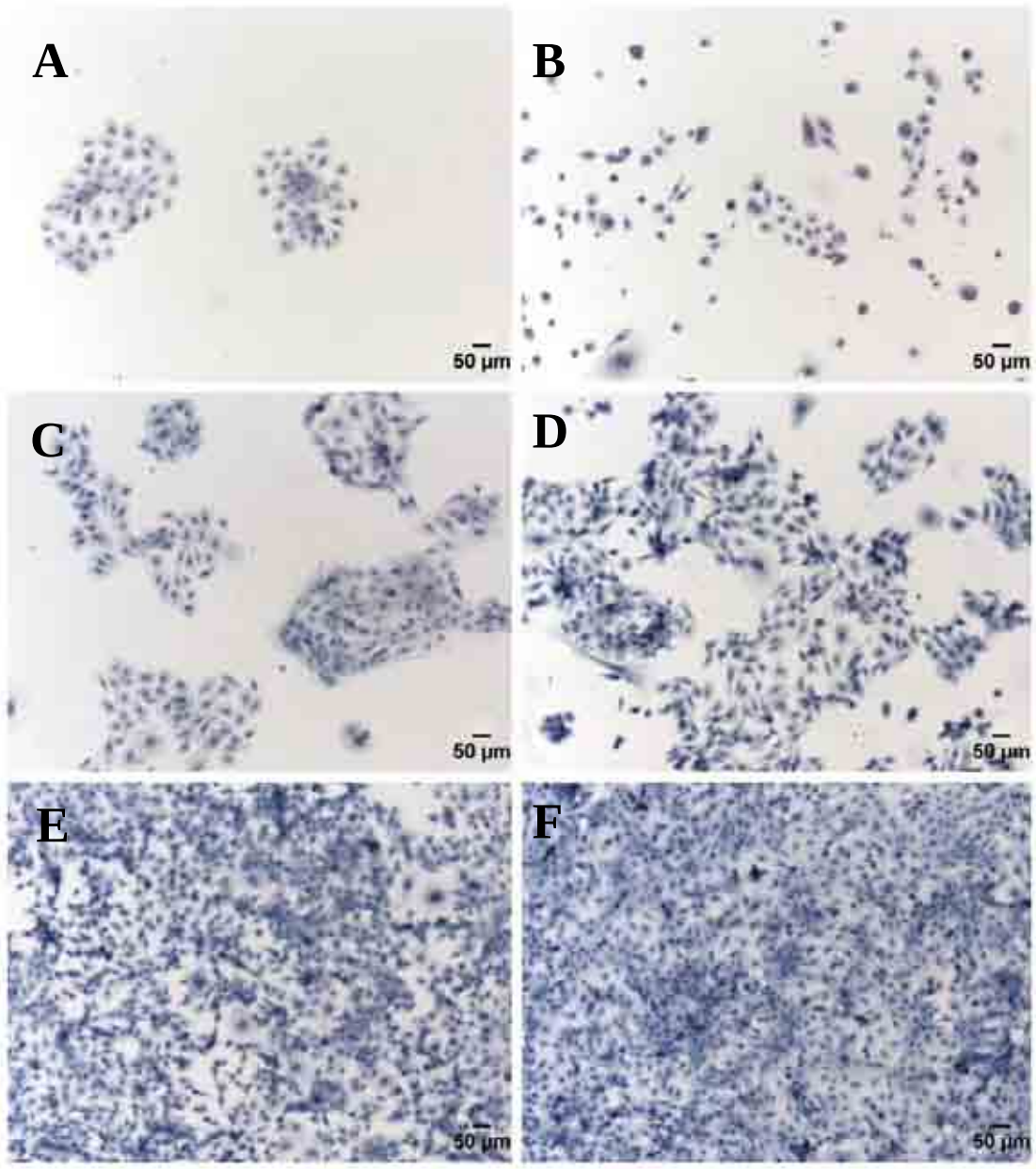

Figure 3.4. **Degree of colonisation of PRK in high and low calcium media.** Light microscopy images of H-only stained cultures of PRKs cultured in high (left) and low (right) calcium media. The degree of colonisation of keratinocytes at day 4, 6 and 8 in high calcium media (A, C, E) was comparatively lower than observed in low calcium media (B, D, F) at each time point.

3.4 Statistical analysis of semi-automated cell counts of monolayer cell cultures

Statistical analysis of semi-automated cell counting data using univariate analysis of variance showed that percentage of area covered by H400 monolayer cultures per microscopic field (field width 1406.5μm), using a x10 objective at 4, 6 and 8 days in low calcium media was significantly higher ($P<0.0001$) than those of cells cultured in high calcium medium (Figure 3.5) as determined by an automated computerised (thresholding) cell counting method (see section 2.4.2).

Percentage area of coverage in H400 is significantly different ($P<0.0001$) amongst 3 different groups of 4/6, 4/8 and 6/8 days of cultures in high and low calcium media. The percentage of area coverage significantly increased between day 4 and 6 ($P<0.0001$) and day 4 and 8 ($P<0.0001$) but not between days 6 and 8 in high and low calcium media as determined using a post-hoc Tukey test univariate general model analysis.

The average area of H400 in low calcium medium was significantly greater than those in high calcium medium at day 6 ($P=0.0001$) and day 8 ($P<0.048$) but not at day 4 ($P=0.668$) determined by the post-hoc Tukey univariate general linear model test The area of coverage of a single keratinocyte in low calcium medium increased between day 4 & 6 ($P=0.077$) and then decreased significantly ($P<0.0001$) between day 6 & 8 of cultures whilst keratinocytes in high calcium media remained similar in size throughout the days of study (Figure 3.6).

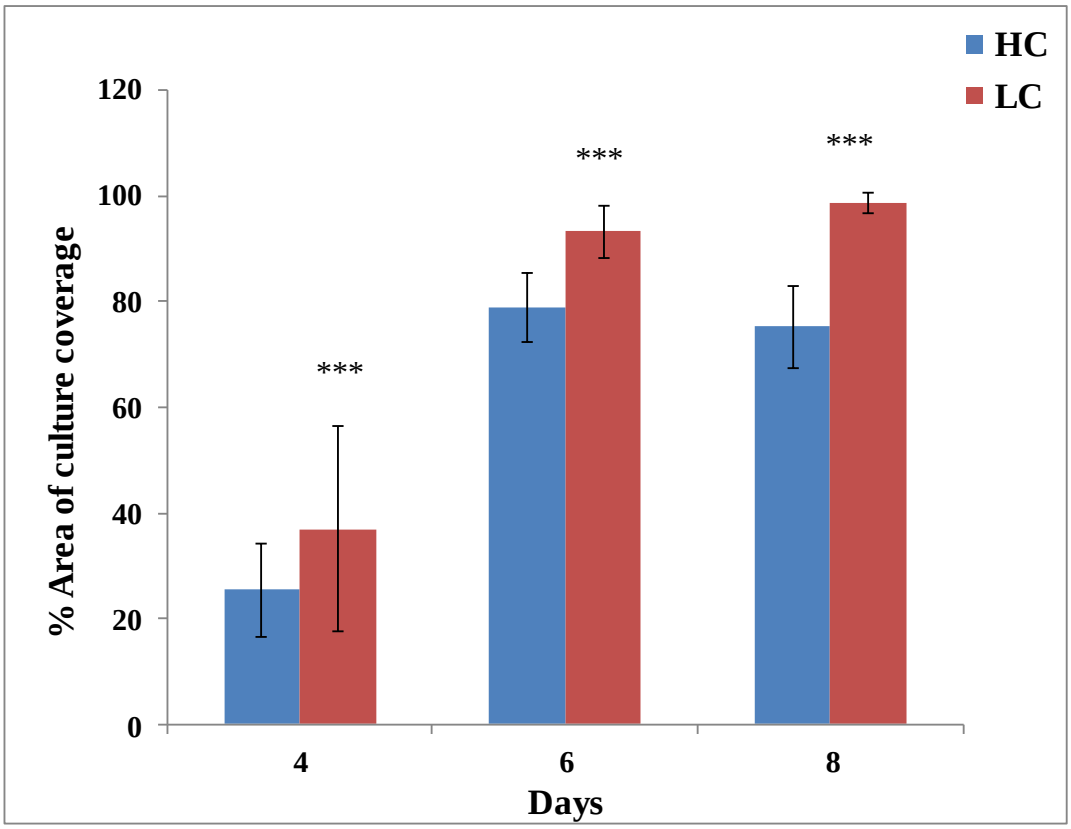

Figure 3.5. **Percentage coverage area for H400 in high and low calcium media.** Graph showing average percentage coverage area for H400 monolayers in low (LC) and high calcium (HC) media after 4, 6 and 8 days of culture. Coverage by H400 keratinocytes was significantly higher compared with those in high calcium medium (*** $P<0.0001$) as determined using a semi-automated cell counting at all time periods analysed.

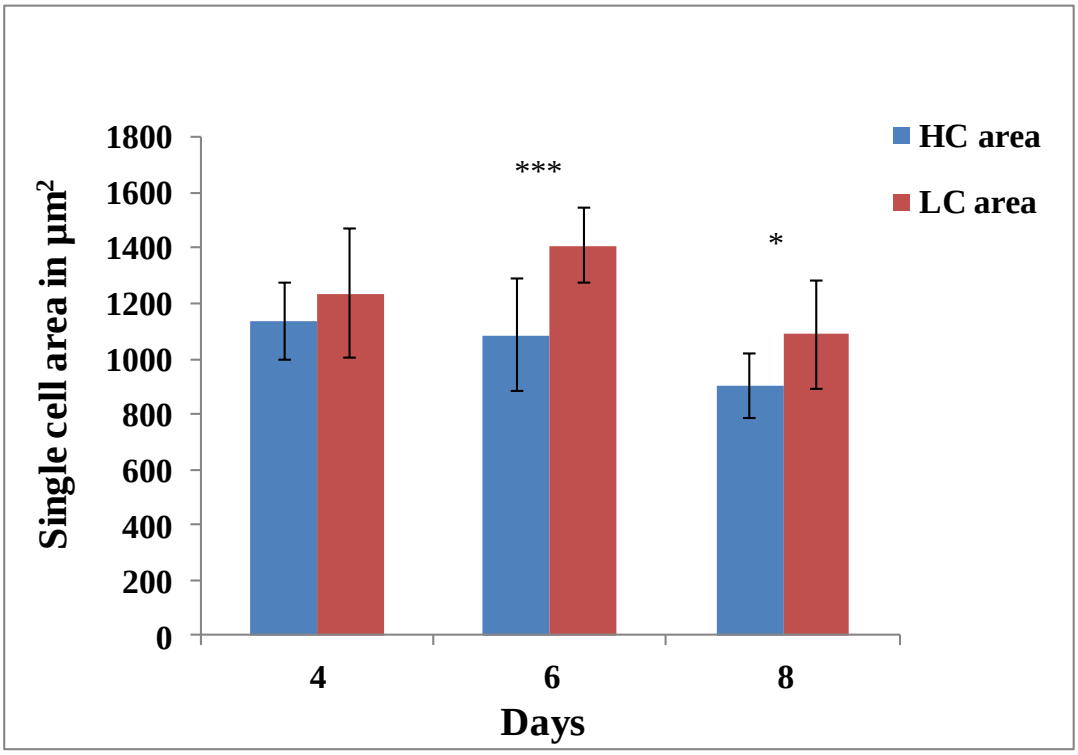

Figure 3.6. **Area of H400 monolayer cultures in high and low calcium media**. Graph showing average area of H400 keratinocytes at 4, 6 and 8 days of culture in high (HC) and low calcium (LC) media as determined by an automated computerised (thresholding) cell counting method. There is no significant difference in the area between cells cultured at high and low calcium medium at day 4 (P=0.668). The cells in low calcium medium have significantly greater area compared to those in high calcium medium at day 6 (***P<0.0001) and day 8 (*P=0.048).

3.5 Immunohistochemical characterisation

Immunohistochemical (IHC) analyses of H400 and PRK monolayer cultures were performed to characterise the expression and distribution of various structural proteins at 8 days of culture when cells had approached full confluence on glass coverslips. Figure 3.7 shows pan-keratin antibody staining, which react with any of the subtype of cytokeratins produced by cell cultures while IgG1, a negative control, did not stain any keratins in the monolayer cell culture with slight background reaction. Figure 3.8 shows expression of suprabasal epithelial proteins including cytokeratins-5, -6, -10, -13 which appeared to be more highly expressed in H400 keratinocyte monolayer cultures in high calcium medium (Figure 3.8 A, C, E) compared with keratinocytes cultured in low calcium medium (Figure 3.8 B, D, F). Ki67, a basal cell marker of proliferation, appeared to be expressed at similar levels in H400 monolayer cultures in high and low calcium media (Figure 3.8 G, H).

The expression of transmembrane proteins including E-cadherin and desmoglein-3 appeared to be more highly expressed in H400 monolayer cultures in high calcium medium (Figure 3.9 A, C) than those produced in low calcium medium (Figure 3.9 B, D). Similarly, PRK monolayer cultures expressed higher levels of structural (cytokeratin) proteins in high calcium medium (Figure 3.10 A, C, E) than those generated in low calcium medium (Figure 3.10 B, D, F). Monolayer cultures also expressed higher levels of intercellular transmembrane proteins in high calcium medium (Figure 3.11 A, C) compared with those cultures generated in low calcium medium (Figure 3.11 B, D). Involucrin appeared highly expressed in high calcium medium in H400 (Figure 3.8 E) and PRK monolayer cultures (Figure 3.11 E) compared with cultures generated in low calcium medium, respectively (Figures 3.8 F & 3.11 F).

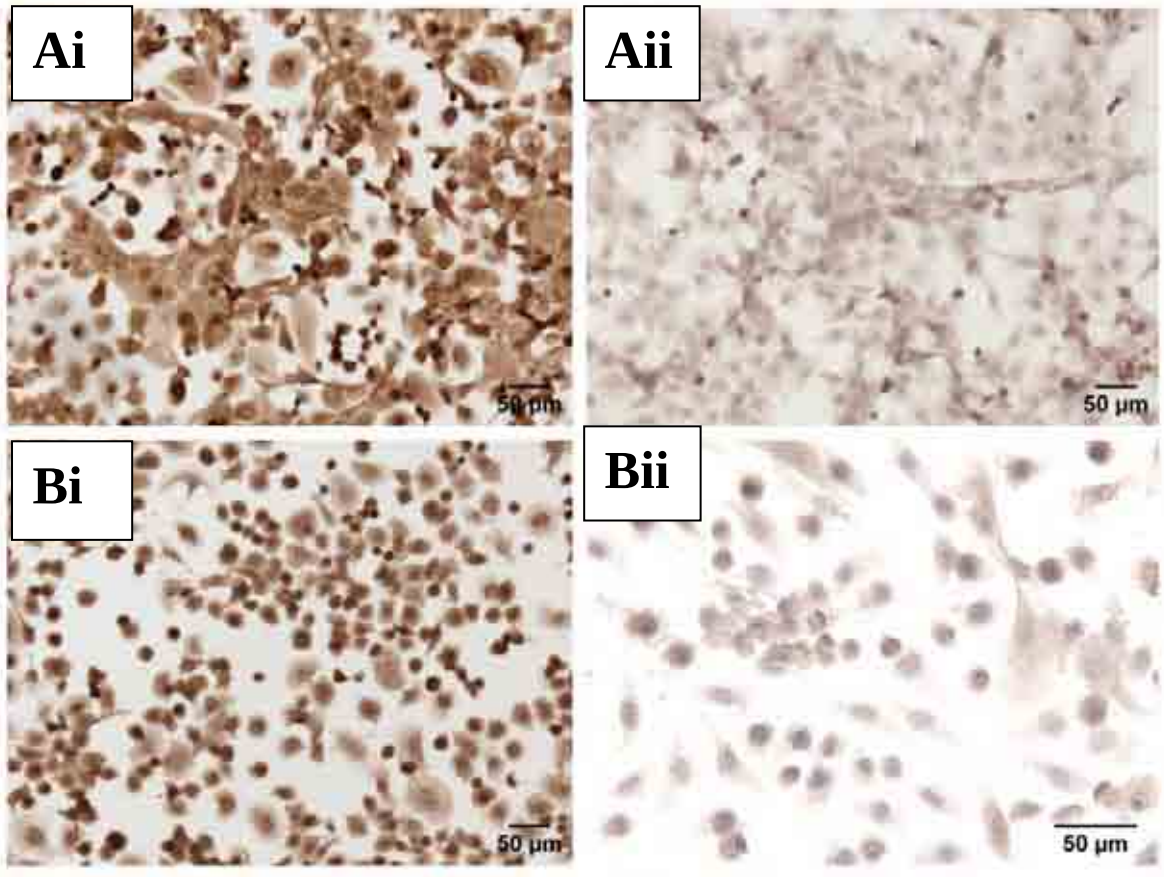

Figure 3.7. **Pan-keratin staining in H400 and PRK monolayer cultures**. Light microscopy images showing immunohistochemical staining for pan-keratin expression in H400 (Ai) and PRK (Bi) monolayer cultures (positive control). Mouse IgG1 (negative control) showing background staining (Aii) and (Bii) and counterstained with haematoxylin.

Figure 3.8. **IHC staining of CK -1, -5, -6, -10, -13 in H400 monolayer culture**s. IHC images of H400 cultured for 8 days in high (left) and low (right) calcium media, stained for the presence of suprabasal cytokeratins, CK1 (A, B), CK5/ CK6 (C, D), CK10 (E, F), CK13 (G, H) in the cytoplasm of the cells. The marker of cell proliferation Ki67 (I, J) stained nuclei of the dividing cells. The expression of suprabasal cytokeratins in H400 cultures were relatively highly expressed in high calcium medium compared with those cultured in low calcium medium. Scale bars are shown.

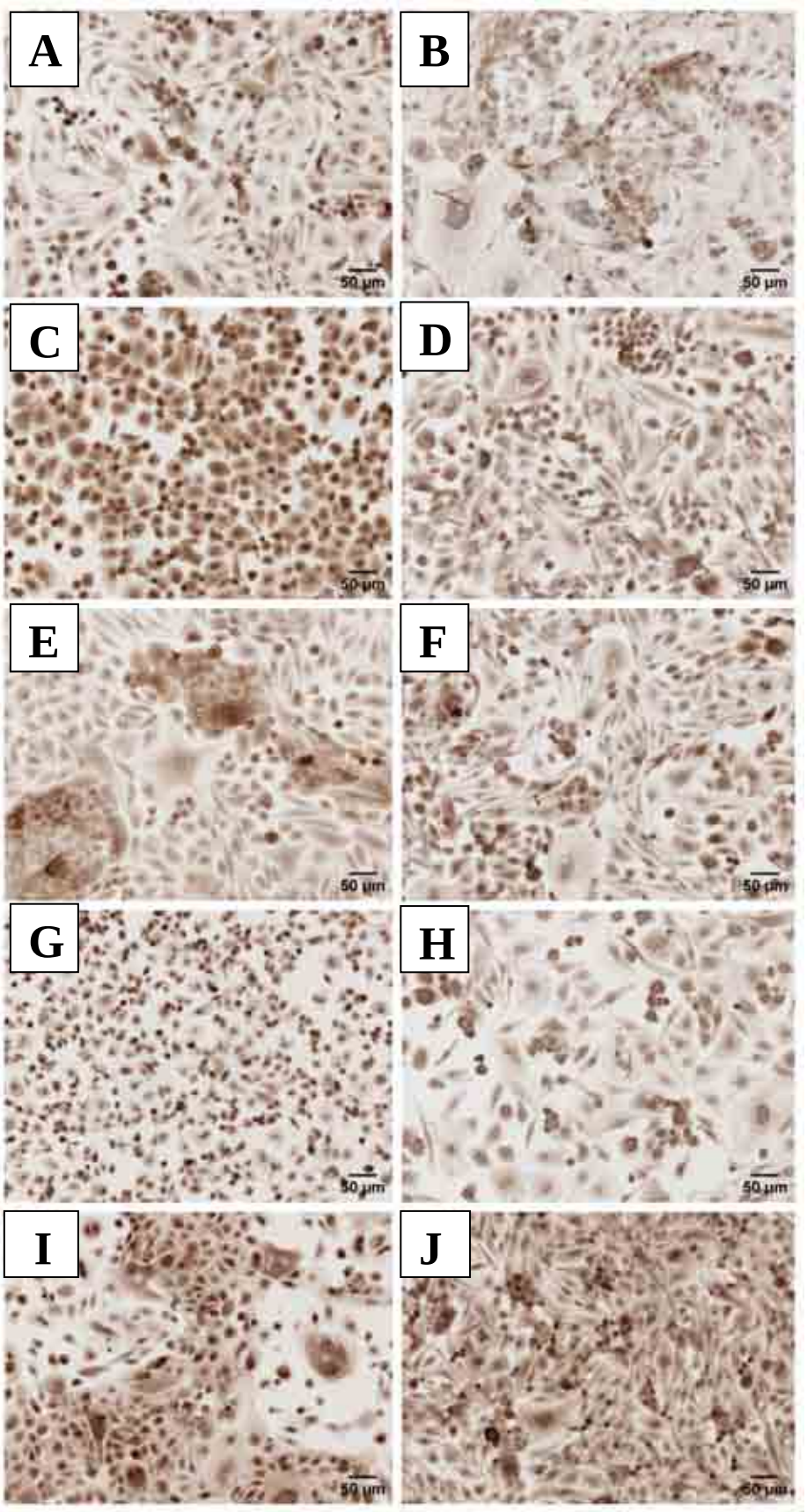
A
B
C
D
E
F
G
H
I
J
50 µm

Figure 3.9. **IHC staining of E-cadherin, desmoglein 3 and involucrin in H400 monolayer cultures.** IHC images of H400 monolayers cultured for 8 days in high (left) and low (right) calcium media, stained for the transmembrane proteins, E-cadherin (A, B) and desmoglein-3 (C, D) responsible for cell-cell adhesion. Involucrin (a marker of keratinocyte differentiation), was also present in the cytoplasm of cells (E, F) cultured in high and low calcium medium. The expression of E-cadherin and desmoglein in H400 cultures are relatively highly expressed in high calcium medium compared with those cultures generated in low calcium medium.

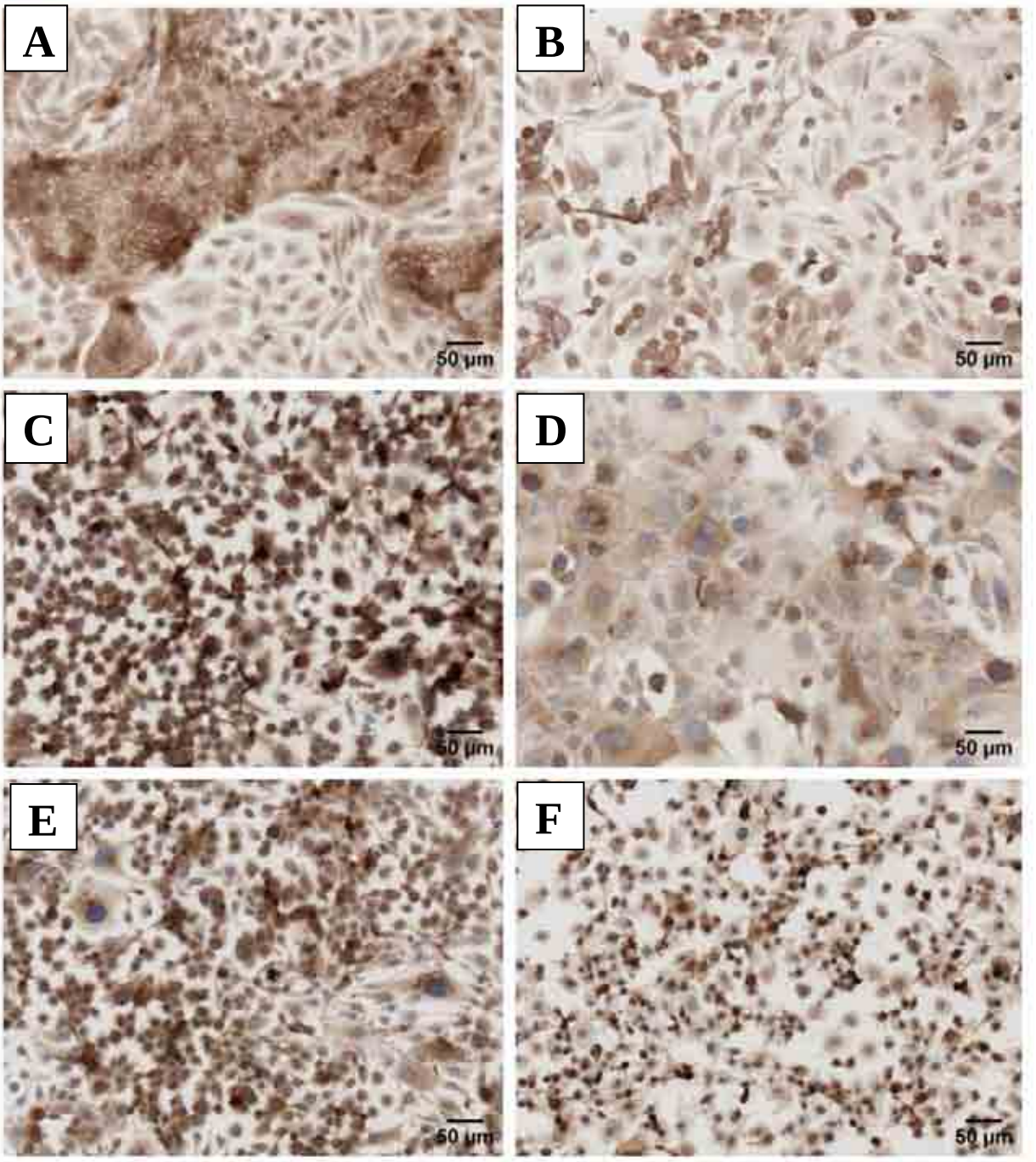
A
50 µm
B
50 µm
C
50 µm
D
50 µm
E
50 µm
F
50 µm

Figure 3.10. **IHC analysis of CK-1, -5, -6, -10, -13 in PRKs monolayer cultures.** IHC images of PRKs cultured for 8 days in high (left) and low (right) calcium media, stained for suprabasal proteins present in the cytoplasm of keratinocytes including CK1 (Figure 3 A, B), CK5/ CK6 (Figure 3 C, D), CK10 (Figure 3 E, F), CK13 (Figure 3 G, H), representing cell differentiation. Expression of suprabasal proteins was greater in high calcium medium compared with those in low calcium medium. The cell proliferation marker, Ki67, was present in the nuclei of some cells of the colonies (I, J). Suprabasal cytokeratins-1, -5, -6, -10, & -13 appeared relatively highly expressed in PRKs in high calcium medium compared with those cultured in low calcium medium.

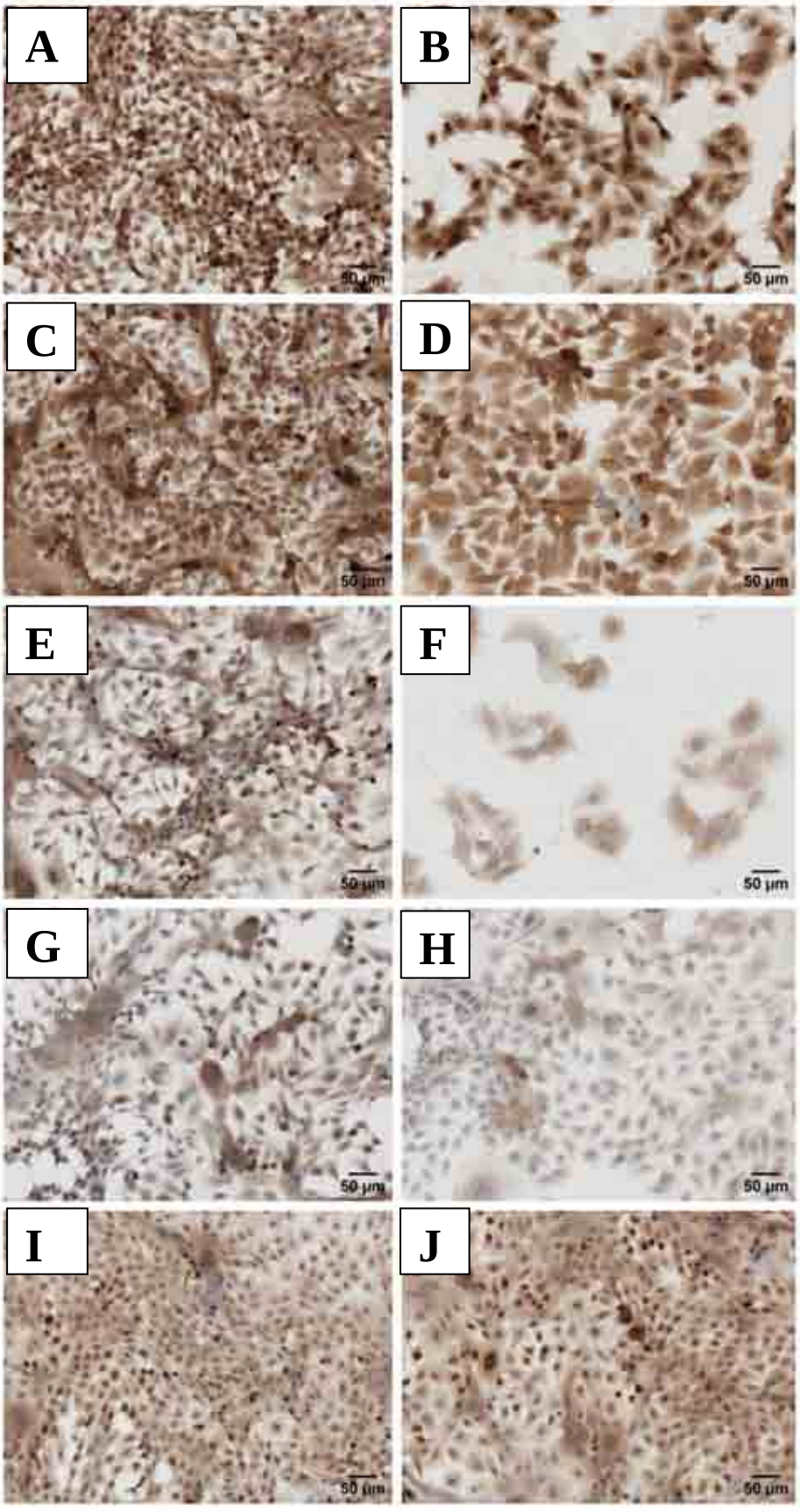
A
B
C
D
E
F
G
H
I
J
50 µm

Figure 3.11. **IHC analysis of E-cadherin, desmoglein 3 and involucrin in PRKs monolayer cultures**. IHC staining of PRKs cultured for 8 days in high (left) and low (right) calcium media, for intercellular transmembrane proteins E-cadherin (A, B), desmoglein-3 (C, D) which are involved in cell adhesion. The cell differentiation marker involucrin was present in the cytoplasm of keratinocytes (E, F). The expression of transmembrane proteins particularly E-cadherin were relatively highly expressed in PRK cultures in high calcium medium compared with those cultured in low calcium medium.

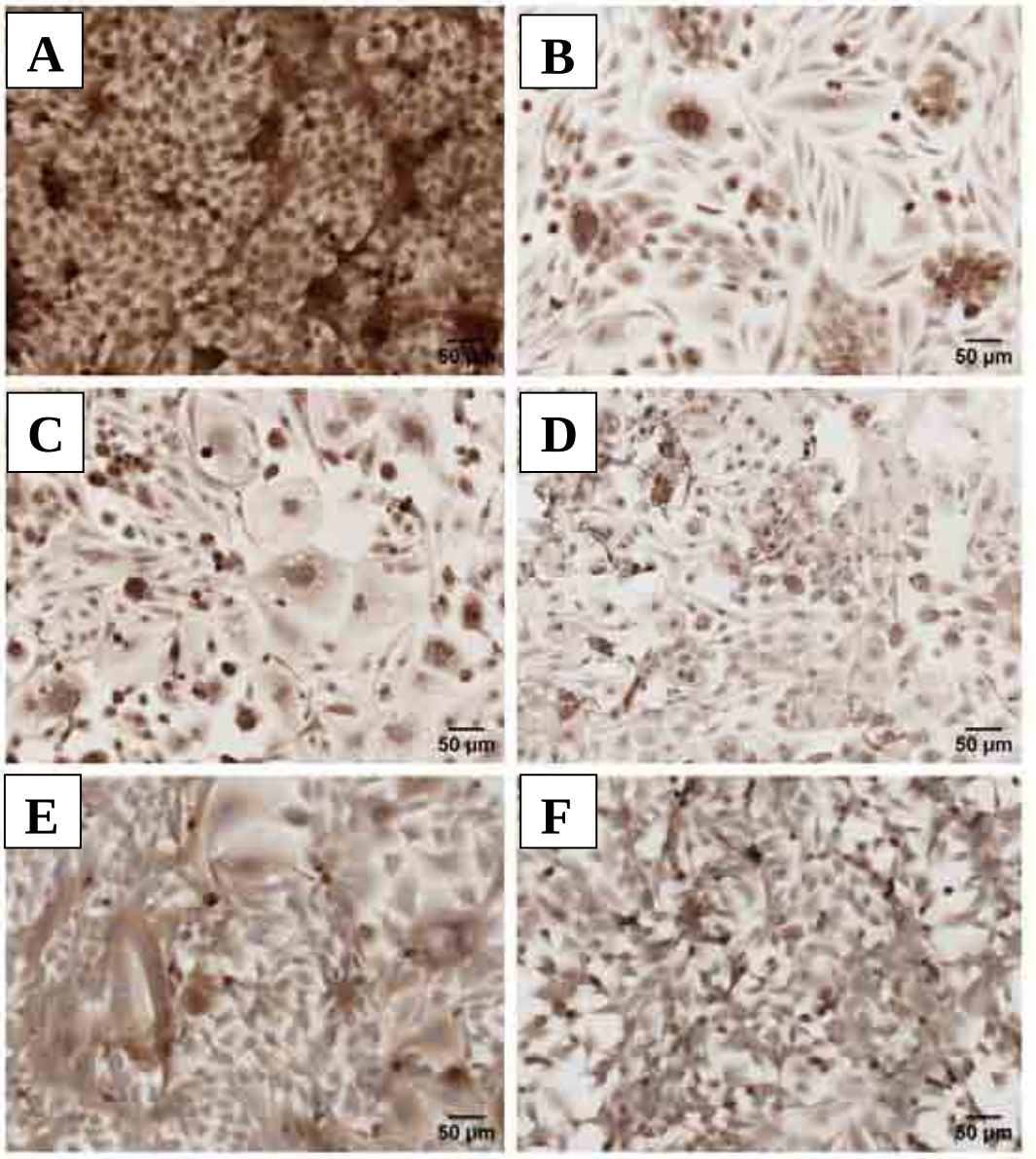
A
B
C
D
E
F
50 µm

3.6 Gene expression analysis in monolayer cell cultures

Following seeding of $1x10^6$ H400 cells or PRKs per $25cm^2$ flask relatively low-, mid- and high-density cultures were obtained at 4, 6 and 8 days of culture.

In Figure 3.12 A, representative gel images for each gene expression of transmembrane molecules including E-cadherin, desmocollin-3, plakophilin and desmoglein-3 and suprabasal cytokeratins-1,-5,-6,-10,-13 transcripts are shown. Figure 3.12 B shows the relative gene expression level for the intercellular transmembrane marker, E-cadherin in H400 keratinocyte monolayer cell cultures in high calcium medium was higher at 8 days of culture compared with day 6 and day 4. Expression of desmocollin-3, plakophilin and desmoglein-3 were higher at day 6 followed by day 8 and day 4. Similarly, the relative levels of gene expression of cytokeratins-1, -6, and -10 were higher at day 6 compared with day 8 and day 4 (Figure 3.12 C). Genes for cytokeratins-5 and-13 were expressed at the highest levels at day 8 followed by day 6 and day 4 expression levels.

Figure 3.13 demonstrates that expression of intercellular transmembrane adhesion molecules such as E-cadherin and desmoglein-3, the cell differentiation marker, involucrin and cytokeratins-1, -4, -5, -6, -10, -13 molecule transcripts were relatively highly up-regulated in H400 (Figure 3.13 A) and PRK (Figure 3.13 B) monolayer cultures in high calcium medium compared with cultures generated in low calcium medium at day 8. Human and rat glyceraldehyde-3-phosphate dehydrogenase (GAPDH) were used for normalisation control.

***Figure 3.12*. Semi-quantitative RT-PCR analysis of GAPDH, CK-1, -4, -5, -6, -10, -13 in H400 monolayer cultures for a range of culture periods.** RT-PCR analysis of selected genes involved in structural integrity of H400 monolayer cultures at 4, 6 and 8 days of culture (A) Representative gel images (from 2 replicate analyses for each gene) of transmembrane molecules (E-cadherin, desmocollin-3, plakophilin and desmoglein-3) and suprabasal cytokeratin transcripts (cytokeratins-1, -4, -5, -6, -10, -13) are shown. GAPDH (top rows) were used for normalisation control and bottom rows for each target gene.

(A)

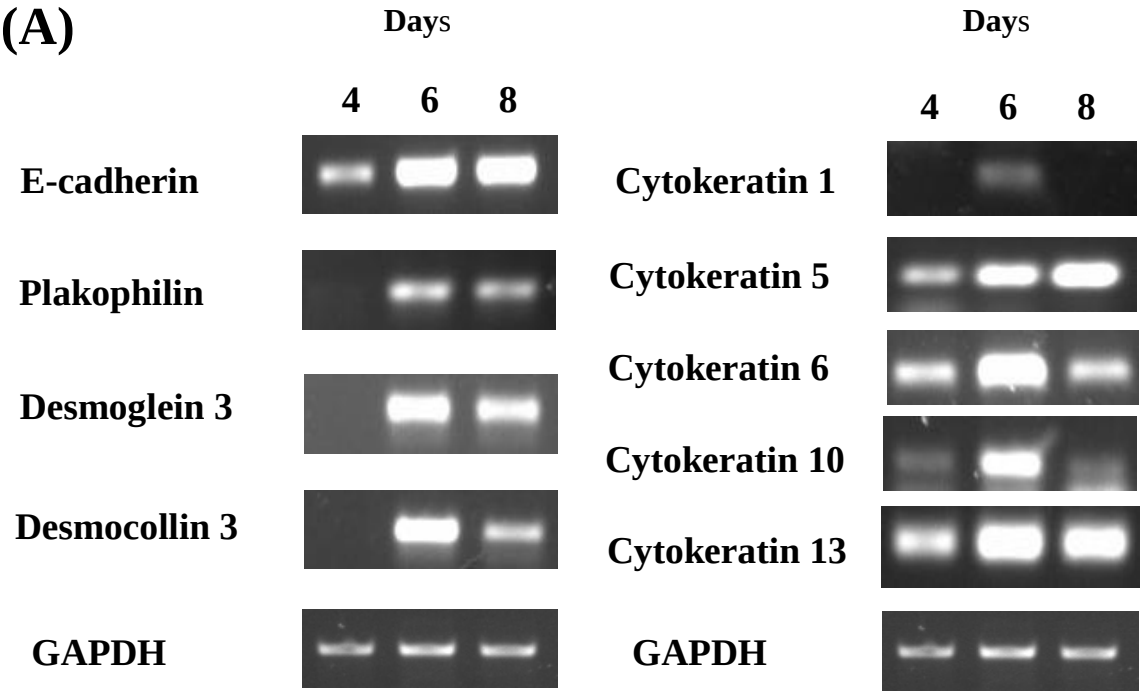
Days
4 6 8
E-cadherin
Plakophilin
Desmoglein 3
Desmocollin 3
GAPDH
Days
4 6 8
Cytokeratin 1
Cytokeratin 5
Cytokeratin 6
Cytokeratin 10
Cytokeratin 13
GAPDH

Figure 3.12. Expression levels are shown as percentage of the highest gene expression level detected (B, C). Amplified product values were normalised to human GAPDH housekeeping gene levels.

(B)

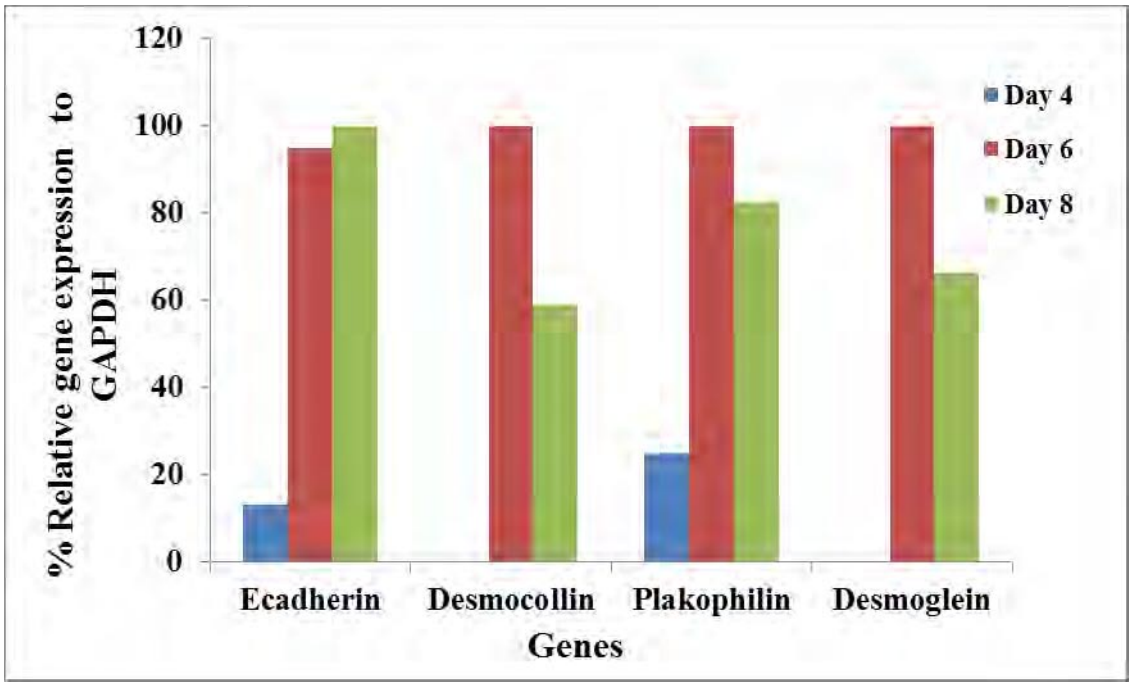
% Relative gene expression to GAPDH
120
100
80
60
40
20
0
Day 4
Day 6
Day 8
Ecadherin
Desmocollin
Plakophilin
Desmoglein
Genes

(C)

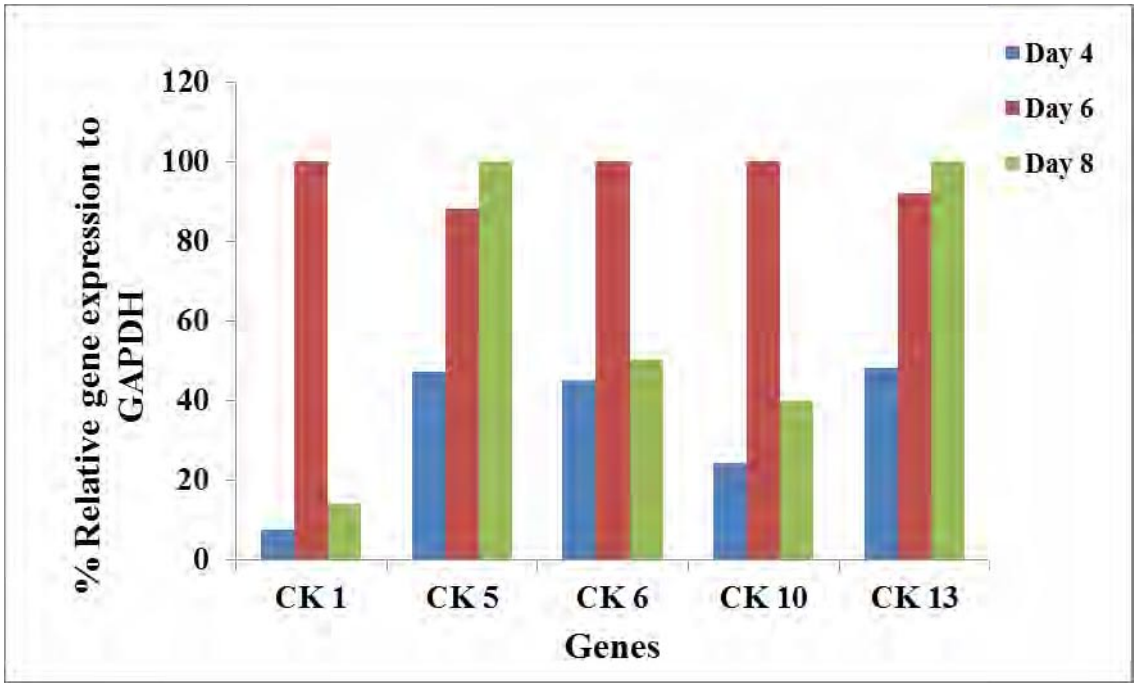
% Relative gene expression to GAPDH
120
100
80
60
40
20
0
Day 4
Day 6
Day 8
CK 1
CK 5
CK 6
CK 10
CK 13
Genes

***Figure 3.13*. Semi-quantitative RT-PCR analysis of selected genes expressed in H400 and PRK monolayer cultures in high calcium (HC) and low calcium (LC) media at 8 days of culture.** (A) Representative gel images (from 2 replicates) of gene expression of suprabasal (cytokeratins-1, -4, -5, -6, -10, -13), adhesive molecules (E-cadherin, desmoglein-3) and differentiation marker involucrin in H400 and PRKs are shown.

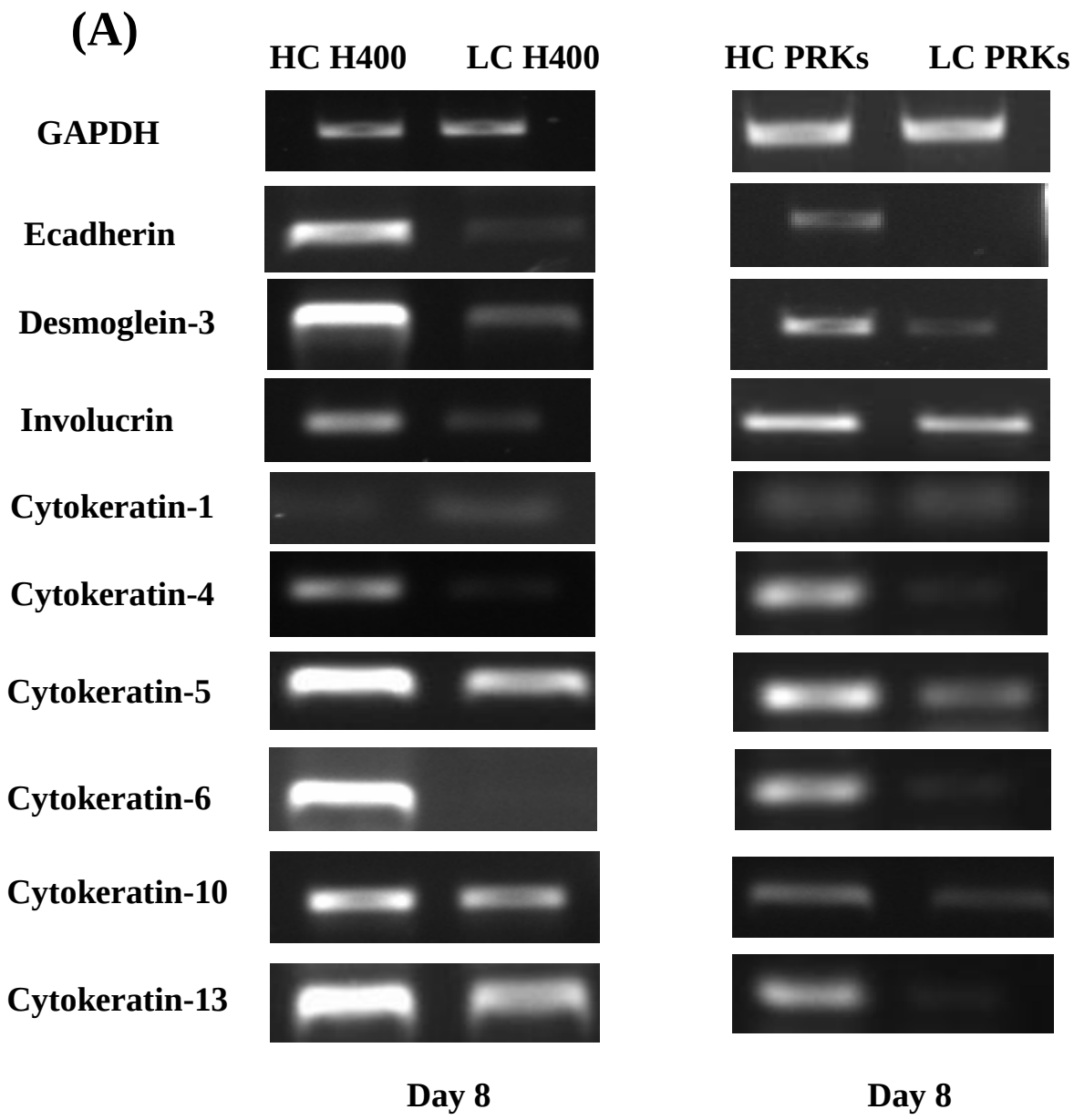
(A)
HC H400
LC H400
HC PRKs
LC PRKs
GAPDH
Ecadherin
Desmoglein-3
Involucrin
Cytokeratin-1
Cytokeratin-4
Cytokeratin-5
Cytokeratin-6
Cytokeratin-10
Cytokeratin-13
Day 8
Day 8

Figure 3.13. Expression levels are shown as percentage of the highest gene level (using human and rat gene primers respectively) detected in (B) H400 and (C) PRK monolayer cultures. Amplified product values were normalised to human and rat GAPDH housekeeping gene levels, respectively.

(B)

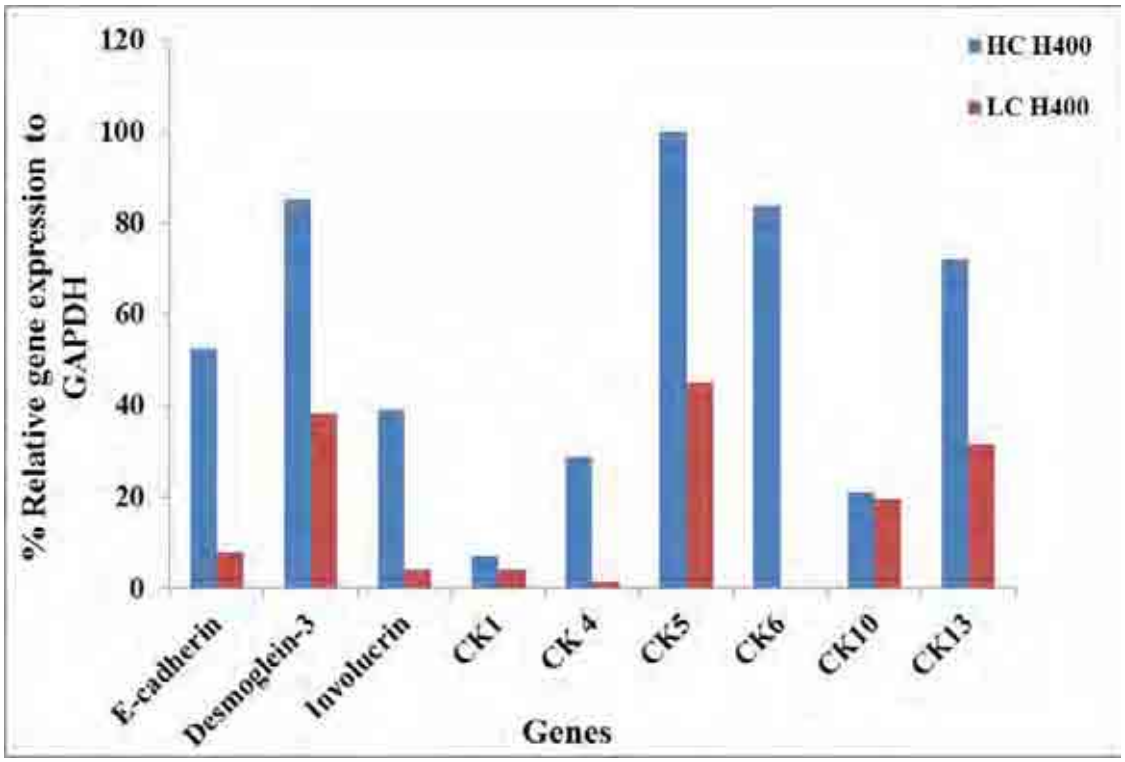
HC H400
LC H400
% Relative gene expression to GAPDH
120
100
80
60
40
20
0
E-cadherin
Desmoglein-3
Involucrin
CK1
CK 4
CK5
CK6
CK10
CK13
Genes

(C)

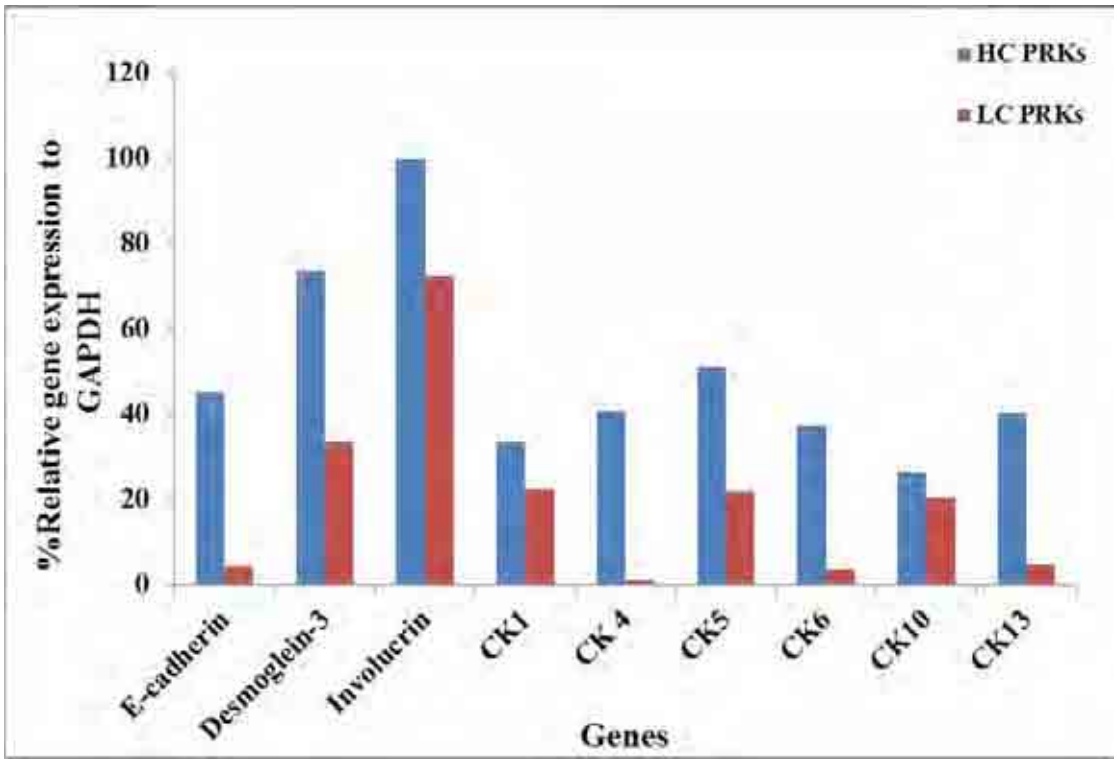
HC PRKs
LC PRKs
%Relative gene expression to GAPDH
120
100
80
60
40
20
0
E-cadherin
Desmoglein-3
Involucrin
CK1
CK 4
CK5
CK6
CK10
CK13
Genes

CHAPTER 4 RESULTS

(3D OCS)

This chapter reports on 3D H400 and PRK oral keratinocyte cultures generated on different scaffolds for a range of culture periods. The three types of scaffolds used in this study were initially examined using scanning electron microscopy (SEM). An unbiased computerised epithelial thickness characterisation and cell layer analysis of H&E stained histological images of H400 and PRKs OCs on DED, collagen and PET at day 3, 5, 7, 10 and 14 days of culture is also reported. Further biochemical and molecular characterisation of the 3D cultures were also performed using immunohistochemistry (IHC) and RT-PCR analyses.

4.1 Examination of OC scaffolds

4.1.1 Scanning electron microscopy (SEM)

SEM examination of PET demonstrated the presence of micro-pores of 0.4 μm diameter (consistent with the manufacturer's data sheet) which enabled cells on one side of the membrane to access necessary nutrients from the culture medium reservoir on the opposite side of the membrane (Figure 4.1 A). Examination of the collagen type I scaffold (rat tail) demonstrated an interwoven fibrillar structure which may facilitate cell attachment (Figure 4.1 B). The DED revealed an undulating surface corresponding with the connective papillae and (absent) rete ridges (Figure 4.1 C).

4.1.2 Immunohistochemical (IHC) analysis of DED

IHC analysis of DED demonstrated that following the removal of the epithelium some constituents of the basement membrane such as collagen type IV (Figure 4.2 A) and laminin-5 (Figure 4.2 B) remained on the culture substrates. PET clearly lacked such biological factors as it is a synthetic material.

Figure 4.1. **Scanning electron microscopy (SEM) of DED, collagen and PET.** SEM secondary electron micrographs showing surfaces of (A) PET membrane, with porosity of approximate diameter 0.4 μm across the surface, (B) collagen type-1 hydrogel, revealing a microfibrillar network, and (C) DED, with rete ridges evident shown by arrow heads. Scale bars are shown.

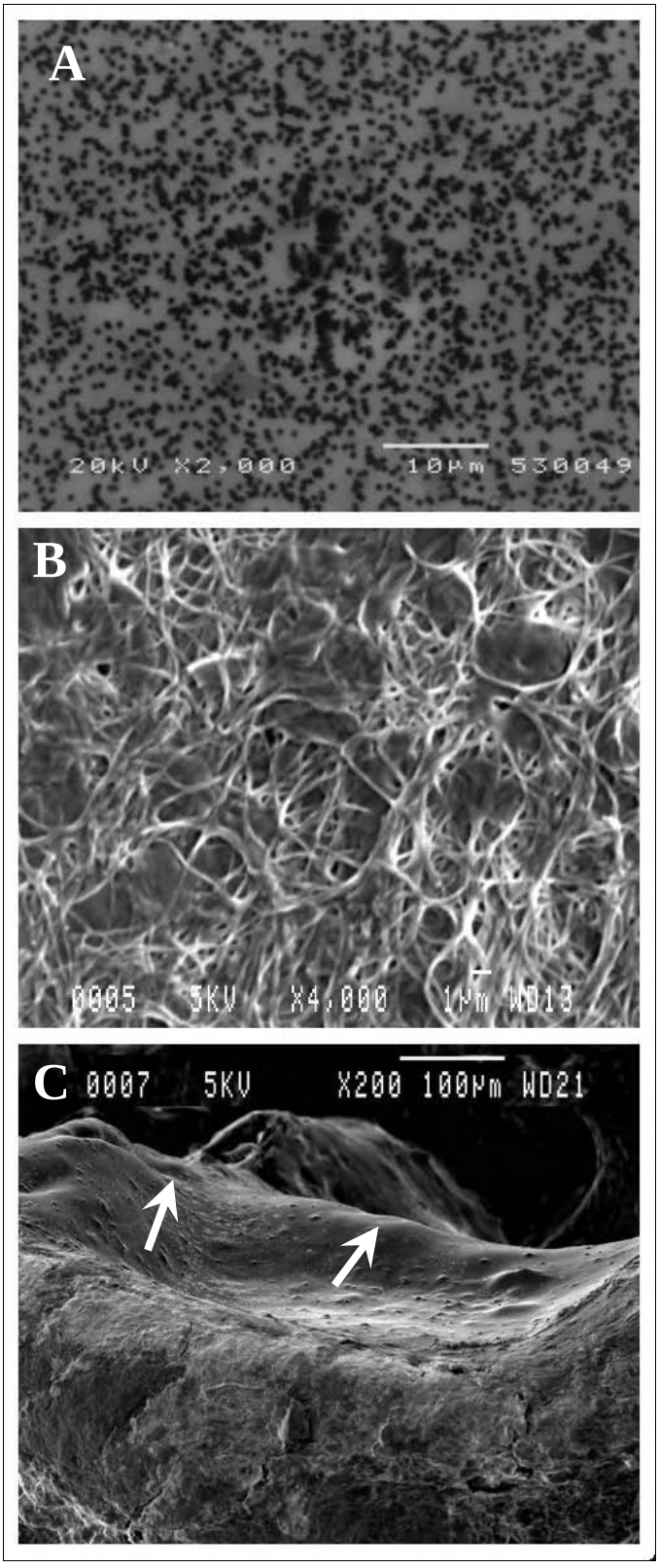
A
20kV X2,000 10µm 530049
B
0005 5KV X4,000 1µm WD13
C 0007 5KV X200 100µm WD21

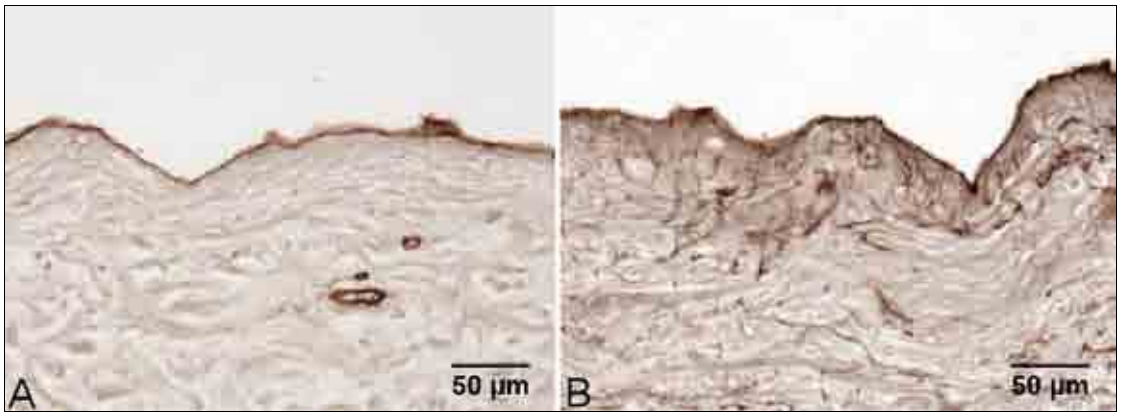

Figure 4.2. **IHC analysis of DED for collagen type IV and laminin-5.** IHC of 5 µm sections of DED for (A) collagen type IV and (B) laminin-5 demonstrating that these two basement membrane components were maintained on the surface of the DED.

4.2 Thickness characterisation of OCs on DED with different culture times

H400 and PRK OCs generated on DED showed variable thickness at 3, 5, 7, 10 and 14 days of culture. The thickness of H400 OCs increased gradually from day 3 (38 µm) and reached a maximum thickness by day 7 (88 µm) but decreased in thickness between day 10 and day 14 (75 µm) possibly due to the desquamation of cornified cells after maturation (Figure 4.3). In contrast the thickness of OCs of PRKs increased steadily between day 3 (23 µm) and day 10 (66 µm) of culture and remained relatively constant through to day 14 (65 µm) (Figure 4.4). The graph presented in Figure 4.4 demonstrates that H400 and PRKs cultured on DED increased in average epithelial thickness with increasing culture time. The increase in thickness between each culture time (3, 5, 7, 10 and 14 days) was significant $P<0.0001$, as analysed using a multivariate general linear model.

4.3 Thickness characterisation of OCs at day 14

Histological staining revealed that OCs generated stratified epithelial structures by 14 days of culture (Figure 4.5). The final thickness of the epithelium as well as the degree of stratification varied significantly depending on the culture substrate used (Figure 4.6). H400 and PRK OCs were polystratified and the epithelial thickness on DED was greater than that observed on the collagen and PET substrates. Moreover, H400 OCs demonstrated a greater thickness compared with PRK OCs on DED measured by the analytical approach described in section 2.8.2.

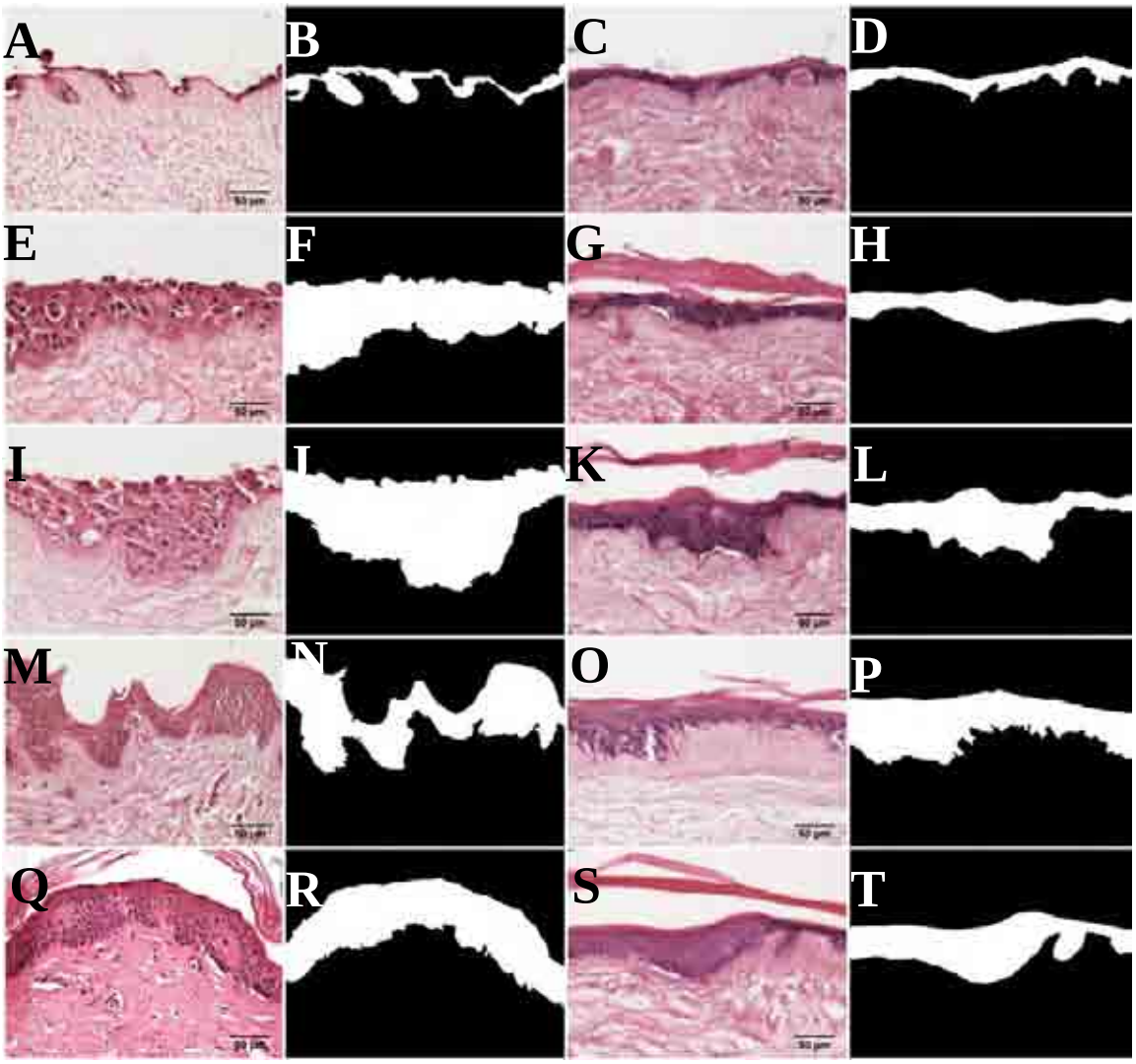

Figure 4.3. **Photomontage of histological sections and thickness characterisation of H400 keratinocytes and PRK OCs on DED at different culture times**. Histological sections (5 µm) of H400 keratinocyte OCs at day 3 (A), 5 (E), 7 (I), 10 (M) and 14 (Q) and PRKs OCs at day 3 (C), 5 (G), 7 (K), 10 (O) and 14 (S) of culture, stained with H&E. The binary (black and white) images of H400 (B, F, J, N, R) and PRK (D, H, L, P, T) represent the epithelial compartmental profiles as segmented using the SIOX procedure.

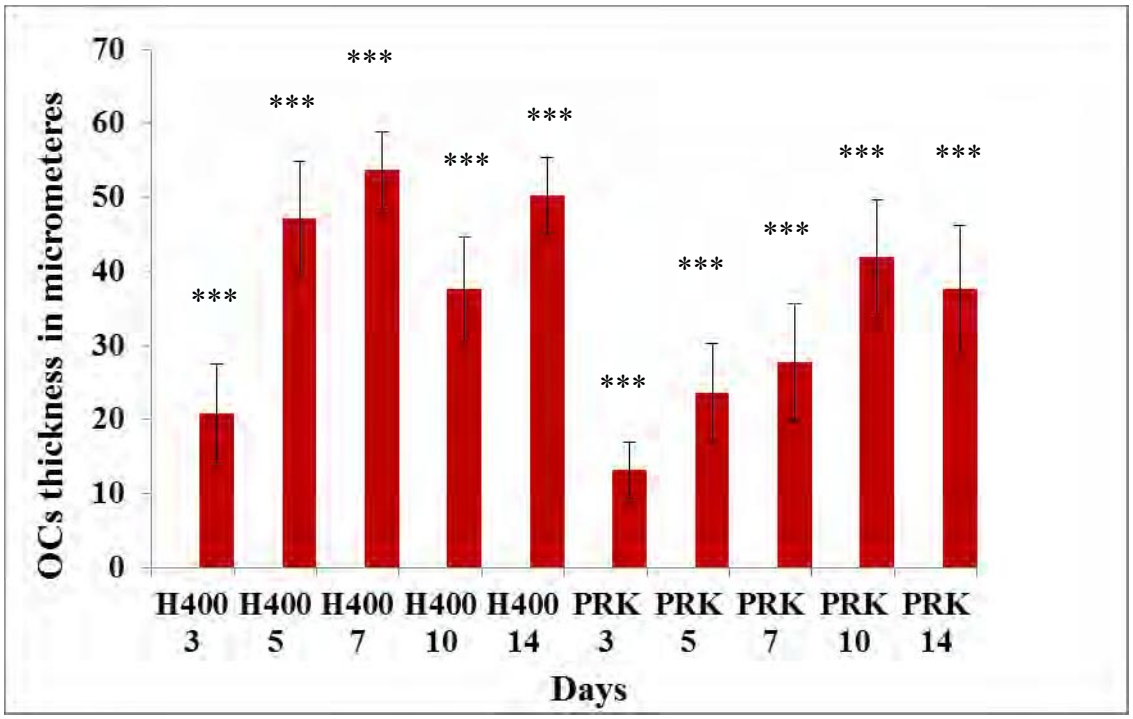

Figure 4.4. **Computed thickness of H400 and PRK OCs on DED (n=80) at different culture times.** The mean thickness (average) for OCs of H400 keratinocytes and PRKs on DED at different culture times determined by multivariate general linear model test was statistically different (***P<0.0001) from each other. Thickness was measured in micrometres and the pixel to micrometre factor was 0.431779. Error bars represent one standard deviation from the mean.

However, cultures of PRKs on collagen and PET were relatively thicker than H400 OCs generated on the same scaffolds (Figure 4.5). Figure 4.5 shows images of H&E stained sections and the segmented binary images from which the epithelial thickness was measured for H400 and PRK OCs at day 14 on the three culture substrates (DED, collagen and PET) using the SIOX procedure. A multivariate general linear model test showed that the differences in thickness of the OCs generated on the three culture materials was statistically significant ($P<0.0001$). The thickness of H400 and PRK OCs on DED was greater than that generated on the collagen and PET scaffolds.

The graph in Figure 4.6 presents the mean thickness of H400 and PRK OCs determined by computerised image processing. There was a significant difference in the thickness generated on DED, collagen and PET with both H400 and PRKs. The maximum thickness of H400 and PRK OCs on DED (75 µm and 65 µm, respectively) was significantly greater than with OCs generated on collagen (38 µm, 43 µm, respectively) and PET (18 µm and 28 µm, respectively).

4.4 Statistical analysis of H400 and PRK OCs at different culture times

Statistical analysis of OCs thickness data using a multivariate general linear model test demonstrated that both H400 keratinocyte and PRK OCs were significantly different on DED at 3, 5, 7, 10 and 14 days of culture (Figure 4.4, Figure 4.6). Moreover, culture time also influenced culture thickness and stratification on scaffolds. The type of cell used on the scaffolds also resulted in significant differences in the thickness of OCs ($P<0.001$) (Table 4.2, Figure 4.3, Figure 4.5).

Figure 4.5. **Histological & binary images of H400 and PRK OCs on DED, collagen and PET.** H&E stained histological sections (5 μm) of H400 and PRKs after culture on DED (A, C), collagen (E, G) and PET (I, K). The binary image of H400 and PRK OC on DED (B, D) collagen (F, H) and PET (J, L) represent the epithelium profiles segmented with the SIOX procedure.

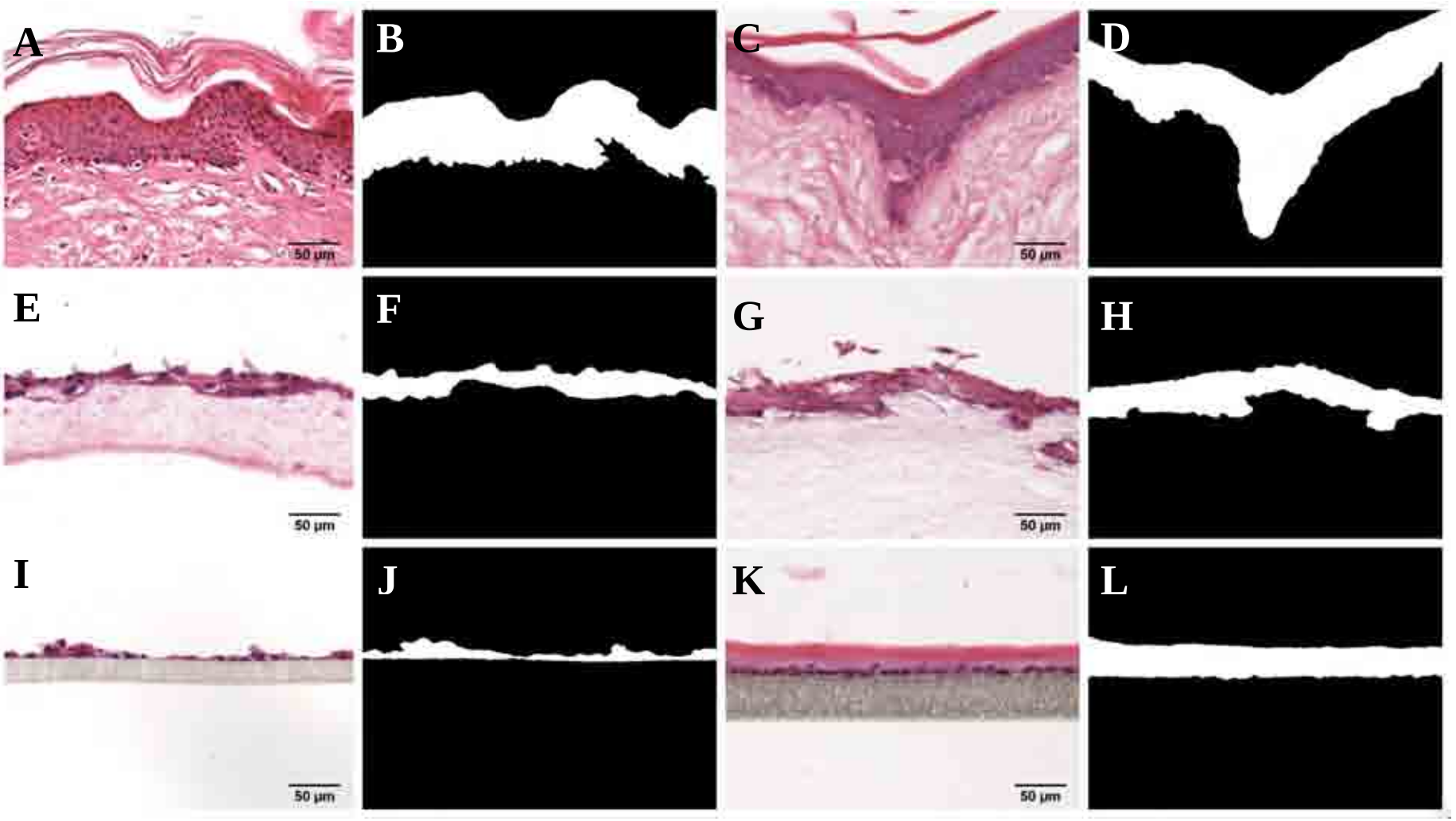
A
B
C
D
E
F
G
H
I
J
K
L
50 µm
50 µm
50 µm
50 µm

Analysis demonstrated significant differences ($P<0.001$) (Table 4.2) in the thickness of the epithelial compartment in OCs of H400 on collagen, PET and those of PRKs on DED, collagen, PET at day 14 (Figure 4.6). At 14 days of culture, the mean thickness of H400 keratinocyte OCs on DED was significantly greater ($P<0.001$) than those generated on collagen and PET scaffolds. Likewise, PRKs exhibited a higher degree of growth and maturation on DED ($P<0.001$) followed by collagen and then PET (Figure 4.6). Notably, H400 cultured on DED appeared to proliferate and differentiate in multiple layers compared with PRK OCs. In contrast, H400 keratinocytes did not appear to grow as efficiently (never more than 2-3 cell layers thick) on collagen and PET compared with PRKs (Figure 4.5). These results indicated that scaffold material played an important role in influencing the behaviour of oral keratinocyte growth and maturation.

Table 4.1 shows that the mean thickness (minimum, maximum, average) of H400 and PRK OCs at day 3, 5, 7, 10 and 14 days on DED are statistical different and identifies as factors “cell types”, “culture times”, and “cell type and culture time”, determined by the multivariate general linear model test at 95 % confidence interval. Values were also analysed using an F-test (this is the ratio of variance between group means to mean of variances within group). F-values larger than 1 indicate that the sample variances are from two different populations (Table 4.1).

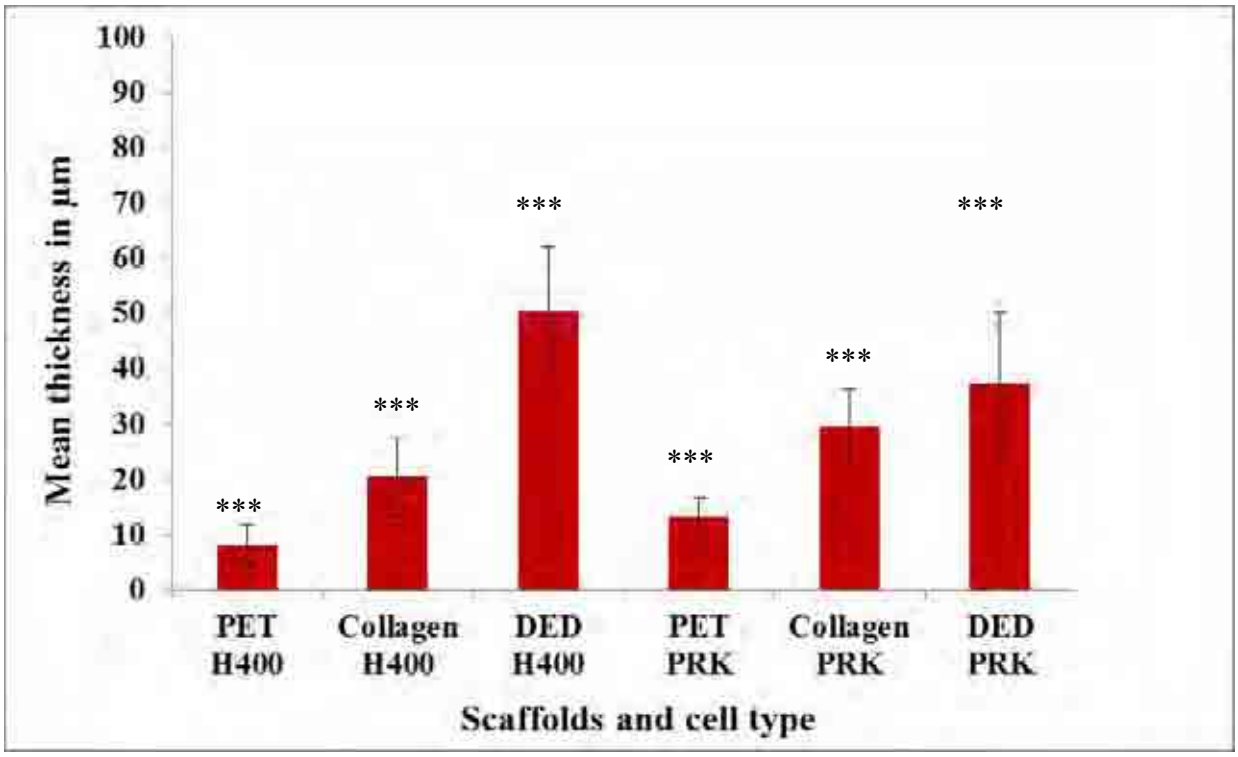

Figure 4.6. **Mean thickness of H400 and PRK OCs on DED, collagen and PET at day 14.** Graph showing mean thickness in microns (average) of H400 and PRK OCs (n=48) on DED, collagen and PET at day 14. (The pixel to micrometre factor was 0.432). The mean average thickness of the three different scaffold groups for H400 and PRK OCs were statistically different (***P<0.0001) determined by a multivariate general linear model test. Error bars represent one standard deviation from the mean.

Table 4.1. H400 and PRK OCs mean thickness on DED for 3, 5, 7, and 10 of culture. Multivariate general linear model analysis showing the significance differences (P<0.001) in the mean thickness influenced by factors (cell type, days and interaction between cell type and days) (df= degrees of freedom, F = F-statistic test).

Factors	Mean thickness	df	F	P
Cell types	Minimum	1	16.141	<0.001
	Maximum	1	33.627	<0.001
	Average	1	40.224	<0.001
	Standard deviation	1	12.525	<0.001
Days	Minimum	4	16.835	<0.001
	Maximum	4	16.909	<0.001
	Average	4	18.934	<0.001
	Standard deviation	4	5.865	<0.001
Cell type and days	Minimum	4	4.701	<0.001
	Maximum	4	2.928	<0.001
	Average	4	5.209	<0.001
	Standard deviation	4	0.978	<0.001

Results in Table 4.2 represent that the mean thickness (minimum, maximum, average) of H400 and PRK OCs at 14 days of culture on DED, collagen and PET is significantly different (P=0.001) as determined by a multivariate general linear model test at 95 % confidence interval (i.e. the mean difference is significant at the interval of 0.05). Mean thickness analysis based on "scaffolds", "cell type and scaffold" as factors were statistically different (P<0.001), while average thickness of OCs based on "cell type" as a factor was not significantly different (P=0.717).

4.5 Analysis of cell layers in OCs

Table 4.3 shows the results of the analysis of cell layer numbers in OCs. The test of the effects between subjects (general linear model) at day 3 showed statistically significant differences when considering "cell types" as a factor, for the number of virtual-cells in the sampled image frames (P=0.001) but not for the number of layers (P=0.061). Furthermore, the average number of H400 (keratinocyte) layers and average number of virtual cells at 5 day of culture was significantly higher (P<0.0001) than those of PRKs. Likewise, at day 7, 10 and 14 of cultures, average number of H400 keratinocytes layers were significantly (P=0.025, P=0.044, P=0.016 respectively) greater compared to PRK (cell) layers. While average number of virtual cells of H400 keratinocyte OCs at 5, 7, 10 and 14 days of cultures was determined significantly greater (P<0.0001), (P=0.007), (P<0.0001) respectively than PRK OCs (Table 4.3).

Analysis of H400 and PRK OCs at 14 days of culture based on scaffold as well as scaffold and cell type used, average number of virtual cells and cell layers of H400 OCs were statistically greater (P<0.0001) than those of PRK OCs (Table 4.3) (Figure 4.7).

Table 4.2. H400 and PRK OCs mean thickness on DED, collagen and PET substrates at 14 days. Results from the multivariate general linear model analysis showing the statistical significance of the differences (P<0.001) in the mean thickness of OCs according to the factors "scaffold" (PET, collagen, DED) and their interactions ("scaffold and cell type") at 14 days of culture. (df= degrees of freedom, F = F-statistic test).

Factors	Mean thickness	df	F	P
Scaffolds	Minimum	2	45.191	<0.001
	Maximum	2	153.701	<0.001
	Average	2	130.916	<0.001
Cell type (H400/ PRKs)	Minimum	1	0.866	0.357
	Maximum	1	3.598	0.065
	Average	1	0.133	0.717
Scaffolds and cell type	Minimum	2	17.465	<0.001
	Maximum	2	11.967	<0.001
	Average	2	28.674	<0.001

Figure 4.7 shows the number of cell layers and number of V-cells and the relationship per image field using H400 and PRKs on DED, collagen and PET splitting the data output according to the culture times and the closest to the human gingiva appears to be the H400-DED-14 days. For days 5, 7, 10 and 14 the differences were statistically significant for both number of layers and V-cells (Figure 4.9, Figure 4.10) according to cell type. In addition, the interactions between cell type and scaffold material at day 14 were also statistically significant ($P<0.001$) (Table 4.3). Note that due to the difficulties in generating cultures on PET and collagen scaffolds for periods of less than 14 days, the interactions of cell type and scaffold material could only be investigated at this time point. This might be because of the absence of basement membrane factors in the collagen and PET, which resulted in poor proliferation and stratification of keratinocytes even after 14 days and generated only 2-3 cells layer.

Results in Figure 4.8 show that average number of cell layers increase with average thickness of H400 and PRK OCs for a range of culture periods, determined by linear regression ($R^2=0.732$). This represents that keratinocytes undergo stratification phase in certain period of time by generating cell layers which results in increased thickness of the epithelia. The average thickness and number of cell layers of H400 and PRK OCs on DED at different culture times are higher compared to those cultured on collagen and PET. Figure 4.8 also shows that average thickness and number of cell layers of PRK OCs on DED increase gradually compared to H400 keratinocyte OCs for a range of culture periods (follow the colour sequence), particularly between day 3 and day 5 where thickness increment and cell layers generation is very rapid.

Table 4.3. Factors influencing the number of V-cells and cell layers in H400 & PRK OCs. Results from the multivariate general linear model analysis showing the statistical significance of the differences in the variables recorded (number of layers and number of V-cells per field) according to the factors "cell type" (H400 or PRCs), "scaffold" (PET, collagen, DED) and their interactions ("scaffold and cell type") at different days of culture. (Multivariate general linear model test, F = F-statistic, P = probability, P values smaller than 0.05 were considered significant).

Source	Factor	Variable	F	P
Day 3	Cell type	Layers	4.133	0.061
Day 3		V-cells	15.541	0.001
Day 5	Cell type	Layers	36.043	<0.0001
Day 5		V-cells	47.793	<0.0001
Day 7	Cell type	Layers	6.326	0.025
Day 7		V-cells	9.903	0.007
Day 10	Cell type	Layers	4.876	0.044
Day 10		V-cells	22.046	<0.0001
Day 14	Scaffold	Layers	84.175	<0.0001
Day 14		V-cells	146.616	<0.0001
Day 14	Cell type	Layers	6.3	0.016
Day 14		V-cells	38.486	<0.0001
Day 14	Scaffold and cell type	Layers	32.025	<0.0001
		V-cells	73.413	<0.0001

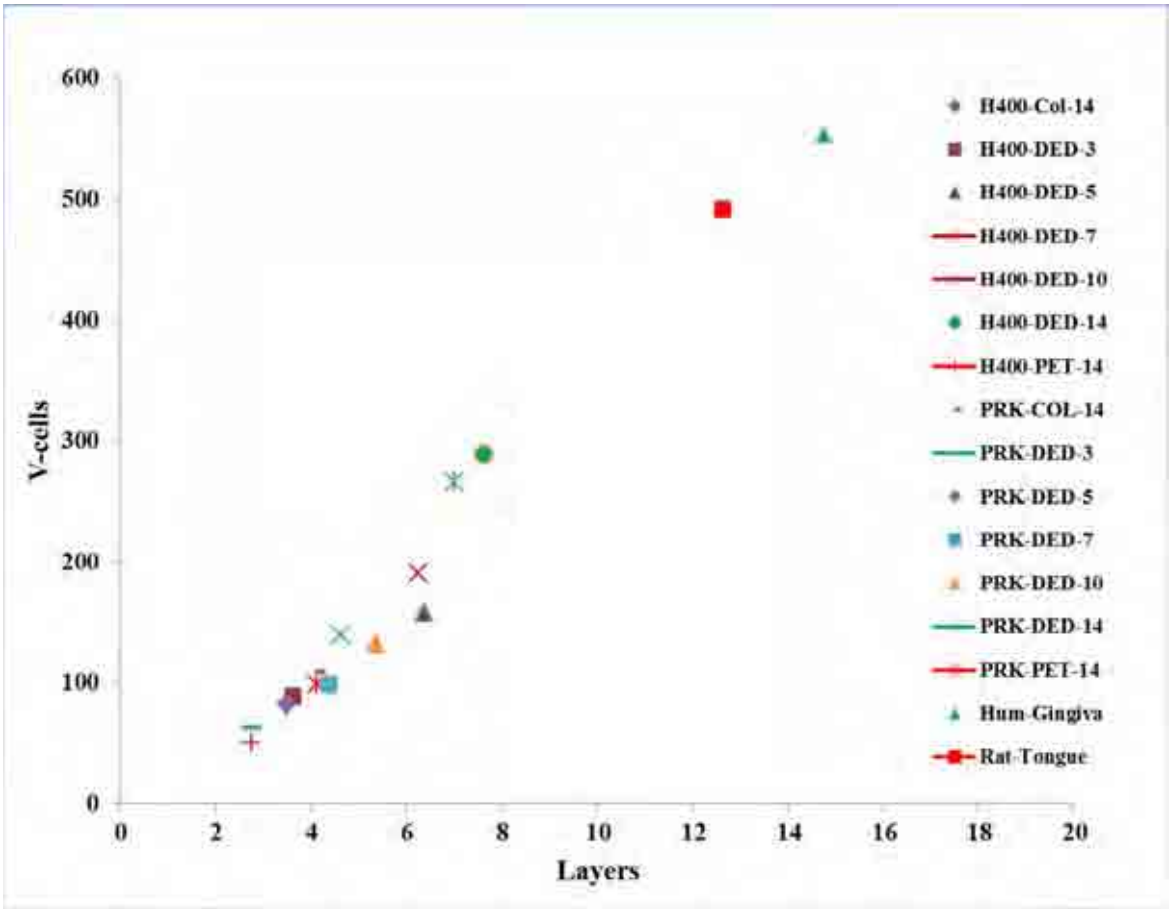

Figure 4.7. **Relationship between average number of layers and number of V-cells in OCs.** Graph showing the linear relation between average number of epithelial layers and number of V-cells per image field (width 353.7 µm) using a x40 objective in samples of human gingiva and rat tongue and in organotypic cultures of H400 & PRK on DED, collagen and PET after different culture periods. All organotypic cultures had less cells and less layers than mucosa samples, however the average layers and number of H400 cells on DED gradually increased with increasing culture days. For PRK cell this trend was also observed (except for 14 days culture, where the average number of layers was less than for 10 days). The number of epithelial layers and number of V-cells was estimated using the method of sequential morphological reconstruction described in section 4.7.

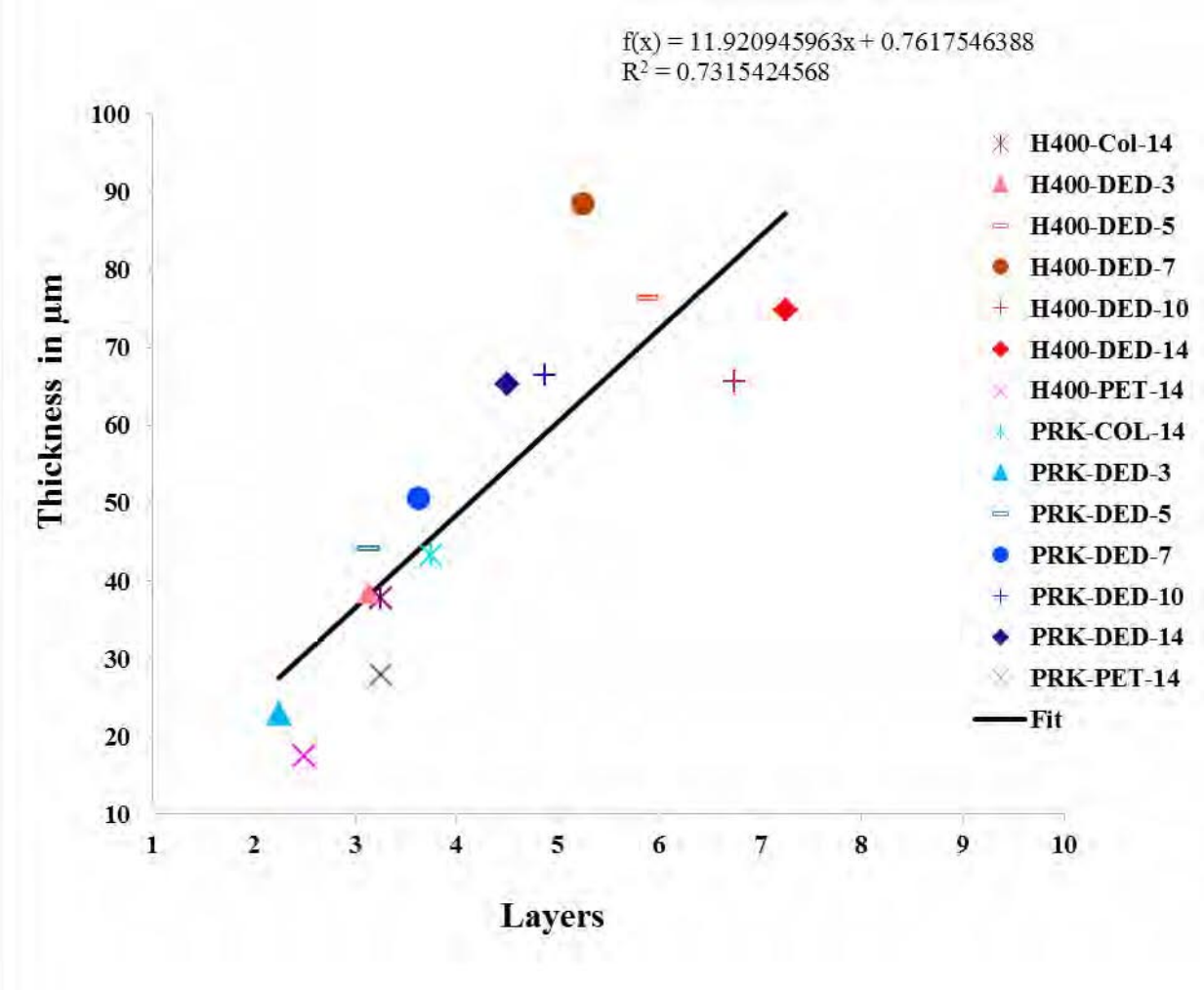

Figure 4.8. **Correlation between average thickness and number of cell layers in OCs.** Graph showing the correlation between average thickness and number of cell layers per image field in samples of H400 & PRK OCs, human gingiva, rat tongue on DED, collagen and PET at different culture times determined by linear regression (R^2= 0.732).

Figure 4.9 shows the average number of V-cells in H400 and PRK OCs on DED at day 3, 5, 7, 10 and 14 of culture which were increased with consecutive days of culture. Likewise, the average number of V-cells in PRK OCs on DED increased with 3, 5, 7 days of culture and remained similar between day 10 and day 14. Noticeably, at 5, 10 and 14 days of culture, the average number of V-cells in H400 and PRK OC was significantly higher compared with days 3 and 7.

Figure 4.10 shows that an average number of cell layers per x40 field of H400 was significantly greater than PRK OCs generated on DED at day 3, 5, 7, 10 and 14 days of culture. Average number of cell layers of H400 OCs increased gradually between day 3 and 5. There was a gradual reduction in the average number of cell layers between day 5 and day 7, however, the average number of cell layers increased again at day 10 and reached to its maximum value at day 14. The average number of cell layers of PRK OCs increased gradually between day 3 and day 10. The number of cell layers of PRK OCs slightly reduced between day 10 and day 14. The units applied are in micrometres and the pixel to micrometre factor is 0.431779.

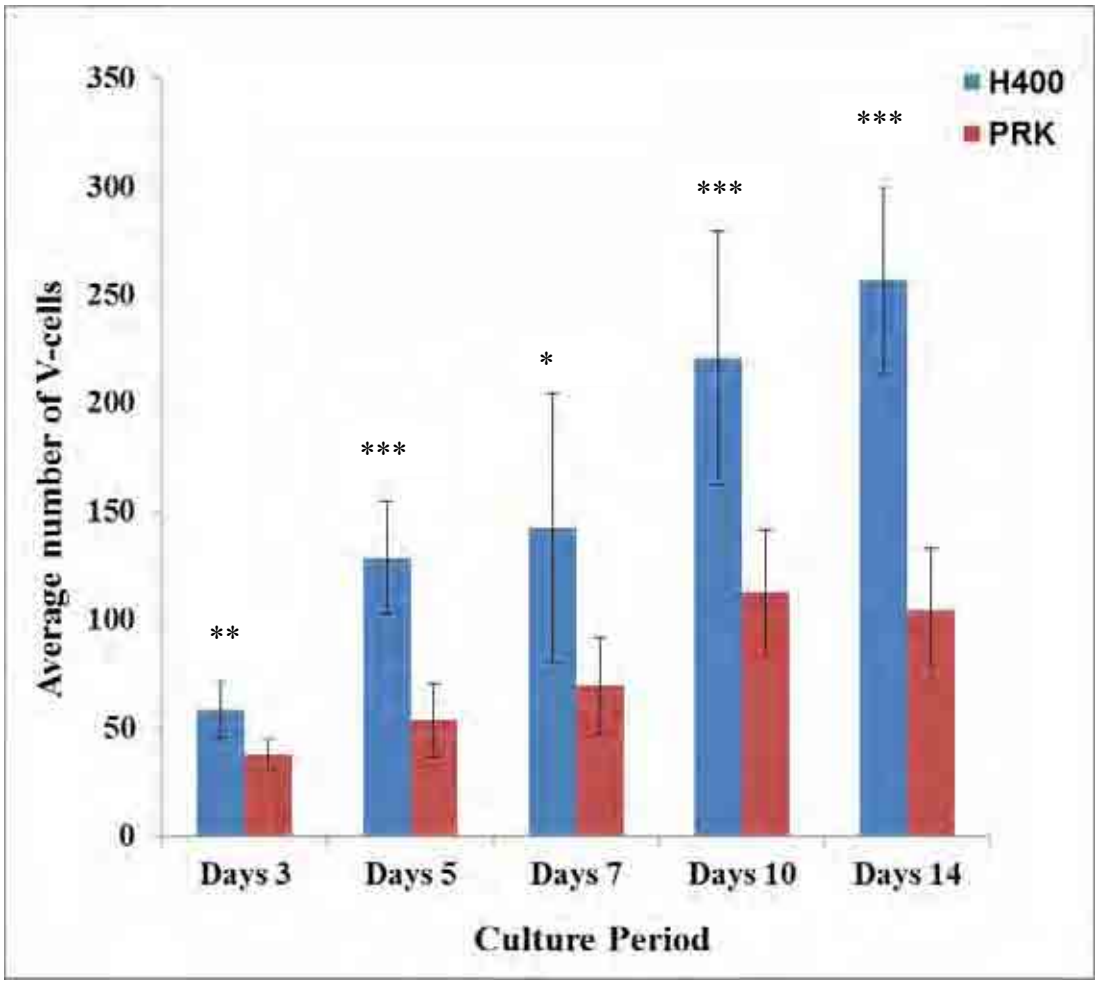

Figure 4.9. **Average number of V-cells in OCs on DED for a range of culture periods.** Number of V-cells per field of view (width 353.7 μm) using a x40 objective in H400 and PRK OCs (n=80) determined by binary reconstruction image processing. The average number of V-cells in H400 and PRK OCs on DED for a range of culture periods was statistically different (*P<0.01, **P<0.001, ***P<0.0001).

Figure 4.11 provides the average number of V-cells of H400 and PRK OCs on DED, collagen and PET at 14 days of culture, determined by binary reconstruction image processing. The number of V-cells from OCs generated on DED (256) was significantly higher than those on collagen (71) and PET (42). Likewise, the average number of V-cells in PRK OCs on DED (104) was significantly greater than those on collagen (83) and PET (60).

The average number of cell layers were determined by image processing of binary reconstruction of H400 and PRK OCs on DED, collagen and PET at day 14 (Figure 4.12). Statistical evaluation also indicates that the average number of cell layers of H400 and PRKs OCs generated on DED was significantly ($P<0.0001$) greater compared with collagen and PET (Table 4.3).

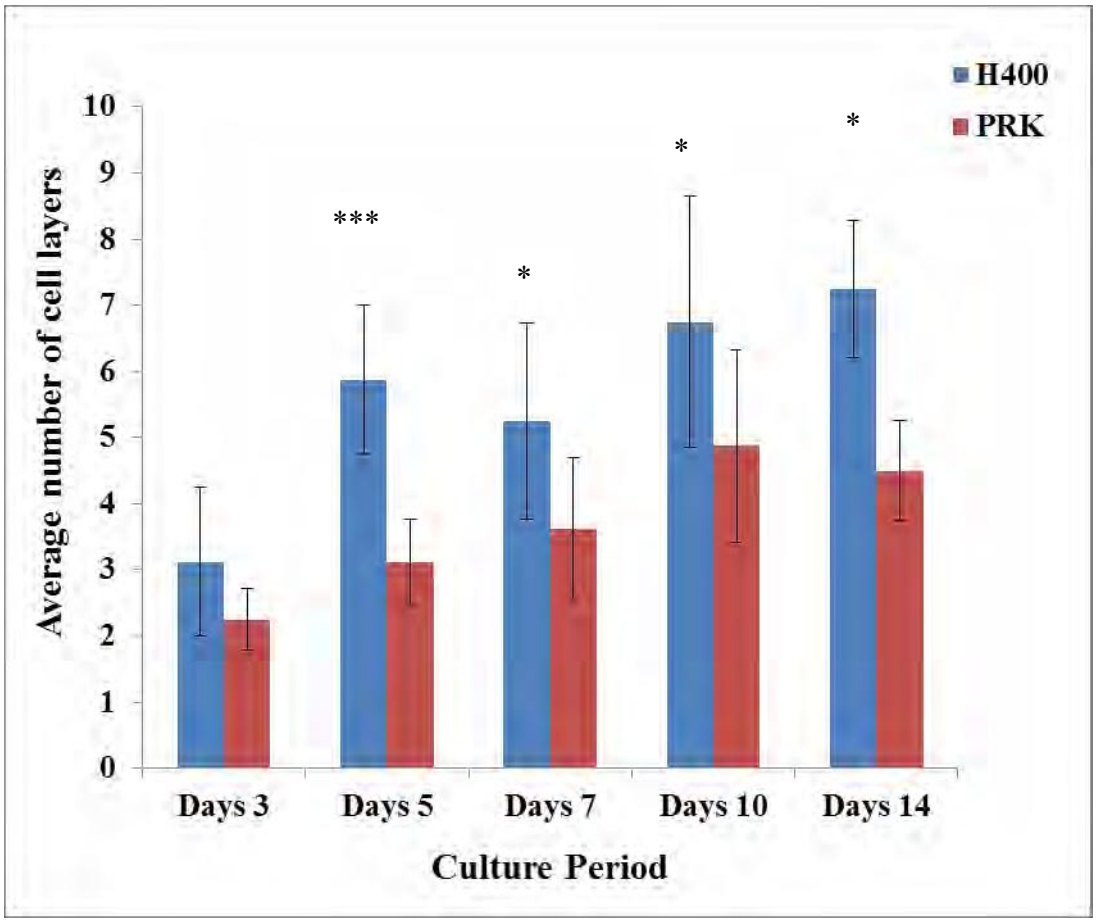

Figure 4.10. **Effect of time on cell layer generation in H400 & PRK OCs on DED.** Graph depicting the effect of time on cell layer generation per field of view (width 353.7 µm) using a x40 objective in H400 and PRK OCs (n=80=number of replicates) determined by image processing. The average number of cell layers of H400 and PRK OCs on DED with different culture time was statistically different (***P<0.0001, *P<0.05).

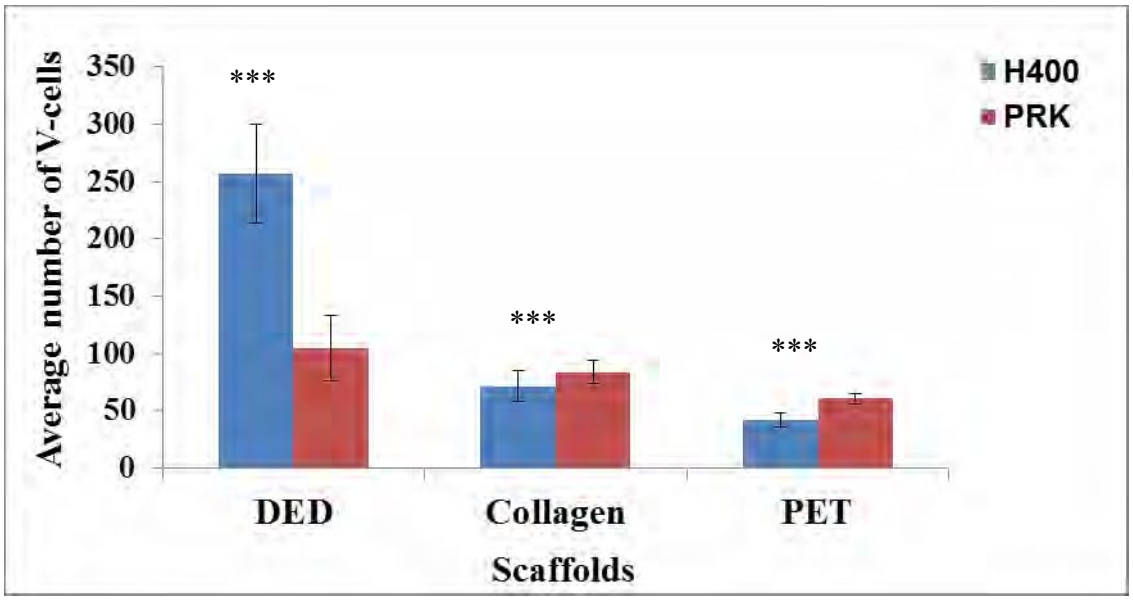

Figure 4.11. **Average number of V-cells in H400 and PRK OCs on DED collagen and PET.** Graph demonstrating the average number of V-cells per field of view (width 353.7 μm) using a x40 objective in H400 and PRK OCs (n= 48=number of replicates) on DED, collagen and PET at 14 days culture. The average number of V-cells in OCs on each scaffold was statistically different (***P<0.0001) from each other.

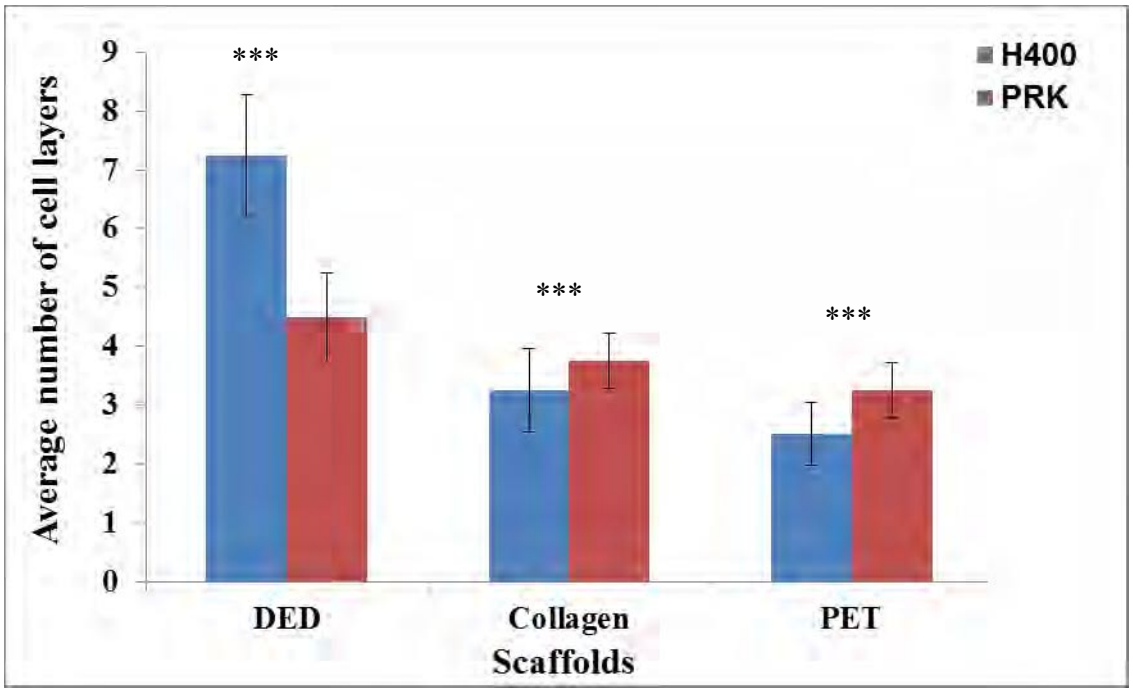

Figure 4.12. **The effect of time on cell layer generation on DED, collagen and PET.** Graph showing average number of cell layers field of view (width 353.7 μm) using a x40 objective of H400 and PRK OCs (n=48=number of replicates) generated on DED, collagen and PET for up to 14 days of culture was statistically different (***P<0.0001) from each other.

4.6 Immunohistochemical (IHC) analyses of 3D OCs

IHC analyses of the expression of several structural proteins on OCs (on the three scaffolds) at 14 days of culture were compared with the patterns of protein expression and distribution in control oral mucosae. The 14 day OCs were selected for this analysis as the epithelia appeared to have achieved a relatively high degree of maturation (e.g. formation of cornified layer) on the scaffolds used.

To compare PRKs and H400 cultures with normal rat tongue and human gingiva (positive controls) respectively, tissue sections were stained using several well characterised parabasal and suprabasal layers (anti-cytokeratins-5, -6, -10, -13) (Figure 4.14, Figure 4.16 A, Figure 4.16 C) markers. Positive staining was detected for the cytokeratins in all PRK and H400 keratinocyte OCs on DED, collagen and PET, which indicated cultures had structurally differentiated suprabasal layers. Involucrin, which is a structural component of the keratinocytes cornified envelope, was also identified in cells cultured at the ALI (Figure 4.15 I, J, K, L, Figure 4.16 B). Moreover, H400 and PRK OCs on DED demonstrated positive staining for the intercellular transmembrane proteins, E-cadherin and desmoglein-3 (Figure 4.15, B, D, F, H). This staining pattern was comparable with that of the normal epithelium controls (Figure 4.15 A, C, E, G) and these data indicated that cell adhesion in OCs likely occurred by means of mature intercellular transmembrane structures.

Analysis using a pan-keratin antibody (anti-keratin positive control) demonstrated the epithelial compartment of normal oral mucosa of human gingiva (Figure 4.13 Ai) and rat tongue (Figure 4.13 Bi) were stained positive for CK 5, 6, 8, 17 and 19. The IgG1 antibody (negative control) showed no visible staining in the

tissue sections of human gingiva (Figure 4.13 Aii) and rat tongue analysed (Figure 4.13 Bii).

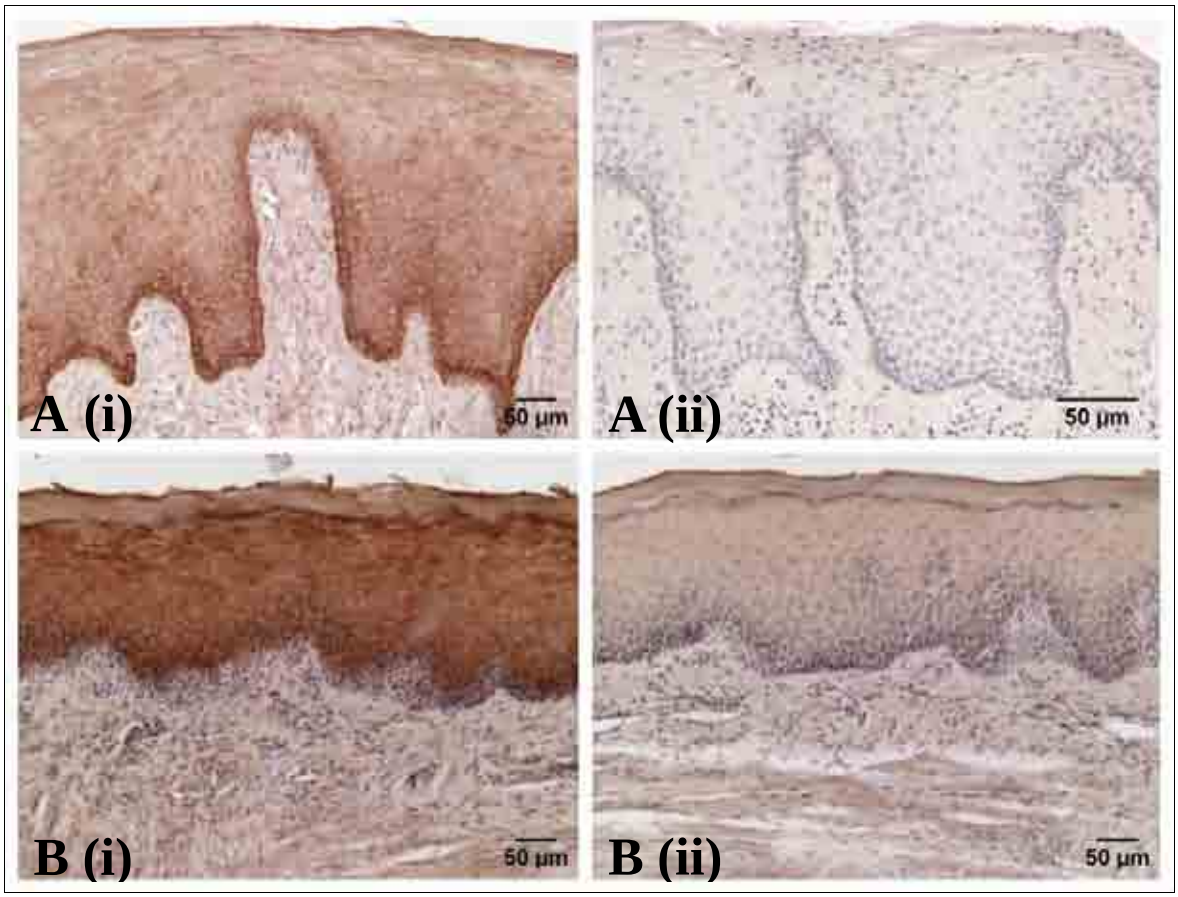

Figure 4.13. **Pan keratin staining of normal human gingiva and rat tongue.** IHC staining of 5 µm sections of normal human gingiva (A) and rat tongue (B) with (i) pan-keratin antibody (positive control) showing presence of cytokeratin in the tissues and (ii) mouse IgG1 (negative control) showing no cross reaction of tissues with staining reagents.

Figure 4.14. **IHC analysis of CK-5, -6, -10, -13 in H400 and PRK OCs on DED and oral mucosa.** 5 µm sections of H400 and PRK OCs cultured for14 days on DED, stained for structural and transmembrane proteins and compared with normal human gingiva and rat tongue. Suprabasal structural protein presence detected for CK5/ CK6 on human gingiva (A), H400 OCs (B), rat tongue (C), PRK OCs (D). CK10 on human gingiva (E) were compared with OCs of H400 (F), rat tongue (G) and PRK OCs (H). CK13 expression profile in human gingiva (I), H400 OCs (J) rat tongue (K), PRK OCs (L).

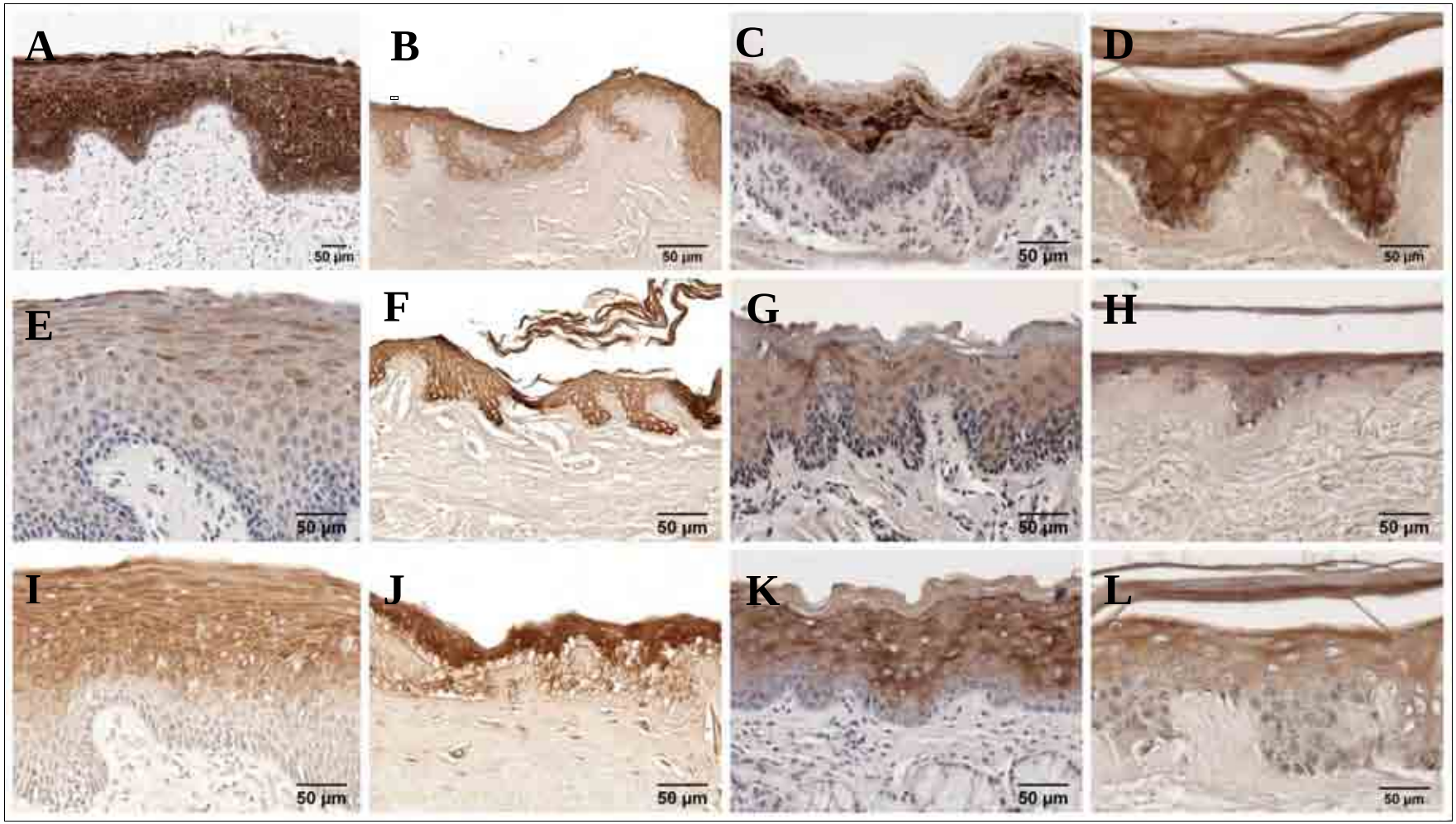
A
B
C
D
E
F
G
H
I
J
K
L
50 µm

Figure 4.15. **E-cadherin, desmoglein-3 and involucrin expression in H400 and PRK OCs on DED and normal oral mucosa.** IHC analysis of 5 μm sections of OCs of H400 and PRKs cultured for 14 days on DED, stained using IHC for structural and transmembrane proteins and compared with normal human gingiva and rat tongue. Presence of cell surface transmembrane proteins, E-cadherin, on human gingiva (A), H400 OCs (B), rat tongue (C) and PRK OCs (D), desmoglein-3, on human gingiva (E), H400 OCs (F), rat tongue (G) and PRK OCs (H). Presence of cell differentiating and superficial layer marker involucrin in human gingiva (I), H400 OCs (J) rat tongue (K), PRK OCs (L).

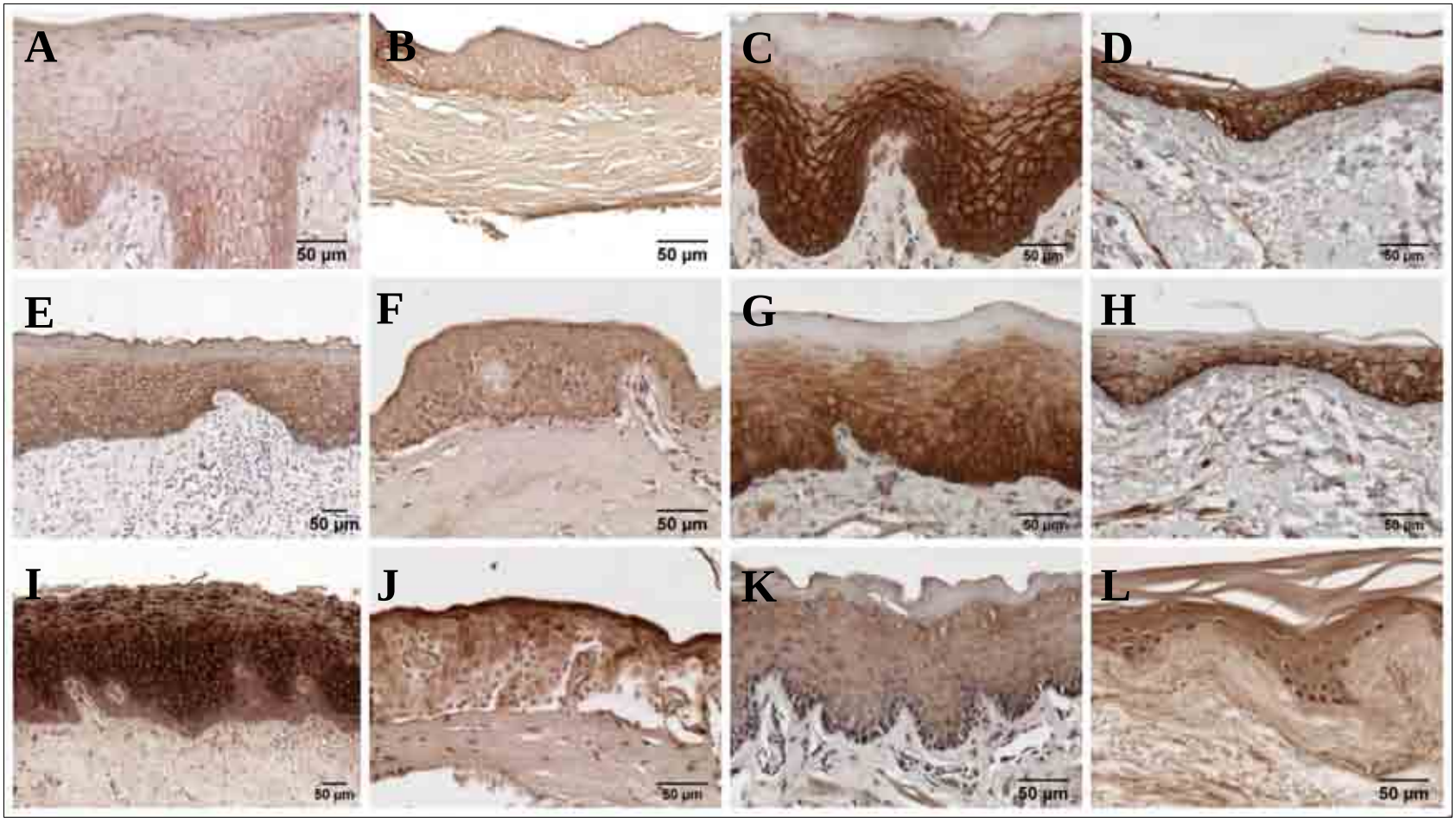
A
50 µm
B
50 µm
C
50 µm
D
50 µm
E
50 µm
F
50 µm
G
50 µm
H
50 µm
I
50 µm
J
50 µm
K
50 µm
L
50 µm

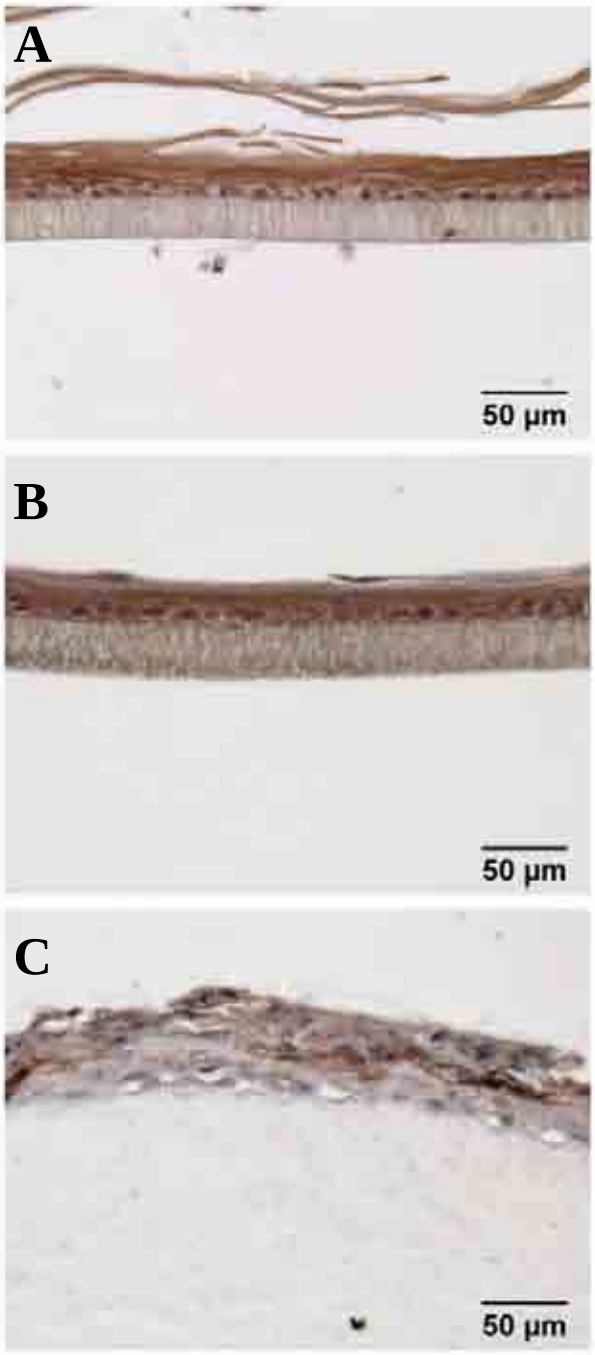

Figure 4.16. **Expression of CK -5, -6, -13 and involucrin in OCs of PRKs on collagen and PET.** IHC of 5 µm sections of OCs of PRKs cultured for 14 days on PET stained with a suprabasal structural protein, CK13 (A), a marker of differentiation found in superficial layers, involucrin (B) and on collagen type I, stained with suprabasal structural proteins, CK5/ CK6 (C).

4.7 RT-PCR analysis of 3D OCs

To determine if H400 keratinocyte and PRK OCs generated on DED, collagen and PET expressed transcript profiles similar to those present within the normal oral epithelium *in vivo*, semi-quantitative RT-PCR analyses were performed. Relative gene expression levels of cytokeratins -1, -5, -6, -10, -13 and the intercellular transmembrane transcripts E-cadherin and desmoglein-3 revealed that H400 and PRK OCs generated on DED scaffolds more closely resembled the expression profile of the control oral epithelium (Figure 4.17 A, 4.17 B, 4.17 C). The results also indicated that the degree of gene expression of involucrin, desmoglein-3, CK-5, -6, -10 and -13 in OCs generated on DED was higher than those of OCs generated on collagen and subsequently PET. This data supported the use of DED as being a better scaffold for 3D OC compared with collagen and PET as it enabled enhanced keratinocyte relevant expression of structural and transmembrane molecules. The degree of gene expression in PCR data was related to the structural and differentiation markers of OCs on DED determined by IHC profile which is comparable to the controls.

Figure 4.17. **Semi-quantitative RT-PCR analysis of selected genes involved in structural integrity of OCs of H400 and PRK analysed at 14 days of ALI culture.** Data demonstrated the degree of gene expression in OCs generated on DED was generally relatively higher compared with that in OCs generated on collagen and PET and more similar to controls (human gingiva and rat tongue). (A) Representative gel images (n = 2=number of replicates) are shown.

(A)

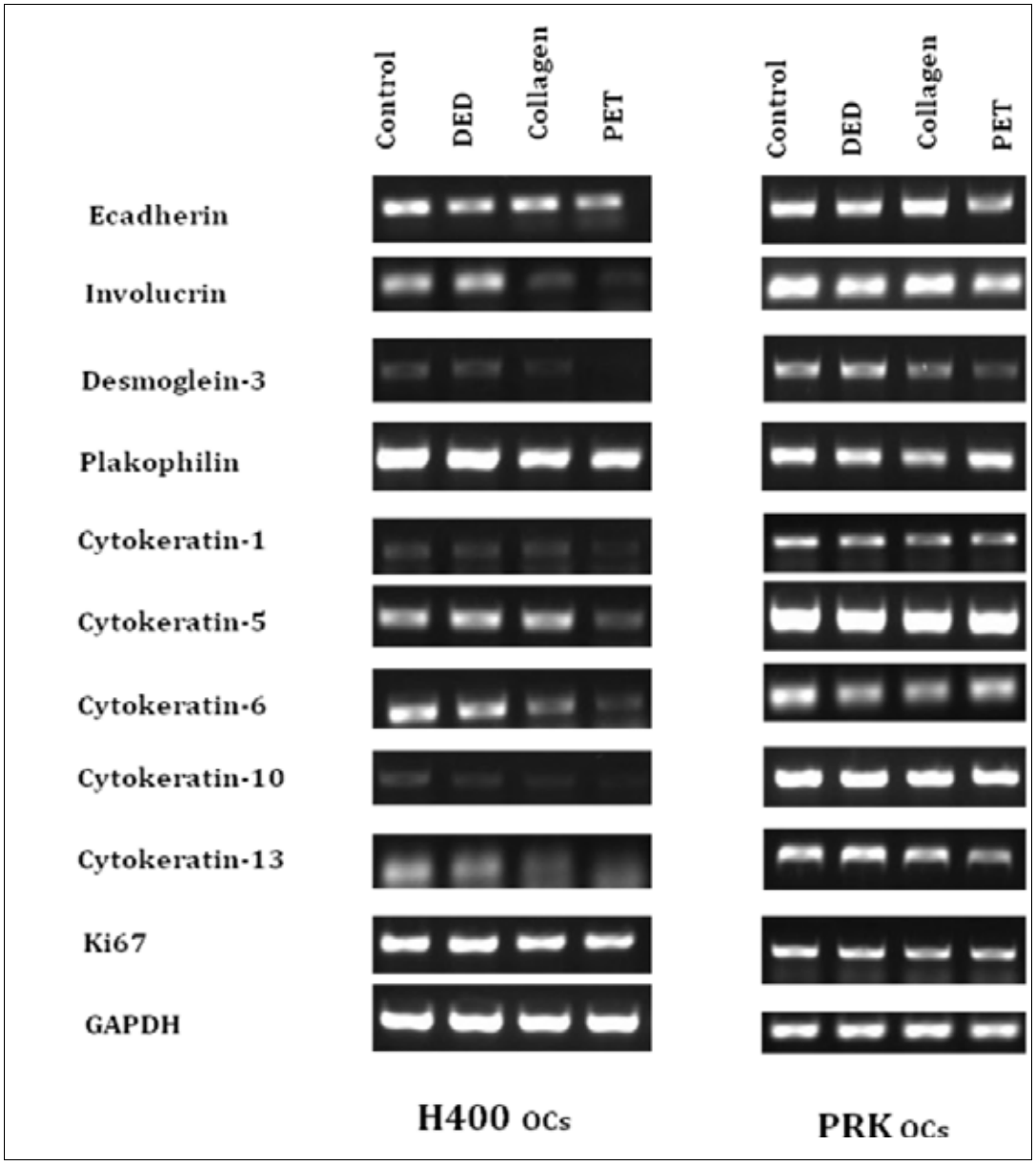
Control
DED
Collagen
PET
Control
DED
Collagen
PET
Ecadherin
Involucrin
Desmoglein-3
Plakophilin
Cytokeratin-1
Cytokeratin-5
Cytokeratin-6
Cytokeratin-10
Cytokeratin-13
Ki67
GAPDH
H400 OCs
PRK OCs

Figure 4.17. Relative expression levels are shown as percentage of the highest level (using human and rat gene primers respectively) detected in OCs of (B) H400 and (C) PRKs. Amplified product values were normalised to human and rat glyceraldehyde-3-phosphate dehydrogenase (GAPDH) housekeeping gene levels respectively.

(B)

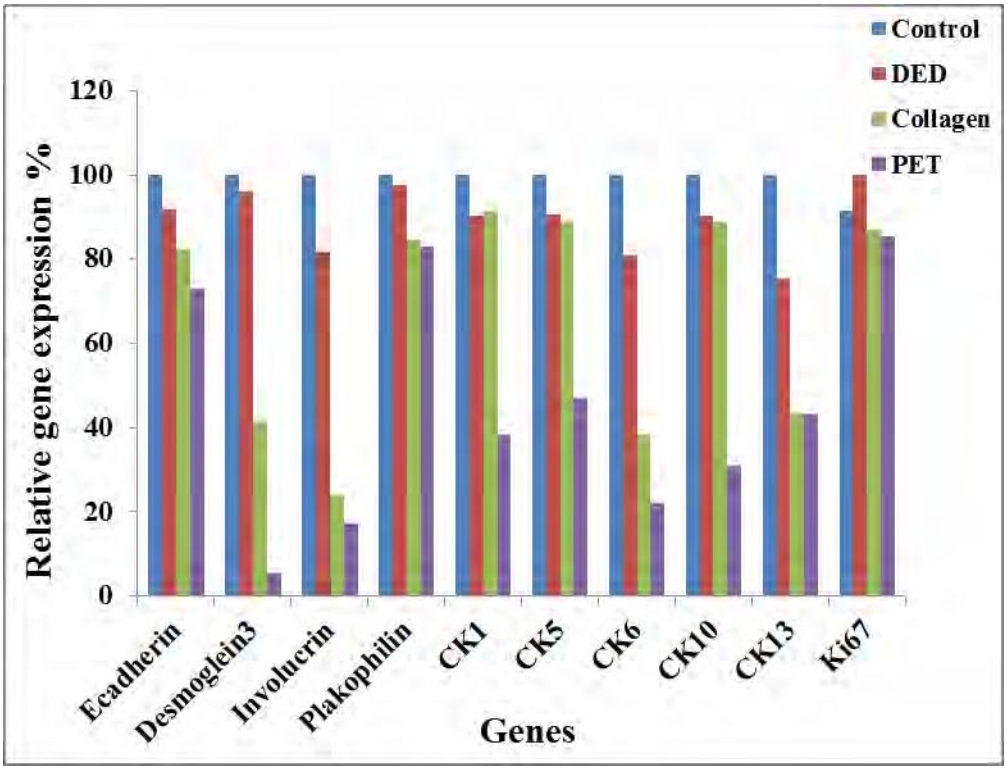
Control
DED
Collagen
PET
120
100
80
60
40
20
0
Relative gene expression %
Ecadherin
Desmoglein3
Involucrin
Plakophilin
CK1
CK5
CK6
CK10
CK13
Ki67
Genes

(C)

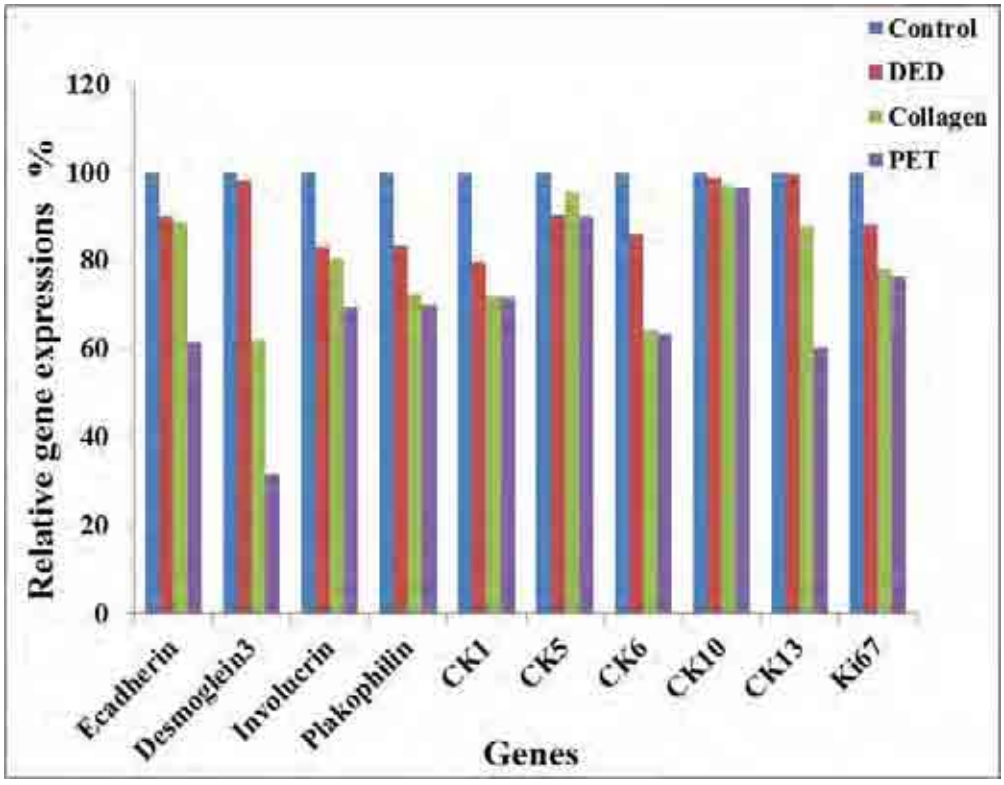
Control
DED
Collagen
PET
120
100
80
60
40
20
0
Relative gene expressions %
Ecadherin
Desmoglein3
Involucrin
Plakophilin
CK1
CK5
CK6
CK10
CK13
Ki67
Genes

CHAPTER 5 DISCUSSION

5 Discussion

The aim of the present study was to generate and characterise OCs to enable identification of the most appropriate methods for generating/engineering oral mucosa *in vitro.* Such OCs, which have been characterised in the present study, provide a useful laboratory study model and may have application in future clinical use. Initially towards this goal, it was therefore important to analyse the cellular and molecular characteristics of 2D keratinocyte monolayer cultures as these cells are the major population within the *in vivo* oral epithelium. In previous studies, immortalised skin keratinocyte cell lines including HaCaT (Boelsma *et al*., 1999), DJM-1, derived from a human skin squamous cell carcinoma (Aoyama *et al.,* 2008; Nagae *et al*., 1987), HFK, from human foreskin, (Lambert *et al.*, 2005) and OKF6/TERT-2 from human oral mucosa (Dongari-Bagtzoglou and Kashleva, 2006) have been used to generate OCs. Data from these studies suggested that the H400 keratinocyte cell line, derived from human alveolar tissue, was appropriate for use in the present study. H400 keratinocytes were relatively easy to culture, particularly as they do not require feeder layers for survival *in vitro* as necessitated for many primary keratinocyte culture systems. However, there are currently no previous studies reporting the use of H400 keratinocytes for generation of OCs. Rat tongue PRKs were the other type of cell used in this study and these cells were more complex to isolate and required a low density fibroblast feeder layer to establish and maintain cultures. Molecular and cellular analysis of monolayer and OCs however indicated that relatively pure populations of PRKs were obtained and enabled comparison of the two cell types with the normal oral mucosa. In general, once established, both PRKs and H400 keratinocytes attached to cultureware and grew relatively rapidly in monolayer cultures and exhibited growth

characteristics similar to those described previously for epidermal cells (Fusenig *et al*., 1983; Kubilus *et al*., 1979).

5.1 Characterisation of monolayer cell cultures generated in high and low calcium media

The quantitative cell counting using a semi-automated thresholding method has been performed and reported here for the first time. Analysis of Haematoxylin stained images of H400 and PRKs demonstrated that these cells were morphologically similar and enabled the growth of monolayer cultures in high and low calcium medium. This study also confirmed that cells exhibit different patterns of culture growth which was calcium-dependent. Data obtained using both the MTT assay (Figure 3.2) and the computerised semi-automated cell counting method (Figure 3.4) demonstrated that exposure of both H400 cells and PRKs to low calcium (0.1 mM) containing media resulted in relatively rapid growth and colonisation compared with culture in high calcium (1.8 mM) containing media.

Indeed there were greater percentage areas of coverage detected for H400 cells cultured in low calcium media at days 4, 6 and 8 compared with cultures in high calcium medium. This data is consistent with previous studies which have demonstrated that keratinocytes proliferate at a faster rate in low calcium compared with high calcium containing medium (Leigh and Watt, 1995). It has been previously proposed that keratinocytes do not efficiently establish desmosomal junctions in low calcium media at concentrations below 0.1 mM which subsequently enables higher rates of proliferation and confluent cultures to occur more rapidly (Aoyama *et al.*, 2008). Cultures of keratinocytes in low calcium medium therefore have the potential for comparatively rapid generation of relatively large cell for future downstream

experimental or clinical application. Furthermore, the average area of a single H400 was increased in low calcium medium compared to those in high calcium medium due to the change in osmolarity.

In this study, elevating the calcium concentration to 1.8 mM within the culture medium stimulated the expression of markers representative of a squamous cell differentiated molecular phenotype as determined by up-regulation of cytokeratins -1, -4, -5, -6, -10 and -13 as compared with expression levels in cultures in low calcium medium (Figure 3.12 A). This data is consistent with previous reports which indicated that epithelial cells more rapidly undergo terminal differentiation in high calcium containing medium as determined by cell and molecular phenotype (Tsutsumi *et al.*, 2000; Jetten, 1987; Rearick *et al*., 1987; Rearick and Jetten, 1986). In addition high calcium concentrations can also influence endogenous involucrin gene expression (Deucher *et al.*, 2002) by increasing transglutaminase type I activity which enhances the cross-linked envelope formation in epithelial cells (Rice *et al*., 1989; Rubin and Rice, 1986). This data is also consistent with that reported here (Figure 3.12 A) and therefore it may also be of interest to compare transglutaminase type I activity in these cultures.

Reportedly higher medium calcium concentrations above 0.1mM also result in greater cell-cell contacts mainly due to adherens junctions and desmosome formation (Leigh and Watt, 1995; Aoyama *et al.*, 2008). Consistent with this, in the present study E-cadherin (a calcium-dependant transmembrane molecule present in epithelial cells) (Bankfalvi *et al.*, 2002), was also up-regulated in high calcium medium cultures. The interaction of desmocollin-3 with plakoglobin and subsequent interaction with desmoglein-3 to form desmosomes is also reportedly sensitive to extracellular calcium

levels (Aoyama *et al.*, 2008) and therefore it also perhaps not surprising to find that this molecule was highly expressed in cultures containing high calcium compared with low calcium medium (Figure 3.12). In the present study cell numbers were much higher at day 8 as compared with day 6 and 4 in high calcium medium likely due to increased cell-cell contact for a range of culture periods which resulted in up-regulation of differentiation and adhesion molecule transcripts (Figure 3.11).

Immunohistochemical analysis presented here demonstrated the distribution of the proliferation associated protein (Ki67), the differentiation markers (CKs -1, -5, -6, -10 & -13) (Figures 3.7 & 3.9), involucrin (Figures 3.8 & 3.10) and the cell-cell adhesive proteins (E-cadherin & desmoglein-3) (Figures 3.8 & 3.10) in monolayer cell cultures generated in high and low calcium medium. This data was also supported by that obtained using RT-PCR (Figure 3.12) and in general demonstrated that monolayer culture cells were relatively poorly stratified in low calcium medium compare with those generated in high calcium containing medium. Combined these findings suggest that in terms of OC generation for clinical applications, it might be possible to initially induce a rapid expansion of the cultures in low calcium media and then having generated an appropriate number of cells, to subsequently trigger stimulation of maturation of the cultures by increasing the calcium content of the media.

5.2 Organotypic cultures

OCs generated using different scaffolds have been previously characterised to some degree using histological (Costea *et al.*, 2005) and immunohistochemical techniques (Boelsma *et al*., 1999; Zacchi *et al*., 1998; Liu *et al*., 2008a). In addition, transmission electron microscopy (Moharamzadeh *et al*., 2008) has been used to investigate ultrastructural features such as desmosomal junctions between

keratinocytes and cytoplasmic keratins in superficial epithelial layers. Although OCs have been previously generated using primary or immortalised keratinocytes (Wan *et al*., 2007; Boelsma *et al*., 1999) detailed quantitative microscopic characterisation in comparison with normal mucosal architecture has not been previously performed. In the present study a semi-automated quantitative imaging method was used for architectural characterisation of H400 and PRK stratified OCs generated on the three different substrates/scaffolds of DED, collagen and PET after 14 days growth at the ALI. In line with the monolayer studies OCs were generated in high calcium concentration media (1.8 mM). Moreover H400 and PRKs were also cultured and analysed on DED for 3, 5, 7, 10 (Figure 4.3) and 14 days (Figure 4.5) of culture to determine the degree of stratification for each day of culture (**see section 2.8)** however, such a detailed time-point study was not possible for OCs generated on collagen and PET due to their poorer rates of maturation**.**

The ALI culture approach is used to generate OCs to facilitate generation of tissues with a relatively normal epithelial architecture and function for oral regenerative procedures (Igarashi *et al*., 2003). Full thickness engineered human oral mucosa has been clinically used as an intra-oral graft for vestibuloplasty, freeing of tongue (Lauer and Schimming, 2001; Sauerbier *et al*., 2006), palatal surgery (Luitaud *et al*., 2007), lip surgery (Xiong *et al*., 2010), periodontal plastic surgery and peri-implant gingival graft (Mohammadi *et al*., 2007; Mohammadi *et al*., 2011). Engineered oral mucosa equivalents have also been used as extra-oral clinical grafts for urethroplasty (Bhargava *et al*., 2008; Selim *et al*., 2011).

3D engineered human oral mucosa have also been used *in vitro* as model of drug delivery (Hearnden *et al*., 2009), oral diseases such as bacterial and fungal

infection (Gursoy *et al*., 2010), cancer invasion (Marsh *et al*., 2011) and to evaluate biocompatibility of dental materials and oral health products (Moharamzadeh *et al*., 2012). New aspects of the engineered oral mucosal research are angiogenesis and radiation-induced oral mucositis (Perez-Amodio *et al*., 2011; Tobita *et al*., 2010).

It is reported that culture at the ALI results in oxygen tension (oxidative stress) necessary to stimulate the OCs to mature and stratify (Tammi and Jansen, 1980). Consistent with previous reports, in the present study this exposure also appeared to play an important role in the growth and differentiation of the OCs. The culture of H400 and PRK OCs at the ALI resulted in direct exposure to oxygen present within air which reportedly promotes OC differentiation (Prunieras *et al*., 1983). The mechanisms involved in this process are reported to involve oxidative stress increasing intracellular levels of glutathione-sulfhydryl group (GSH) and at the ALI and the cellular GSH levels have been reported to be increased by 4 - 5 fold (Kameyama *et al*., 2003). Others (Kang *et al*., 1994; Kameyama *et al*., 2003) have previously reported that high levels of GSH enhance intracellular glutamine synthesis which stimulates cell proliferation and growth. Keratinocyte exposure to air has also been shown to accelerate cellular differentiation and the synthesis of membrane-coating granules containing lipids (Prunieras *et al*., 1983) which resulted in the formation of a permeability barrier. Future studies could therefore involve the analysis of oxidative stress signalling within OC generated below, and at, the ALI as this may identify pathways important in regulating key keratinocyte differentiation pathways.

5.2.1 Scaffold thickness and cell layer number of OCs

Engineered oral mucosa equivalents have been developed for clinical application and also for *in vitro* studies of biocompatibility, mucosal irritants and

disease (Moharamzadeh *et al.,* 2007). Several studies have reported successfully generating engineered oral mucosa by culturing oral keratinocytes with or without fibroblasts on collagen (Masuda, 1996; Rouabhia and Deslauriers, 2002), de-epidermalised dermis (DED) (Patterson *et al*., 2011; Colley *et al*., 2011; Ophof *et al*., 2002) and polyethylene terephthalate (PET) (Moharamzadeh *et al.,* 2008). In the present study the thickness, in terms of actual size as well as in cell layers, of H400 and PRK OCs after 14-days on DED was found to be significantly greater than OCs generated on collagen and PET as demonstrated by means of quantitative imaging (Figure 4.5, 4.12). Clearly, the thickness of cultured epithelium in OCs was significantly influenced by the scaffold material used.

5.2.1.1 DED

DED has been used *in vitro* for generation of OCs for reconstruction of human hard palate mucosal epithelium (Cho *et al*., 2000) and is regarded as the 'gold standard' scaffold for culture of keratinocytes (Ojeh *et al*., 2001). In the present study oral keratinocytes cultured on DED demonstrated similar histological and immunohistochemical characteristics (Figure 4.14, 4.15) to those of normal oral epithelium. It is possible that due to the presence of the basement membrane components (laminin 5 and collagen IV) in DED (Figure 4.2) (Krejci *et al*., 1991; Prunieras *et al*., 1983) that these molecules enable keratinocyte attachment to connective tissue and therefore contribute to the generation of a basal layer which consequently modulates and facilitates cell growth and differentiation. In the present study H400 and PRKs were co-cultured with fibroblasts on DED. The presence of fibroblasts has previously been shown to inhibit the cell death of basal cells and to increase terminal differentiation of cells towards the superficial layers of stratified

epithelia (which is also a normal pattern of differentiation in native oral mucosa) resulting in the development of stratum spinosum (Costea *et al.,* 2003) and stratum corneum (when present). In addition, keratinocyte growth factor (KGF) is endogenously secreted by fibroblasts in co-cultures and this growth factor has been shown to be important in modulating keratinocyte growth and differentiation (Potten *et al.,* 2002) in OCs *in vitro* (Costea *et al.,* 2003) as well as epithelium *in vivo.* (Danilenko, 1999). Interestingly, it has previously been reported that poor fibroblast migration occurs through DED and epithelial islands can form due to the invasion of keratinocytes from the papillary (epithelial) surface of DED affecting the thickness of the engineered oral mucosa (Moharamzadeh *et al.,* 2007). In the present study, however, no such epithelial islands were detected at the culture times investigated and therefore this appeared not to contribute to the thickness and cell layer number generated in OCs. Alternatively the connective tissue invasion by epithelial cells might require longer culture times than those studied providing a possible explanation as to why this was not observed here. Squier and Kremer (2001) reported that epithelial tissue homeostasis is modulated by proliferation of the basal cell layer followed by differentiation and desquamation at the epithelial surface. The average number of cell layers produced on DED was greater than that observed on collagen and PET and although there were fewer layers when compared with normal human oral epithelium, the pattern of maturation appeared to be maintained (showing keratinocytes which grew, underwent differentiation and migrated to the surface as a cornified layer of epithelium). This resulted in an increased thickness of OCs on DED compared with those generated on collagen and PET.

In the present study the thickness of H400 OCs generated on DED gradually increased from day 3 and reached a maximum thickness by day 7 due to cell proliferation and differentiation. Between day 7 and day 10 the thickness of OCs was slightly reduced possibly due to the onset of desquamation of surface epithelial cells. At day 14 the thickness appeared to be greater than day 10, when the formation of a cornified thick layer was noted. In the case of PRK OCs, however, the thickness gradually increased between day 3 and 10 but reduced at day 14, also most likely due to desquamation of surface keratinocytes as observed histologically.

5.2.1.2 Collagen

Collagen gels have been reported to provide a suitable substrate for keratinocytes to form multilayers on and prevent epithelial cell invasion and island formation within the scaffold (MacCallum and Lillie, 1990). Collagen has high compatibility for supporting growth and function of oral keratinocytes and can be manufactured into devices that are adhesive and can be sutured for clinical use (Glowacki and Mizuno, 2008). The presence of ECM components within a substrate is likely to influence the establishment and maintenance of cell proliferation and differentiation and therefore collagen in the form of highly porous lattice sponges were utilised (Moharamzadeh *et al.*, 2008; Navarro *et al*., 2001; Breitkreutz *et al*., 1997). In the present study, when fibroblasts were incorporated in gels the cells appeared contracted and were found to be unsuitable for further keratinocyte surface culture (Bell *et al*., 1981; Lopez Valle *et al.*, 1992). Although the thickness of OCs was 3 to 4 cells (Figure 4.12), the histological appearance of H400 and PRK OCs on collagen gels indicated regular stratification and uniform differentiation (Figure 4.5). It is possible that manipulation of the collagen gel concentrations may enable incorporation of

fibroblasts to better support the generation of keratinocyte OCs. Additionally incorporation of other types of structural molecules (laminin 5, or collagen type IV or VII) might facilitate adhesion to the scaffold and formation of basement-like membrane structures.

5.2.1.3 PET

PET is a synthetic relatively inert porous polymer that does not contain an organic or ECM component. It is therefore likely that for these reasons that a lower degree of maturation and stratification (only 2-3 cell layers) occurred on this substrate compared with DED and collagen (Figures 4.8 and 4.12). PRKs appeared to attach better to PET compared with H400 cells (Figure 4.5) resulting in better PRK OC generation however as only minimal cell layers were generated after 14 day culture OCs on PET were not able to be analysed at earlier time-points. The coating of the PET substrate with basement membrane components or the inclusion of growth factor stimulants, such as KGF, may also enable improved OCs to be generated using this material and represents a possible future direction for research.

5.2.2 Quantitative imaging to determine OCs thickness and cell layer number

Quantitative imaging enabled the determination of the thickness of OCs on a morphometric basis (Figure 4.4, 4.6). Furthermore quantitative microscopy provided an unbiased quantitative determination of OCs thickness and cell layer number in the OCs of H400 and PRKs on DED, collagen and PET (Figure 4.8, 4.10) for different culture periods by means of segmentation of the epithelial compartment using the computation of theoretical cells (Figure 4.7, 4.9) based on the positioning of the cell nuclei.

The present study has shown that the thickness of the epithelium is a parameter that might enable tissue architectural characterisation by providing quantitative feature that can be subjected to statistical analysis. The formation of a multi-layered epithelium by keratinocytes seeded on the surface on DED was compared with that of keratinocytes seeded onto a collagen type I and PET. On collagen and PET, only a relatively few cell layers were produced and appeared to lack a stratum corneum (Figure 4.5, 4.12). The image analysis approach applied here provided a better understanding of tissue architecture and enabled identification of the morphological markers that might contribute to the identification of the most appropriate methods for generating/engineering oral mucosa *in vitro.* In future the application of this analytical technique may enable improvement in strategies for tissue engineering compared with the current more qualitative comparative approaches.

5.2.3 IHC analysis

In skin and oral mucosa stratified squamous epithelia demonstrate the expression of structural and differentiation markers in different region of suprabasal cell layers (Figure 4.14, 4.15) (Mackenzie and Fusenig, 1983b). In this study, stratified OCs of H400 and PRKs generated on DED expressed *in vivo*-like patterns of differentiation. IHC analysis of H400 and PRK OCs generated on DED at day 14 indicated that involucrin was expressed in several layers but in particular was more predominant in the upper suprabasal layers of the stratified epithelium (Figure 4.15). This finding was consistent with previous reports demonstrating its expression in human oral mucosa during terminal differentiation (Carroll *et al*., 1993; Stark *et al*., 1999; Barrett *et al*., 2005) and that its expression is reportedly due to the accumulation of cholesterol sulphate resulting in cross-linked envelope formation in epithelial cells

(Nagae *et al*., 1987). The differentiation of OCs on DED is supported by the presence of involucrin which appeared in its typical distribution and is associated with the transition of the cells from the spinous to the corneum layer in keratinised epithelia. (Thacher and Rice, 1985; Banks-Schlegel and Green, 1981).

In the present study the stratified organotypic epithelium also demonstrated the synthesis of a number of cytokeratins. In H400 and PRK OCs generated on DED keratinocytes in the suprabasal compartment expressed the differentiation markers including CK-5, -6, -10 and the distribution of these proteins was similar to that in the normal oral mucosa (Figures 4.14) (Stark *et al*., 1999; Liu *et al*., 2008b; Moharamzadeh *et al*., 2008). Similarly, CK-13 showed a significant and uniform staining in the suprabasal layers of OCs and this expression also closely resembled that detected in the native oral mucosa shown here (Figures 4.14 and 4.16) and reported elsewhere (Costea *et al*., 2003). The presence of E-cadherin in OCs (Figure 4.15) supports the hypothesis that E-cadherin maintained polarity and tissue structure by establishing cell-cell contact which contributed to the tissue architecture resulting in increased thickness of OCs generated on DED (Figure 4.4) (Gumbiner *et al*., 1988). In addition to the E-cadherins, desmosomal cadherins (desmoglein-3 and desmocollin) were expressed as membrane-spanning glycoproteins (Delva *et al*., 2009) in OCs and regulated calcium dependent cell adhesion (Green and Jones, 1996) by linking with intermediate filament (Michels *et al*., 2009; Kowalczyk *et al*., 1999). OCs generated on collagen and PET did not show such a high degree of differentiation as was detected in OCs on DED however a few cell layers were generated and analysed by IHC which indicated that cells on collagen and PET had not proliferated and migrated well from the basal to the surface layers. In contrast the surface cell layers generated at the ALI

stained positive for CK-5, -6 (on collagen) and CK-13 and involucrin (on PET) (Figure 4.16) typically located more superficially in native oral mucosa. Combined this data on protein expression and profile supported the use of DED for generating OCs that best resemble normal oral epithelium. In the present study, image analysis for measuring expression of an antigen using DAB was not performed because the antigen-antibody reactions are not stoichiometric.

5.2.4 RT-PCR analysis of OCs

The gene expression profiles of structural and differentiation molecules including E-cadherin, desmoglein-3, involucrin and cytokeratins -1, -4, -5, -6, -10, -13 were analysed in H400 and PRK OCs generated at 14 days culture (Figure 4.17). RT-PCR data indicated that these transcripts were more abundantly expressed in OCs generated on DED compared with collagen and PET and were also at comparable levels with those detected in the oral mucosa (Figure 4.17). This data provided further support for that which already indicated that culture on DED generated OCs was more comparable with normal oral epithelium compared with those generated on collagen and PET. It is possible that cell-cell contact may lead to activation of transcription for a range of cell membrane and suprabasal molecules in 3D OCs (which may also occur *in vivo*) as keratinocytes differentiate from the basal to the superficial cell layers. It is also likely that due to the limited adhesion of keratinocytes to the surface of the collagen and PET that this process is a key step in the regulation of epithelial development and maturation.

5.2.5 Effects of growth supplements

Studies *in vitro* have also reported that proliferation of keratinocytes is induced by EGF and insulin-like growth factors. EGF (5-20 ng/ml) not only increased cell growth 2.5-fold but also increased cell layering in culture (Lechner *et al.*, 1981). In the present study, keratinocyte culture medium was supplemented with EGF (20 ng/ml) and insulin (5 mg/ml) in order to promote cell proliferation and differentiation. It is likely that these regulatory factors also play a role in maintaining a balance between proliferation and differentiation *in vivo* (Jetten *et al*., 1986). Further work could be performed to determine more optimal culture conditions, including addition of chemical and protein supplements, which would support OC generation on a variety of substrates.

6. Conclusions

H400 and PRKs were used to generate monolayer and organotypic cultures of oral epithelium. Cellular interactions and changes in gene expression were determined as oral keratinocytes grew in two and three dimensional cultures for a range of culture periods. Computerised quantitative microscopy allowed identification of architectural characteristics of cell cultures.

- During growth, increased cell-cell contact resulted in activation of transcription for a range of cell membrane molecules which may also occur *in vivo* as cells migrate and differentiate from the basal cell layer to the surface layer. In monolayer cultures, a high degree of confluency with respect to range of culture periods provided a better understanding of the expression of structural molecules within the oral mucosa.
- Low calcium concentration in culture medium influenced increased cell growth rates in monolayer cultures compared with keratinocyte cultures generated in high calcium medium as determined by the MTT assay and semi-automated cell counting. Furthermore, high calcium concentration resulted in up-regulation of adhesion and differentiation molecules including E-cadherin, plakophilin, desmocollin-3, desmogleins-3 and cytokeratins-1, -5, -6, -10, -13 in monolayer cultures as determined by RT-PCR analysis.
- Quantitative microscopy of OCs of H400 and PRKs a novel method which enabled unbiased quantitative determination of thickness and cell layer number in the OCs by means of segmentation of the epithelial compartment based on computation of theoretical cells and layers based on the identification of cell nuclei.

- Image analysis also enabled a quantitative comparison of tissue structure and maturation of OCs with the normal architecture of oral mucosa by relating epithelial thickness and cell layer numbers for a range of culture periods.
- The scaffold materials used in the present study (DED, collagen type I and PET) differentially influenced cell behaviour in OCs of oral epithelia. Cultures generated on DED showed greater similarity to normal mucosa compared with OCs on collagen and PET as determined by image analysis, immunohistochemistry (IHC) profiles and RT-PCR data patterns.
- Due to the architectural similarity of OC models with normal oral epithelium, OCs have the potential to contribute in tissue repairing and for the study of mucosal biology. Further characterisation of OC models will enable optimisation of the most appropriate methods for generating oral epithelial structures for clinical use.
- Full thickness engineered oral mucosa grafts facilitate in healing and repairing of intra-oral and extra-oral defects and oral mucosa disease models provide a better understanding of the phenomenon of oral diseases and their treatment, therefore it is important to identify the most suitable methods for production and delivery of these tissues.

7. Future work

In future, it is highly likely that human oral keratinocytes will be used to engineer full-thickness oral mucosa for tissue replacement. Human blood serum/ plasma (Pena *et al*., 2010) would be preferably used to culture human oral keratinocytes rather fetal calf serum (FCS) and Ham's F-12 serum to avoid tissue antigenicity in the recipient body. Further development of culture techniques and their architectural characterisation will hopefully enable more quantitative comparisons between engineered oral mucosa and their natural counterparts to make it more clinical acceptable. For example it is speculated that the dynamics of epithelium maintenance depend on stem cell positioning and density and therefore organotypic cultures might facilitate the understanding of such interactions.

Further work should seek modification of scaffold materials to facilitate stratified epithelial layering and maturation and investigate to what degree it might be possible to control the type of epithelium produced (i.e. keratinising or non-keratinising) as well as making it possible to easily transfer the engineered tissues to the patient.

PET is a synthetic material which does not exhibit antigenicity or other known biological safety risks and therefore may be suited for future clinical use. While only 2-3 cell layers of OCs were generated on PET, the thickness of OCs could potentially be improved by incorporating factors such as KGF, TGF-α, TGF-β and IL-1 either within the scaffold material or added to the media to promote faster keratinocyte proliferation and differentiation *in vitro* so the thicker epithelial tissues generated can be made available relatively rapidly for patients.

Further gene and protein expression characterisation by IHC, RT-PCR and microarray technology over longer periods of time in OCs generated on different substrates will also contribute to the understanding of the sustained expression of structural molecules to produce more accurate tissue models. It is hoped that future characterisation of those OC models will enable identification of the most appropriate methods for generating replacement tissues for clinical use. Such models could also be used to study cancer cell invasion capacity using H400 immortalised cell line by quantitative microscopy.

8. REFERENCES

ABU-EID, R. & LANDINI, G. 2006. Morphometrical differences between pseudo-epitheliomatous hyperplasia in granular cell tumours and squamous cell carcinomas. *Histopathology,* 48**,** 407-16.

ADAMS, D. 1976. Keratinization of the oral epithelium. *Ann R Coll Surg Engl,* 58**,** 351-8.

ALBERTS, B., JOHNSON, A., LEWIS, J., RAFF, M., ROBERTS, K. & WALTER, P. 2008. *Molecular Biology of the Cell,* New York, Garland Science.

ALEXANDER, H. 1995. The clinical impact of tissue engineering. *Tissue Eng,* 1**,** 197-202.

AOYAMA, Y., YAMAMOTO, Y., YAMAGUCHI, F. & KITAJIMA, Y. 2009. Low to high Ca2+ -switch causes phosphorylation and association of desmocollin 3 with plakoglobin and desmoglein 3 in cultured keratinocytes. *Exp Dermatol,* 18**,** 404-8.

AUMAILLEY, M. & KRIEG, T. 1996. Laminins: a family of diverse multifunctional molecules of basement membranes. *J Invest Dermatol,* 106**,** 209-214.

AVERY, J. K. & DANIEL J., J. C. 2005. *Essentials of Oral Histology and Embryology: A Clinical Approach*, Elsevier, Mosby.

BALE, E. & WHITE, F. H. 1982. Quantitative light and electron microscopical studies of the epithelial-connective tissue junction in intraoral mucosae. *J Microsc,* 128**,** 69-78.

BANKS-SCHLEGEL, S. & GREEN, H. 1981. Involucrin synthesis and tissue assembly by keratinocytes in natural and cultured human epithelia. *J Cell Biol,* 90**,** 732-7.

BARRETT, A. W., MORGAN, M., NWAEZE, G., KRAMER, G. & BERKOVITZ, B. K. 2005. The differentiation profile of the epithelium of the human lip. *Arch Oral Biol,* 50**,** 431-8.

BAUM, B. J. & MOONEY, D. J. 2000. The impact of tissue engineering on dentistry. *J Am Dent Assoc,* 131**,** 309-18.

BECKER, J., SCHUPPAN, D., HAHN, E. G., ALBERT, G. & REICHART, P. 1986. The immunohistochemical distribution of collagens type IV, V, VI and of laminin in the human oral mucosa. *Arch Oral Biol,* 31**,** 179-86.

BECKER, W. M., KLEINSMITH, L. J., HARDIN, J. & BERTONI, G. P. 2008. *The World of the Cell*, Benjamin Cummings.

BELL, E., EHRLICH, H. P., BUTTLE, D. J. & NAKATSUJI, T. 1981. Living tissue formed in vitro and accepted as skin-equivalent tissue of full thickness. *Science,* 211**,** 1052-4.

BERNSTAM, L. I., VAUGHAN, F. L. & BERNSTEIN, I. A. 1990. Stratified cornified primary cultures of human keratinocytes grown on microporous membranes at the air-liquid interface. *J Dermatol Sci,* 1**,** 173-81.

BHARGAVA, S., PATTERSON, J. M., INMAN, R. D., MACNEIL, S., CHAPPLE, C. R. 2008. Tissue-engineered buccal mucosa urethroplasty—clinical outcomes. *Eur Urol,* 53**,** 1263-1269.

BLACK, A. F., BOUEZ, C., PERRIER, E., SCHLOTMANN, K., CHAPUIS, F. & DAMOUR, O. 2005. Optimization and characterization of an engineered human skin equivalent. *Tissue Eng,* 11**,** 723-33.

BLACKER, K. L., WILLIAMS, M. L. & GOLDYNE, M. 1987. Mitomycin C-treated 3T3 fibroblasts used as feeder layers for human keratinocyte culture retain the capacity to generate eicosanoids. *J Invest Dermatol,* 89**,** 536-9.

BLOOR, B. K., SEDDON, S. V. & MORGAN, P. R. 2000. Gene expression of differentiation-specific keratins (K4, K13, K1 and K10) in oral non-dysplastic keratoses and lichen planus. *J Oral Pathol Med,* 29**,** 376-84.

BLOOR, B. K., SEDDON, S. V. & MORGAN, P. R. 2001. Gene expression of differentiation-specific keratins in oral epithelial dysplasia and squamous cell carcinoma. *Oral Oncol,* 37**,** 251-61.

BLOOR, B. K., SU, L., SHIRLAW, P. J. & MORGAN, P. R. 1998. Gene expression of differentiation-specific keratins (4/13 and 1/10) in normal human buccal mucosa. *Lab Invest,* 78**,** 787-95.

BLUMENBERG, M. & TOMIC-CANIC, M. 1997. Human epidermal keratinocyte: keratinization processes. *EXS,* 78**,** 1-29.

BOELSMA, E., VERHOEVEN, M. C. & PONEC, M. 1999. Reconstruction of a human skin equivalent using a spontaneously transformed keratinocyte cell line (HaCaT). *J Invest Dermatol,* 112**,** 489-98.

BOLAND, M. V. & MURPHY, R. F. 2001. A neural network classifier capable of recognizing the patterns of all major subcellular structures in fluorescence microscope images of HeLa cells. *Bioinformatics,* 17**,** 1213-23.

BREITKREUTZ, D., STARK, H. J., MIRANCEA, N., TOMAKIDI, P., STEINBAUER, H. & FUSENIG, N. E. 1997. Integrin and basement membrane normalization in mouse grafts of human keratinocytes--implications for epidermal homeostasis. *Differentiation,* 61**,** 195-209.

BURGESON, R. E., CHIQUET, M., DEUTZMANN, R., EKBLOM, P., ENGEL, J., KLEINMAN, H., MARTIN, G. R., MENEGUZZI, G., PAULSSON, M., SANES, J. & ET AL. 1994. A new nomenclature for the laminins. *Matrix Biol,* 14**,** 209-11.

CANCEDDA, R. & DE LUCA, M. 1993. Tissue engineering for clinical application. *Year Immunol,* 7**,** 193-8.

CARROLL, J. M., ALBERS, K. M., GARLICK, J. A., HARRINGTON, R. & TAICHMAN, L. B. 1993. Tissue- and stratum-specific expression of the human involucrin promoter in transgenic mice. *Proc Natl Acad Sci U S A,* 90**,** 10270-4.

CARTER, W. G., KAUR, P., GIL, S. G., GAHR, P. J. & WAYNER, E. A. 1990. Distinct functions for integrins alpha 3 beta 1 in focal adhesions and alpha 6 beta 4/bullous pemphigoid antigen in a new stable anchoring contact (SAC) of keratinocytes: relation to hemidesmosomes. *J Cell Biol,* 111**,** 3141-54.

CHAMBARD, M., VERRIER, B., GABRION, J. & MAUCHAMP, J. 1983. Polarisation of thyroid cells in culture: evidence for the baso-lateral localisation of the iodide "pump" and of the thyroid-stimulating hormone receptor-adenyl cyclase complex. *J Cell Biol,* 96**,** 1172-7.

CHAN, B. P. & LEONG, K. W. 2008. Scaffolding in tissue engineering: general approaches and tissue-specific considerations. *Eur Spine J,* 17 Suppl 4**,** 467-79.

CHANDRA, S., CHANDRA, S., CHANDRA, M., CHANDRA, G. & CHANDRA, N. 2010. *Textbook of Dental and Oral Histology with Embryology,* Jaypee Brothers Medical Publishers.

CHEN, X. & MURPHY, R. 2004. Robust classification of subcellular location patterns in high resolution 3D fluorescence microscope images. *Conf Proc IEEE Eng Med Biol Soc,* 3**,** 1632-5.

CHO, K. H., AHN, H. T., PARK, K. C., CHUNG, J. H., KIM, S. W., SUNG, M. W., KIM, K. H., CHUNG, P. H., EUN, H. C. & YOUN, J. I. 2000. Reconstruction of human hard-palate mucosal epithelium on de-epidermized dermis. *J Dermatol Sci,* 22**,** 117-24.

CLAUSEN, H., VEDTOFTE, P., MOE, D., DABELSTEEN, E., SUN, T. T. & DALE, B. 1986. Differentiation-dependent expression of keratins in human oral epithelia. *J Invest Dermatol,* 86**,** 249-54.

CLUGSTON, P. A., SNELLING, C. F., MACDONALD, I. B., MALEDY, H. L., BOYLE, J. C., GERMANN, E., COURTEMANCHE, A. D., WIRTZ, P., FITZPATRICK, D. J., KESTER, D. A. & ET AL. 1991. Cultured epithelial autografts: three years of clinical experience with eighteen patients. *J Burn Care Rehabil,* 12**,** 533-9.

COLLEY, H. E., HEARNDEN, V., JONES, A. V., WEINREB, P. H., VIOLETTE, S. M., MACNEIL, S., THORNHILL, M. H. & MURDOCH, C. 2011. Development of tissue-engineered models of oral dysplasia and early invasive oral squamous cell carcinoma. *Br J Cancer,* 105**,** 1582-92.

COOPER, M. L., ANDREE, C., HANSBROUGH, J. F., ZAPATA-SIRVENT, R. L. & SPIELVOGEL, R. L. 1993. Direct comparison of a cultured composite skin substitute containing human keratinocytes and fibroblasts to an epidermal sheet graft containing human keratinocytes on athymic mice. *J Invest Dermatol,* 101**,** 811-9.

COSTEA, D. E., DIMBA, A. O., LORO, L. L., VINTERMYR, O. K. & JOHANNESSEN, A. C. 2005. The phenotype of in vitro reconstituted normal human oral epithelium is essentially determined by culture medium. *J Oral Pathol Med,* 34**,** 247-52.

COSTEA, D. E., LORO, L. L., DIMBA, E. A., VINTERMYR, O. K. & JOHANNESSEN, A. C. 2003. Crucial effects of fibroblasts and keratinocyte growth factor on morphogenesis of reconstituted human oral epithelium. *J Invest Dermatol,* 121**,** 1479-86.

COULOMBE, P. A., KERNS, M. L. & FUCHS, E. 2009. Epidermolysis bullosa simplex: a paradigm for disorders of tissue fragility. *J Clin Invest,* 119**,** 1784-93.

CUTRIGHT, D. E. & BAUER, H. 1967. Cell renewal in the oral mucosa and skin of the rat. I. Turnover time. *Oral Surg Oral Med Oral Pathol,* 23**,** 249-59.

DANILENKO, D. M. 1999. Preclinical and early clinical development of keratinocyte growth factor, an epithelial-specific tissue growth factor. *Toxicol Pathol,* 27**,** 64-71.

DELVA, E., TUCKER, D. K. & KOWALCZYK, A. P. 2009. The desmosome. *Cold Spring Harb Perspect Biol,* 1**,** a002543.

DENIZOT, F. & LANG, R. 1986. Rapid colorimetric assay for cell growth and survival. Modifications to the tetrazolium dye procedure giving improved sensitivity and reliability. *J Immunol Methods,* 89**,** 271-7.

DEUCHER, A., EFIMOVA, T. & ECKERT, R. L. 2002. Calcium-dependent involucrin expression is inversely regulated by protein kinase C (PKC)alpha and PKCdelta. *J Biol Chem,* 277**,** 17032-40.

DOGIC, D., ROUSSELLE, P. & AUMAILLEY, M. 1998. Cell adhesion to laminin 1 or 5 induces isoform-specific clustering of integrins and other focal adhesion components. *J Cell Sci,* 111 (Pt 6)**,** 793-802.

DONGARI-BAGTZOGLOU, A. & KASHLEVA, H. 2006. Development of a highly reproducible three-dimensional organotypic model of the oral mucosa. *Nat Protoc,* 1**,** 2012-8.

DUNCAN, C. O., SHELTON, R. M., NAVSARIA, H., BALDERSON, D. S., PAPINI, R. P. & BARRALET, J. E. 2005. In vitro transfer of keratinocytes: comparison of transfer from fibrin membrane and delivery by aerosol spray. *J Biomed Mater Res B Appl Biomater,* 73**,** 221-8.

ELIAS, P. M. & FRIEND, D. S. 1975. The permeability barrier in mammalian epidermis. *J Cell Biol,* 65**,** 180-91.

ENOCH, S., MOSELEY, R., STEPHENS, P., THOMAS, D. W. 2008. The oral mucosa: a model of wound healing with reduced scarring. *Oral Surg,* 1**,** 11-21.

FEINBERG, S.E., AGHALOO, T.L. & CUNNINGHAM, L.L. JR. 2005. Role of tissue engineering in oral and maxillofacial reconstruction: findings of the 2005 AAOMS Research Summit. *J Oral Maxillofac Surg,* 63**,** 1418-25.

FELICIANI, C., GUPTA, A. K. & SAUDER, D. N. 1996. Keratinocytes and cytokine/growth factors. *Crit Rev Oral Biol Med,* 7**,** 300-18.

FREEDBERG, I. M., TOMIC-CANIC, M., KOMINE, M. & BLUMENBERG, M. 2001. Keratins and the keratinocyte activation cycle. *J Invest Dermatol,* 116**,** 633-40.

FREIMOSER, F. M., JAKOB, C. A., AEBI, M. & TUOR, U. 1999. The MTT [3-(4,5-dimethylthiazol-2-yl)-2,5-diphenyltetrazolium bromide] assay is a fast and reliable method for colorimetric determination of fungal cell densities. *Appl Environ Microbiol,* 65**,** 3727-9.

FRESHNEY, R. I. & FRESHNEY, M. G. 2002. *Culture of Epithelial Cells*, Wiley-Liss.

FRIEDLAND, G. 2007. Image cut and paste in images and videos. *Inter J of Semantic Computing,* 1, 221-247.

FUKUYAMA, K., INOUE, N., SUZUKI, H. & EPSTEIN, W. L. 1976. Keratinization. *Int J Dermatol,* 15**,** 473-89.

FUSENIG, N. E., BREITKREUTZ, D., DZARLIEVA, R. T., BOUKAMP, P., BOHNERT, A. & TILGEN, W. 1983. Growth and differentiation characteristics of transformed keratinocytes from mouse and human skin in vitro and in vivo. *J Invest Dermatol,* 81**,** 168s-75s.

GACHE, C., BERTHOIS, Y., MARTIN, P. M. & SAEZ, S. 1998. Positive regulation of normal and tumoral mammary epithelial cell proliferation by fibroblasts in coculture. *In Vitro Cell Dev Biol Anim,* 34**,** 347-51.

GARCIA, Y., BREEN, A., BURUGAPALLI, K., DOCKERY, P. & PANDIT, A. 2007. Stereological methods to assess tissue response for tissue-engineered scaffolds. *Biomaterials,* 28**,** 175-86.

GARROD, D. & CHIDGEY, M. 2008. Desmosome structure, composition and function. *Biochim Biophys Acta,* 1778**,** 572-87.

GARROD, D. R. 1993. Desmosomes and hemidesmosomes. *Curr Opin Cell Biol,* 5**,** 30-40.

GLOWACKI, J. & MIZUNO, S. 2008. Collagen scaffolds for tissue engineering. *Biopolymers,* 89**,** 338-44.

GREEN, K. J. & JONES, J. C. 1996. Desmosomes and hemidesmosomes: structure and function of molecular components. *FASEB J,* 10**,** 871-81.

GUMBINER, B., STEVENSON, B. & GRIMALDI, A. 1988. The role of the cell adhesion molecule uvomorulin in the formation and maintenance of the epithelial junctional complex. *J Cell Biol,* 107**,** 1575-87.

GURSOY, U. K., POLLANEN, M., KONONEN, E., UITTO, V. J. 2010. Biofilm formation enhances the oxygen tolerance and invasiveness of *Fusobacterium nucleatum* in an oral mucosa culture model. *J Periodontol,* 81**,** 1084-1091.

HAFEMANN, B., ENSSLEN, S., ERDMANN, C., NIEDBALLA, R., ZUHLKE, A., GHOFRANI, K. & KIRKPATRICK, C. J. 1999. Use of a collagen/elastin-membrane for the tissue engineering of dermis. *Burns,* 25**,** 373-84.

HANSSON, A., BLOOR, B. K., HAIG, Y., MORGAN, P. R., EKSTRAND, J. & GRAFSTROM, R. C. 2001. Expression of keratins in normal, immortalized and malignant oral epithelia in organotypic culture. *Oral Oncol,* 37**,** 419-30.

HAUG, H. 1972. Stereological methods in the analysis of neuronal parameters in the central nervous system. *J Microsc,* 95**,** 165-80.

HEARNDEN, V., LOMAS, H., MACNEIL, S., THORNHILL, M., MURDOCH, C., LEWIS, A. 2009. Diffusion studies of nanometer polymersomes across tissue engineered human oral mucosa. *Pharm Res,* 26**,** 1718-1728.

HECK, E. L., BERGSTRESSER, P. R. & BAXTER, C. R. 1985. Composite skin graft: frozen dermal allografts support the engraftment and expansion of autologous epidermis. *J Trauma,* 25**,** 106-12.

HENNINGS, H., MICHAEL, D., CHENG, C., STEINERT, P., HOLBROOK, K. & YUSPA, S. H. 1980. Calcium regulation of growth and differentiation of mouse epidermal cells in culture. *Cell,* 19**,** 245-54.

HILDEBRAND, H. C., HAKKINEN, L., WIEBE, C. B. & LARJAVA, H. S. 2002. Characterization of organotypic keratinocyte cultures on de-epithelialised bovine tongue mucosa. *Histol Histopathol,* 17**,** 151-63.

HOFLAND LJ, VAN DER BURG B, VAN EIJCK CH, SPRIJ DM, VAN KOETSVELD PM, LAMBERTS SW. 1995. Role of tumor-derived fibroblasts in the growth of primary cultures of human breast-cancer cells: effects of epidermal growth factor and the somatostatin analogue octreotide. *Int J Cancer,* 3**,** 93-9.

HUANG, K. & MURPHY, R. F. 2004. From quantitative microscopy to automated image understanding. *J Biomed Opt,* 9**,** 893-912.

HUNT, N. C., SHELTON, R. M. & GROVER, L. 2009. An alginate hydrogel matrix for the localised delivery of a fibroblast/keratinocyte co-culture. *Biotechnol J,* 4**,** 730-7.

HYNES, R. O. 1992. Integrins: versatility, modulation, and signaling in cell adhesion. *Cell,* 69**,** 11-25.

IGARASHI, M., IRWIN, C. R., LOCKE, M. & MACKENZIE, I. C. 2003. Construction of large area organotypical cultures of oral mucosa and skin. *J Oral Pathol Med,* 32**,** 422-30.

IZUMI, K., FEINBERG, S. E., IIDA, A. & YOSHIZAWA, M. 2003. Intraoral grafting of an ex vivo produced oral mucosa equivalent: a preliminary report. *Int J Oral Maxillofac Surg,* 32**,** 188-97.

IZUMI, K., TERASHI, H., MARCELO, C. L. & FEINBERG, S. E. 2000. Development and characterization of a tissue-engineered human oral mucosa equivalent produced in a serum-free culture system. *J Dent Res,* 79**,** 798-805.

JAMORA, C. & FUCHS, E. 2002. Intercellular adhesion, signalling and the cytoskeleton. *Nat Cell Biol,* 4**,** E101-8.

JETTEN, A. M., SHIRLEY, J. E. & STONER, G. 1986. Regulation of proliferation and differentiation of respiratory tract epithelial cells by TGF beta. *Exp Cell Res,* 167**,** 539-49.

JUHL, M., REIBEL, J. & STOLTZE, K. 1989. Immunohistochemical distribution of keratin proteins in clinically healthy human gingival epithelia. *Scand J Dent Res,* 97**,** 159-70.

KAIGLER, D. & MOONEY, D. 2001. Tissue engineering's impact on dentistry. *J Dent Educ,* 65**,** 456-62.

KAMATA, T. 1992. Histological study of human lingual tonsil, especially changes with aging. *Nihon Jibiinkoka Gakkai Kaiho,* 95**,** 825-43.

KAMEYAMA, S., KONDO, M., TAKEYAMA, K. & NAGAI, A. 2003. Air exposure causes oxidative stress in cultured bovine tracheal epithelial cells and produces a change in cellular glutathione systems. *Exp Lung Res,* 29**,** 567-83.

KANG, Y. J., FENG, Y. & HATCHER, E. L. 1994. Glutathione stimulates A549 cell proliferation in glutamine-deficient culture: the effect of glutamate supplementation. *J Cell Physiol,* 161**,** 589-96.

KIM, J. P., ZHANG, K., CHEN, J. D., WYNN, K. C., KRAMER, R. H. & WOODLEY, D. T. 1992. Mechanism of human keratinocyte migration on fibronectin: unique roles of RGD site and integrins. *J Cell Physiol,* 151**,** 443-50.

KINIKOGLU, B., AUXENFANS, C., PIERRILLAS, P., JUSTIN, V., BRETON, P., BURILLON, C., HASIRCI, V. & DAMOUR, O. 2009. Reconstruction of a full-thickness collagen-based human oral mucosal equivalent. *Biomaterials,* 30**,** 6418-25.

KLAUSNER, M., AYEHUNIE, S., BREYFOGLE, B. A., WERTZ, P. W., BACCA, L. & KUBILUS, J. 2007. Organotypic human oral tissue models for toxicological studies. *Toxicol In Vitro,* 21**,** 938-49.

KOWALCZYK, A. P., BORNSLAEGER, E. A., NORVELL, S. M., PALKA, H. L. & GREEN, K. J. 1999. Desmosomes: intercellular adhesive junctions specialized for attachment of intermediate filaments. *Int Rev Cytol,* 185**,** 237-302.

KOWALCZYK, A. P., STAPPENBECK, T. S., PARRY, D. A., PALKA, H. L., VIRATA, M. L., BORNSLAEGER, E. A., NILLES, L. A. & GREEN, K. J. 1994. Structure and function of desmosomal transmembrane core and plaque molecules. *Biophys Chem,* 50**,** 97-112.

KREJCI, N. C., CUONO, C. B., LANGDON, R. C. & MCGUIRE, J. 1991. In vitro reconstitution of skin: fibroblasts facilitate keratinocyte growth and differentiation on acellular reticular dermis. *J Invest Dermatol,* 97**,** 843-8.

KUBILUS, J., MACDONALD, M. J. & BADEN, H. P. 1979. Epidermal proteins of cultured human and bovine keratinocytes. *Biochim Biophys Acta,* 578**,** 484-92.

LAMBERT, P. F., OZBUN, M. A., COLLINS, A., HOLMGREN, S., LEE, D. & NAKAHARA, T. 2005. Using an immortalized cell line to study the HPV life cycle in organotypic "raft" cultures. *Methods Mol Med,* 119**,** 141-55.

LANDINI, G. 2006. Quantitative analysis of the epithelial lining architecture in radicular cysts and odontogenic keratocysts. *Head Face Med,* 2**,** 4.
LANDINI, G. & OTHMAN, I. E. 2003. Estimation of tissue layer level by sequential morphological reconstruction. *J Microsc,* 209**,** 118-25.
LANDINI, G. & OTHMAN, I. E. 2004. Architectural analysis of oral cancer, dysplastic, and normal epithelia. *Cytometry A,* 61**,** 45-55.
LANGER, R. & VACANTI, J. P. 1993. Tissue engineering. *Science,* 260**,** 920-6.
LANZA, R., LANGER, R. & VACANTI, J. 2007. *Principles of Tissue Engineering,* Academic Press.
LAUER, G. & SCHIMMING, R. 2001. Tissue-engineered mucosa graft for reconstruction of the intraoral lining after freeing of the tongue: a clinical and immunohistologic study. *J Oral Maxillofac Surg,* 59**,** 169-75; discussion 175-7.
LECHNER, J. F., HAUGEN, A., AUTRUP, H., MCCLENDON, I. A., TRUMP, B. F. & HARRIS, C. C. 1981. Clonal growth of epithelial cells from normal adult human bronchus. *Cancer Res,* 41**,** 2294-304.
LEE, C. H., SINGLA, A. & LEE, Y. 2001. Biomedical applications of collagen. *Int J Pharm,* 221**,** 1-22.
LEE, K. H. 2000. Tissue-engineered human living skin substitutes: development and clinical application. *Yonsei Med J,* 41**,** 774-9.
LEE, K. Y. & MOONEY, D. J. 2001. Hydrogels for tissue engineering. *Chem Rev,* 101**,** 1869-79.
LEESON, C. R., LEESON, T. S. & PAPARO, A. A. 1985. *Textbook of Histology,* Philadelphia, Saunders.
LEIGH, I. M. & WATT, F. M. 1995. *Keratinocyte Methods* Cambridge University Press.
LEWIS, J. E., JENSEN, P. J., JOHNSON, K. R. & WHEELOCK, M. J. 1994. E-cadherin mediates adherens junction organization through protein kinase C. *J Cell Sci,* 107 (Pt 12)**,** 3615-21.
LI, C., YANG, S., CHEN, L., LU, W., QIU, X., GUNDERSEN, H. J. & TANG, Y. 2009. Stereological methods for estimating the myelin sheaths of the myelinated fibers in white matter. *Anat Rec (Hoboken),* 292**,** 1648-55.
LIU, C. Z., XIA, Z. D., HAN, Z. W., HULLEY, P. A., TRIFFITT, J. T. & CZERNUSZKA, J. T. 2008a. Novel 3D collagen scaffolds fabricated by indirect printing technique for tissue engineering. *J Biomed Mater Res B Appl Biomater,* 85**,** 519-28.
LI, W. J., LAURENCIN, C. T., CATERSON, E. J., TUAN, R. S. & KO, F. K. 2002. Electrospun nanofibrous structure: A novel scaffold for tissue engineering. *JBMR,* 60**,** 613–621.
LIU, J., LAMME, E. N., STEEGERS-THEUNISSEN, R. P., KRAPELS, I. P., BIAN, Z., MARRES, H., SPAUWEN, P. H., KUIJPERS-JAGTMAN, A. M. & VON DEN HOFF, J. W. 2008b. Cleft palate cells can regenerate a palatal mucosa in vitro. *J Dent Res,* 87**,** 788-92.
LIU, X., TAN, J., HATEM, I. & SMITH, B. L. 2004. Image processing of hematoxylin and eosin-stained tissues for pathological evaluation. *Toxicol Mech Methods,* 14**,** 301-7.
LIVESEY, S. A., HERNDON, D. N., HOLLYOAK, M. A., ATKINSON, Y. H. & NAG, A. 1995. Transplanted acellular allograft dermal matrix. Potential as a template for the reconstruction of viable dermis. *Transplantation,* 60**,** 1-9.

LOPEZ VALLE, C. A., AUGER, F. A., ROMPRE, P., BOUVARD, V. & GERMAIN, L. 1992. Peripheral anchorage of dermal equivalents. *Br J Dermatol,* 127**,** 365-71.

LUITAUD, C., LAFLAMME, C., SEMLALI, A., SAIDI, S., GRENIER, G., ZAKRZEWSKI, A. & ROUABHIA, M. 2007. Development of an engineering autologous palatal mucosa-like tissue for potential clinical applications. *J Biomed Mater Res B Appl Biomater,* 83**,** 554-61.

MA, L., GAO, C., MAO, Z., ZHOU, J., SHEN, J., HU, X. & HAN, C. 2003. Collagen/chitosan porous scaffolds with improved biostability for skin tissue engineering. *Biomaterials,* 24**,** 4833-41.

MA, P. X. & ELISSEEFF, J. H. 2005. *Scaffolding in tissue engineering,* Boca Raton, Taylor&Francis.

MA, Z. W., KOTAKI, M., YONG, T., HE, W. & RAMAKRISHNA, S. 2005. *Biomaterials,* 26**,** 2527–2536.

MACCALLUM, D. K. & LILLIE, J. H. 1990. Evidence for autoregulation of cell division and cell transit in keratinocytes grown on collagen at an air-liquid interface. *Skin Pharmacol,* 3**,** 86-96.

MACNEIL, S. 2008. Biomaterials for tissue engineering of skin. *Materials today,* 11, 26-35.

MACNEIL, S., SHEPHERD, J. & SMITH, L. 2011. Production of tissue-engineered skin and oral mucosa for clinical and experimental use. *Meth Mol Biol,* 695**,** 129-53.

MACKENZIE, I. C. & BINNIE, W. H. 1983a. Recent advances in oral mucosal research. *J Oral Pathol,* 12**,** 389-415.

MACKENZIE, I. C. & FUSENIG, N. E. 1983b. Regeneration of organized epithelial structure. *J Invest Dermatol,* 81**,** 189s-94s.

MADISON, K. C., SWARTZENDRUBER, D. C., WERTZ, P. W. & DOWNING, D. T. 1987. Presence of intact intercellular lipid lamellae in the upper layers of the stratum corneum. *J Invest Dermatol,* 88**,** 714-8.

MAGIN, T. M., VIJAYARAJ, P. & LEUBE, R. E. 2007. Structural and regulatory functions of keratins. *Exp Cell Res,* 313, 2021-32.

MARINKOVICH, M. P., VERRANDO, P., KEENE, D. R., MENEGUZZI, G., LUNSTRUM, G. P., ORTONNE, J. P. & BURGESON, R. E. 1993. Basement membrane proteins kalinin and nicein are structurally and immunologically identical. *Lab Invest,* 69**,** 295-9.

MARSH, D., SUCHAK, K., MOUTASIM, K. A., VALLATH, S., HOPPER, C. & JERJES, W. 2011. Stromal features are predictive of disease mortality in oral cancer patients. *J Pathol,* 223**,** 470-481.

MASUDA, I. 1996. [An in vitro oral mucosal model reconstructed from human normal gingival cells]. *Kokubyo Gakkai Zasshi,* 63**,** 334-53.

MATOLTSY, A. G. 1976. Keratinization. *J Invest Dermatol,* 67, 20-5.

MATOLTSY, A. G. 1975. Desmosomes, filaments, and keratohyaline granules: their role in the stabilization and keratinization of the epidermis. *J Invest Dermatol,* 65**,** 127-42.

MCGRATH, J. A., GATALICA, B., CHRISTIANO, A. M., LI, K., OWARIBE, K., MCMILLAN, J. R., EADY, R. A. & UITTO, J. 1995. Mutations in the 180-kD bullous pemphigoid antigen (BPAG2), a hemidesmosomal transmembrane

collagen (COL17A1), in generalized atrophic benign epidermolysis bullosa. *Nat Genet,* 11**,** 83-6.

MEFI, R. C., ALLEY, K. & PERMER, D. 2000. *Permar's Oral Embryology and Microscopic Anatomy,* Lippincott Williams and Wilkins.

MICHELS, C., BUCHTA, T., BLOCH, W., KRIEG, T. & NIESSEN, C. M. 2009. Classical cadherins regulate desmosome formation. *J Invest Dermatol,* 129**,** 2072-5.

MILWARD, M. R., CHAPPLE, I. L., WRIGHT, H. J., MILLARD, J. L., MATTHEWS, J. B. & COOPER, P. R. 2007. Differential activation of NF-kappaB and gene expression in oral epithelial cells by periodontal pathogens. *Clin Exp Immunol,* 148**,** 307-24.

MOHAMMADI, M., SHOKRGOZAR, M. A., MOFID, R. 2007. Culture of human gingival fibroblasts on a biodegradable scaffold and evaluation of its effect on attached gingiva: a randomised, controlled pilot study. *J Periodontol,* 78**,** 1897-1903.

MOHAMMADI, M., MOFID, R., SHOKRGOZAR, M. A. 2011. Peri-implant soft tissue management through use of cultured gingival graft: a case report. *Acta Med Iran,* 49**,** 319-324.

MOHARAMZADEH, K., BROOK, I. M., VAN NOORT, R., SCUTT, A. M., SMITH, K. G. & THORNHILL, M. H. 2008. Development, optimization and characterization of a full-thickness tissue engineered human oral mucosal model for biological assessment of dental biomaterials. *J Mater Sci Mater Med,* 19**,** 1793-801.

MOHARAMZADEH, K., BROOK, I. M., VAN NOORT, R., SCUTT, A. M. & THORNHILL, M. H. 2007. Tissue-engineered oral mucosa: a review of the scientific literature. *J Dent Res,* 86**,** 115-24.

MOHARAMZADEH, K., COLLEY, H., MURDOCH, C., HEARNDEN, V., CHAI, W. L., BROOK, I. M., THORNHILL, M. H. & MACNEIL, S. 2012. Tissue-engineered oral mucosa. *J Dent Res,* 86**,** 115-124.

MOLINARI, B. L., TASAT, D. R., PALMIERI, M. A. & CABRINI, R. L. 2005. Kinetics of MTT-formazan exocytosis in phagocytic and non-phagocytic cells. *Micron,* 36**,** 177-83.

MOLL, R., FRANKE, W. W., SCHILLER, D. L., GEIGER, B. & KREPLER, R. 1982. The catalog of human cytokeratins: patterns of expression in normal epithelia, tumors and cultured cells. *Cell,* 31**,** 11-24.

MORGAN, P. R. & SU, L. 1994. Intermediate filaments in oral neoplasia. I. Oral cancer and epithelial dysplasia. *Eur J Cancer B Oral Oncol,* 30B**,** 160-6.

MOSMANN, T. 1983. Rapid colorimetric assay for cellular growth and survival: application to proliferation and cytotoxicity assays. *J Immunol Methods,* 65**,** 55-63.

MURPHY, R. F., VELLISTE, M., PORRECA, G. 2003 Robust numerical features for description and classification of subcellular location patterns in fluorescence microscope images. *J. VLSI Sig. Proc.*35, 311–321.

MUSCHLER, G. F., NAKAMOTO, C. & GRIFFITH, L. G. 2004. Engineering principles of clinical cell-based tissue engineering. *J Bone Joint Surg Am,* 86-A**,** 1541-58.

NAGAE, S., LICHTI, U., DE LUCA, L. M. & YUSPA, S. H. 1987. Effect of retinoic acid on cornified envelope formation: difference between spontaneous

envelope formation in vivo or in vitro and expression of envelope competence. *J Invest Dermatol,* 89**,** 51-8.
NANCI, A. 2007. *Ten Cate's Oral Histology: Development, Structure, and Function*, Mosby.
NAVARRO, F. A., MIZUNO, S., HUERTAS, J. C., GLOWACKI, J. & ORGILL, D. P. 2001. Perfusion of medium improves growth of human oral neomucosal tissue constructs. *Wound Repair Regen,* 9**,** 507-12.
NAVSARIA, H. A., OJEH, N. O., MOIEMEN, N., GRIFFITHS, M. A. & FRAME, J. D. 2004. Reepithelialization of a full-thickness burn from stem cells of hair follicles micrografted into a tissue-engineered dermal template (Integra). *Plast Reconstr Surg,* 113**,** 978-81.
NEWBY, C. S., BARR, R. M., GREAVES, M. W. & MALLET, A. I. 2000. Cytokine release and cytotoxicity in human keratinocytes and fibroblasts induced by phenols and sodium dodecyl sulfate. *J Invest Dermatol,* 115**,** 292-8.
NIESSEN, C. M. 2007. Tight junctions/adherens junctions: basic structure and function. *J Invest Dermatol,* 127**,** 2525-32.
O'TOOLE, E. A., MARINKOVICH, M. P., HOEFFLER, W. K., FURTHMAYR, H. & WOODLEY, D. T. 1997. Laminin-5 inhibits human keratinocyte migration. *Exp Cell Res,* 233**,** 330-9.
OTTO, W. R., NANCHAHAL, J., LU, Q. L., BODDY, N. & DOVER, R. 1995. Survival of allogeneic cells in cultured organotypic skin grafts. *Plast Reconstr Surg,* 96**,** 166-76.
OJEH, N. O., FRAME, J. D. & NAVSARIA, H. A. 2001. In vitro characterization of an artificial dermal scaffold. *Tissue Eng,* 7**,** 457-72.
OKADA, N., KITANO, Y. & ICHIHARA, K. 1982. Effects of cholera toxin on proliferation of cultured human keratinocytes in relation to intracellular cyclic AMP levels. *J Invest Dermatol,* 79**,** 42-7.
OPHOF, R., VAN RHEDEN, R. E., VON DEN, H. J., SCHALKWIJK, J. & KUIJPERS-JAGTMAN, A. M. 2002. Oral keratinocytes cultured on dermal matrices form a mucosa-like tissue. *Biomaterials,* 23**,** 3741-8.
ORGEL, J. P., IRVING, T. C., MILLER, A. & WESS, T. J. 2006. Microfibrillar structure of type I collagen in situ. *Proc Natl Acad Sci U S A,* 103**,** 9001-5.
PACHENCE, J. M. 1996. Collagen-based devices for soft tissue repair. *J Biomed Mater Res,* 33**,** 35-40.
PALSSON, B. O. & BHATIA, S. N. 2003. *Tissue Engineering*, Prentice Hall.
PANG, Y. Y., SCHERMER, A., YU, J. & SUN, T. T. 1993. Suprabasal change and subsequent formation of disulfide-stabilized homo- and hetero-dimers of keratins during esophageal epithelial differentiation. *J Cell Sci,* 104 (Pt 3)**,** 727-40.
PATTERSON, J. M., BULLOCK, A. J., MACNEIL, S. & CHAPPLE, C. R. 2011. Methods to reduce the contraction of tissue-engineered buccal mucosa for use in substitution urethroplasty. *Eur Urol,* 60**,** 856-61.
PAULING, L. & COREY, R. B. 1951. The structure of fibrous proteins of the collagen-gelatin group. *Proc Natl Acad Sci U S A,* 37**,** 272-81.
PENA, I., JUNQUERA, L. M., MEANA, A., GARCIA, E., AGUILAR, C., FRESNO, M. F. 2011. In vivo behaviour of complete human oral mucosa equivalents: characterisation in athymic mice. *J Periodontal Res,* 46**,** 214-220.
PEREZ-AMODIO, S., TRA, W. M., RAKHORST, H. A., HOVIUS, S. E., VAN

NECK, J. W. 2011. Hypoxia preconditioning of tissue-engineered mucosa enhances its angiogenic capacity in vitro. *Tissue Eng Part A,* 17**,** 1583-1593.

PINS, G. D., TONER, M. & MORGAN, J. R. 2000. Microfabrication of an analog of the basal lamina: biocompatible membranes with complex topographies. *FASEB J,* 14**,** 593-602.

PONEC, M. & BOONSTRA, J. 1987. Effects of retinoids and hydrocortisone on keratinocyte differentiation, epidermal growth factor binding and lipid metabolism. *Dermatologica,* 175 Suppl 1**,** 67-72.

PONEC, M., WEERHEIM, A., KEMPENAAR, J., MOMMAAS, A. M. & NUGTEREN, D. H. 1988. Lipid composition of cultured human keratinocytes in relation to their differentiation. *JLipid Res,* 29**,** 949-961.

POTTEN, C. S., BOOTH, D., CRAGG, N. J., O'SHEA, J. A., TUDOR, G. L. & BOOTH, C. 2002. Cell kinetic studies in the murine ventral tongue epithelium: the effects of repeated exposure to keratinocyte growth factor. *Cell Prolif,* 35 Suppl 1**,** 22-31.

PRESLAND, R. B. & DALE, B. A. 2000. Epithelial structural proteins of the skin and oral cavity: function in health and disease. *Crit Rev Oral Biol Med,* 11**,** 383-408.

PRESLAND, R. B. & JUREVIC, R. J. 2002. Making sense of the epithelial barrier: what molecular biology and genetics tell us about the functions of oral mucosal and epidermal tissues. *J Dent Educ,* 66**,** 564-74.

PRIME, S. S., NIXON, S. V., CRANE, I. J., STONE, A., MATTHEWS, J. B., MAITLAND, N. J., REMNANT, L., POWELL, S. K., GAME, S. M. & SCULLY, C. 1990. The behaviour of human oral squamous cell carcinoma in cell culture. *J Pathol,* 160**,** 259-69.

PRUNIERAS, M., REGNIER, M. & WOODLEY, D. 1983. Methods for cultivation of keratinocytes with an air-liquid interface. *J Invest Dermatol,* 81**,** 28s-33s.

PURDUE, G. F. 1997. Dermagraft-TC pivotal efficacy and safety study. *J Burn Care Rehabil,* 18**,** S13-4.

RASBAND, W.S., ImageJ, U.S. National Institutes of Health, Bethesda, Maryland USA, imagej.nih.gov/ij/, 1997–2011.

RAULT, I., FREI, V., HERBAGE, D. 1996. Evaluation of different chemical methods for cross-linking collagen gel, films and sponges. J Mater Sci Mater Med, 215-221.

REARICK, J. I., HESTERBERG, T. W. & JETTEN, A. M. 1987. Human bronchial epithelial cells synthesize cholesterol sulfate during squamous differentiation in vitro. *J Cell Physiol,* 133**,** 573-8.

REARICK, J. I. & JETTEN, A. M. 1986. Accumulation of cholesterol 3-sulfate during in vitro squamous differentiation of rabbit tracheal epithelial cells and its regulation by retinoids. *J Biol Chem,* 261**,** 13898-904.

RHEINWALD, J. G. & GREEN, H. 1975. Serial cultivation of strains of human epidermal keratinocytes: the formation of keratinizing colonies from single cells. *Cell,* 6**,** 331-43.

RICE, R. H. & GREEN, H. 1977. The cornified envelope of terminally differentiated human epidermal keratinocytes consists of cross-linked protein. *Cell,* 11**,** 417-22.

ROSDY, M. & CLAUSS, L. C. 1990. Terminal epidermal differentiation of human keratinocytes grown in chemically defined medium on inert filter substrates at the air-liquid interface. *J Invest Dermatol,* 95**,** 409-14.

ROUABHIA, M. & DESLAURIERS, N. 2002. Production and characterization of an in vitro engineered human oral mucosa. *Biochem Cell Biol,* 80**,** 189-95.

ROY, R., BOSKEY, A. & BONASSAR, L. J. 2010. Processing of type I collagen gels using nonenzymatic glycation. *J Biomed Mater Res A,* 93**,** 843-51.

RUBIN, A. L. & RICE, R. H. 1986. Differential regulation by retinoic acid and calcium of transglutaminases in cultured neoplastic and normal human keratinocytes. *Cancer Res,* 46**,** 2356-61.

RUIFROK, A. C. & JOHNSTON, D. A. 2001. Quantification of histochemical staining by color deconvolution. *Anal Quant Cytol Histol,* 23**,** 291-9.

SAKAMOTO, K., ARAGAKI, T., MORITA, K., KAWACHI, H., KAYAMORI, K., NAKANISHI, S., OMURA, K., MIKI, Y., OKADA, N., KATSUBE, K., TAKIZAWA, T. & YAMAGUCHI, A. 2011. Down-regulation of keratin 4 and keratin 13 expression in oral squamous cell carcinoma and epithelial dysplasia: a clue for histopathogenesis. *Histopathology,* 58**,** 531-542.

SALONEN, J., PELLINIEMI, L. J., FOIDART, J. M., RISTELI, L. & SANTTI, R. 1984. Immunohistochemical characterization of the basement membranes of the human oral mucosa. *Arch Oral Biol,* 29**,** 363-8.

SAUERBIER, S., GUTWALD, R., WIEDMANN-AL-AHMAD, M., LAUER, G. & SCHMELZEISEN, R. 2006. Clinical application of tissue-engineered transplants. Part I: mucosa. *Clin Oral Implants Res,* 17**,** 625-32.

SAUNDERS, N. A., BERNACKI, S. H., VOLLBERG, T. M. & JETTEN, A. M. 1993. Regulation of transglutaminase type I expression in squamous differentiating rabbit tracheal epithelial cells and human epidermal keratinocytes: effects of retinoic acid and phorbol esters. *Mol Endocrinol,* 3**,** 387-98.

SAWAF, M. H., OUHAYOUN, J. P., SHABANA, A. H. & FOREST, N. 1990. Cytokeratin expression in human tongue epithelium. *Am J Anat,* 189**,** 155-66.

SCHMELZEISEN, R., SCHIMMING, R., SITTINGER, M. 2002. Soft tissue and hard tissue engineering in oral and maxillofacial surgery. *Ann R Australas Coll Dent Surg,* 16, 50-3.

SCHMID, B., SCHINDELIN, J., CARDONA, A., LONGAIR, M. & HEISENBERG, M. 2010. A high-level 3D visualization API for Java and ImageJ. *BMC Bioinformatics,* 11**,** 274.

SELIM, M., BULLOCK, A. J., BLACKWOOD, K. A., CHAPPLE, C. R. & MACNEIL, S. 2011. Developing biodegradable scaffolds for tissue engineering of the urethra. *BJU Int,* 107**,** 296-302.

SIPE, J. D. 2002. Tissue engineering and reparative medicine. *Ann N Y Acad Sci,* 961**,** 1-9.

SKALAK, R. & FOX, C. F. 1988. *Tissue Engineering,* Liss (New York).

SLOAN, P., PICARDO, M. & SCHOR, S. L. 1991. The structure and function of oral mucosa. *Dent Update,* 18**,** 208-12.

SMACK, D. P., KORGE, B. P. & JAMES, W. D. 1994. Keratin and keratinization. *J Am Acad Dermatol,* 30**,** 85-102.

SMITH, E. & EVERETT, M. A. 1962. Keratinization: A review. *J Okla State Med Assoc,* 55**,** 459-62.

SMITH, L.A., LIU, X. & MA, P.X. 2008. Tissue engineering with nano-fibrous scaffolds. *Soft Matter,* 4**,** 2144-2149.

SQUIER, C. & BROGDEN, K. 2011. *Human Oral Mucosa: Development, Structure and Function,* Wiley-Blackwell.

SQUIER, C. A. 1968. Ultrastructural observations on the keratinization process in rat buccal epithelium. *Arch Oral Biol,* 13**,** 1445-51.

SQUIER, C. A. & KREMER, M. J. 2001. Biology of oral mucosa and esophagus. *J Natl Cancer Inst Monogr***,** 7-15.

STARK, H. J., BAUR, M., BREITKREUTZ, D., MIRANCEA, N. & FUSENIG, N. E. 1999. Organotypic keratinocyte cocultures in defined medium with regular epidermal morphogenesis and differentiation. *J Invest Dermatol,* 112**,** 681-91.

STEINERT, P. M., STEVEN, A. C. & ROOP, D. R. 1983. Structural features of epidermal keratin filaments reassembled in vitro. *J Invest Dermatol,* 81**,** 86s-90s.

STEVENS, A. & LOWE, J. S. 2005. *Human Histology*, Philadelphia : Elsevier/Mosby.

SU, L., MORGAN, P. R. & LANE, E. B. 1994. Protein and mRNA expression of simple epithelial keratins in normal, dysplastic, and malignant oral epithelia. *Am J Pathol,* 145**,** 1349-57.

TAMMI, R. & JANSEN, C. 1980. Effect of serum and oxygen tension on human skin organ culture: a histometric analysis. *Acta Derm Venereol,* 60**,** 223-8.

THACHER, S. M. & RICE, R. H. 1985. Keratinocyte-specific transglutaminase of cultured human epidermal cells: relation to cross-linked envelope formation and terminal differentiation. *Cell,* 40**,** 685-95.

THOMSON, P. J., POTTEN, C. S. & APPLETON, D. R. 1999. Mapping dynamic epithelial cell proliferative activity within the oral cavity of man: a new insight into carcinogenesis? *Br J Oral Maxillofac Surg,* 37**,** 377-83.

TODARO, G. J. & GREEN, H. 1963. Quantitative studies of the growth of mouse embryo cells in culture and their development into established lines. *J Cell Biol,* 17**,** 299-313.

TOMAKIDI, P., BREITKREUTZ, D., FUSENIG, N. E., ZOLLER, J., KOHL, A. & KOMPOSCH, G. 1998. Establishment of oral mucosa phenotype in vitro in correlation to epithelial anchorage. *Cell Tissue Res,* 292**,** 355-66.

TROTT, J. R. & BANOCZY, J. 1962. The oral mucosa and keratinization. *Acta Morphol Acad Sci Hung,* 11**,** 217-28.

TSUTSUMI, K., IWATAKE, H., KUWABARA, D., HYODO, A., KOBAYASHI, T., KOIZUKA, I. & KATO, I. 2000. [Effects of calcium on HPV16 gene transcription in cultured laryngeal epithelial cells]. *Nihon Jibiinkoka Gakkai Kaiho,* 103**,** 727-33.

UEDA, M., EBATA, K. & KANEDA, T. 1991. In vitro fabrication of bioartificial mucosa for reconstruction of oral mucosa: basic research and clinical application. *Ann Plast Surg,* 27**,** 540-9.

VAISSIERE, G., CHEVALLAY, B., HERBAGE, D. & DAMOUR, O. 2000. Comparative analysis of different collagen-based biomaterials as scaffolds for long-term culture of human fibroblasts. *Med Biol Eng Comput,* 38**,** 205-10.

VERRANDO, P., SCHOFIELD, O., ISHIDA-YAMAMOTO, A., ABERDAM, D., PARTOUCHE, O., EADY, R. A. & ORTONNE, J. P. 1993. Nicein (BM-600) in junctional epidermolysis bullosa: polyclonal antibodies provide new clues for pathogenic role. *J Invest Dermatol,* 101**,** 738-43.

VILA TORRES, J., PINEDA MARFA, M., GONZALEZ ENSENAT, M. A. & LLORETA TRULL, J. 1994. Pathology of the elastic tissue of the skin in Costello syndrome. An image analysis study using mathematical morphology. *Anal Quant Cytol Histol,* 16**,** 421-9.

VINCENT, L. 1993. Morphological grayscale reconstruction in image analysis: applications and efficient algorithms. *IEEE Trans Image Process,* 2**,** 176-201.

WAN, H., YUAN, M., SIMPSON, C., ALLEN, K., GAVINS, F. N., IKRAM, M. S., BASU, S., BAKSH, N., O'TOOLE, E. A. & HART, I. R. 2007. Stem/progenitor cell-like properties of desmoglein 3dim cells in primary and immortalized keratinocyte lines. *Stem Cells,* 25**,** 1286-97.

WATT, F. M. 1989. Terminal differentiation of epidermal keratinocytes. *Curr Opin Cell Biol,* 1**,** 1107-15.

WATT, F. M. 1998. Epidermal stem cells: markers, patterning and the control of stem cell fate. *Philos Trans R Soc Lond B Biol Sci,* 353**,** 831-7.

WATT, F. M. & GREEN, H. 1982. Stratification and terminal differentiation of cultured epidermal cells. *Nature,* 295**,** 434-6.

WINNING, T. A. & TOWNSEND, G. C. 2000. Oral mucosal embryology and histology. *Clin Dermatol,* 18**,** 499-511.

WOO, K. M., JUN, J. H., CHEN, V. J., SEO, J., BAEK, J. H., RYOO, H. M., KIM, G. S., SOMERMAN, M. J. & MA, P. X. 2007. *Biomaterials,* 28**,** 335–343.

XIONG, X., JIA, J., HE, S., ZHAO, Y. 2010. Cryopreserved lip mucosa tissue derived keratinocytes can fabricate tissue engineered palatal mucosa equivalent. *J Biomed Mater Res B Appl Biomater,* 94**,** 165-170.

XIONG, X., ZHAO, Y., ZHANG, W., XIE, W. & HE, S. 2008. In vitro engineering of a palatal mucosa equivalent with acellular porcine dermal matrix. *J Biomed Mater Res A,* 86**,** 544-51.

YOSHIMOTO, H., SHIN, Y. M, TERAI, H. & VACANTI, J. P. 2003. *Biomaterials,* 24**,** 2077-2082.

YOUNG, B., LOWE, J. S., STEVENS, A., HEATH, J. W. & DEAKIN, P. J. 2000. *Wheater's Functional Histology: A Text and Colour Atlas,* Mosby.

ZACCHI, V., SORANZO, C., CORTIVO, R., RADICE, M., BRUN, P. & ABATANGELO, G. 1998. In vitro engineering of human skin-like tissue. *J Biomed Mater Res,* 40**,** 187-94.

ZDRAHALA, R. J. & ZDRAHALA, I. J. 1999. In vivo tissue engineering: Part I. Concept genesis and guidelines for its realization. *J Biomater Appl,* 14**,** 192-209.